Universidade do Minho
Escola de Engenharia

Miguel Angelo da Rocha Peixoto

Microporous tin silicates – synthesis, crystal structure, ion exchange, isomorphic substitution and thermal properties

novembro de 2013

Microporous tin silicates – synthesis, crystal structure, ion exchange, isomorphic substitution and thermal properties
Miguel Angelo da Rocha Peixoto
UMinho | 2013

Universidade do Minho
Escola de Engenharia

Miguel Angelo da Rocha Peixoto

Microporous tin silicates – synthesis, crystal structure, ion exchange, isomorphic substitution and thermal properties

Tese de Mestrado
Ciclo de Estudos Integrados Conducentes ao
Grau de Mestre em Engenharia de Materiais

Trabalho efetuado sob a orientação do
Professor Doutor Carlos Tavares
e
Stanislav Ferdov

novembro de 2013

Declaração

Nome

Miguel Angelo Rocha Peixoto

Endereço eletrónico: miguel52633@gmail.com **Telefone**: 913705334

Titulo dissertação:

Microporous tin silicates – synthesis, crystal structure, ion exchange, isomorphic substitution and thermal properties

Orientadores:

Carlos Tavares e Stanislav Ferdov

Designação do mestrado:

Mestrado Integrado em Engenharia de Materiais

Universidade do Minho 31 de Outubro 2013

Assinatura: _____

I Acknowledges

My acknowledgments go to my fellow colleges that have been a great source of support and guidance in my learning process. Also to my teachers that have provided me with the tools and means not only to complete this work but also to start a future career as a materials engineer.

In particular I would like to thank Professor Carlos Tavares for its support and promptitude that allowed me to enter this work. I would also like to thank Professor Mario Pereira and Ana Claudia Mota for providing the tools needed for me to conclude this work.

To my family, for their love and sacrifice, I leave the most sincere gratitude, without them I would never be where I am today. To Sara, for the days spend at my side, in every failure or success, with outstanding patience and comprehension. I give the guaranty that I'll be there when you'll need me.

Most importantly I would like to thank my tutor Professor Stanislav Ferdov. His never-ending patience and care gave me the motivation to never quit and to always look for answers. In all the days spend with him I have gain the love for science and investigation. As my mentor he showed me a kind of materials that I had never seen and infused me with the knowledge to understand them. As a friend he has given me the passion to complete this work and the courage to face any future challenge. For everything, thank you very much professor Stanislav Ferdov.

II Resume

The present work introduces the transparent precursor as a new media for synthesis of tin silicates. Based on this approach a systematic work exploiting the potential for formation of various tin silicates and process optimization of the existing ones has been carried out. The conducted syntheses resulted in the creation of crystallization fields showing the dependence of the run product on initial molar composition. Within various synthesis compositions the typical structures of the sodium based silicate (AV-10) the potassium based tin silicate (AV-6) the sodium and potassium based tin silicate (AV-7) has been achieved. Another novelty is the fine control of the crystalline product by the time of agitation of the initial transparent precursor. This type of phase control has never been studied in tin silicates.

The close structural and synthesis relation between the microporous phases AV-6 and AV-7 has been studied. The studies on the time of precursor agitation revealed that the transition between these two structures is time dependent and that AV-7 can be produced in absence of sodium ions. In the course of creation of the crystallization fields a new potassium tin silicate with layered structure was prepared. The structure was successfully indexed and the structural determination is in progress. Ion exchange properties of AV-6 and AV-7 were also explored. AV-6 was exchanged to copper and zinc forms and for the first time it has been revealed the ion exchange potential of AV-7. The phase was successfully converted into copper, zinc, chromium and lead forms. It was also seen that upon ion exchanged with divalent ions and coordination number 8, AV-7, changes differently depending on the captured ion. This behavior may serve to identify and confirm exchanges in multi ions solutions.

Isomorphous substitutions produced no effects on the synthesized phases. However, the presence of amorphous germanium in the initial batch of AV-7 resulted in decreased thermal stability and lower temperature transformation of the AV-7 framework into the Sn-AV-11 phase.

In other thermal studies it was seen that amorphous stannosilicate compositions turn into cassiterite upon high temperature exposure. The same transformation was seen in Cu-AV-6 that totally degrades after 700°C and recrystallizes into cassiterite (SnO_2) at 750°C. The thermal studies also showed the high temperatures transformations of the new layered potassium tin silicate into Sn-AV-11 and Sn-wadeite. In the ion exchanged forms of AV-7 it was seen that the Zn-AV-7 gained a thermal stability higher than any other exchanged form and possibly higher than the unchanged AV-7.

III Resumo

Silicatos de estanho microporosos: A Síntese, a estrutura cristalina, as suas trocas iónicas e substituições isomórficas, e a sua estabilidade térmica.

Este trabalho introduz um método que utiliza soluções transparentes como nova fonte para a síntese hidrotérmica de silicatos de estanho. Baseado nesta nova forma, este trabalho explora o potencial deste novo método para a produção de várias fases cristalinas e para o aperfeiçoamento das fases já conhecidas. As sínteses realizadas resultaram na criação de campos de cristalização que indicam a dependência na composição molar inicial no produto final. Com diferentes composições foi possível sintetizar estruturas de silicatos de estanho baseadas em sódio (AV-10), em potássio (AV-6 e baseadas em sódio e potássio (AV-7). Outra novidade foi o controlo do produto final pela manipulação do tempo de agitação do precursor. Este parâmetro nunca tinha sido estudado para silicatos de estanho.

Também foram estudadas as semelhanças na síntese e na estrutura entre os materiais AV-6 e AV-7. O estudo da variação do tempo de agitação do percursor mostrou que é possível fazer a transição entre estas duas estruturas. Graças a este estudo, a estrutura AV-7 foi produzida pela primeira vez sem iões de sódio. Enquanto foram criados os campos de cristalização foi produzida uma forma lamelar de silicatos de estanho. Esta fase foi identificada e reproduzida com sucesso e o processo de caracterização estrutural ainda é alvo de estudo. Algumas trocas iónicas também foram exploradas nas estruturas AV-6 e AV-7. Para AV-6 foi possível produzir uma forma com iões de cobre e uma forma com iões de zinco. Foi também possível, e pela primeira vez, produzir diferentes formas AV-7. Através de troca iónica foi possível introduzir nesta estrutura iões de cobre, zinco, crómio e chumbo. Para além disso foi encontrado um comportamento característico na estrutura quando é trocada com iões de carga $^{2+}$ e coordenação 8. Cada ião capturado produz uma alteração característica, isto pode facilitar na identificação do ião de captura em soluções multi-iões. As substituições isomórficas não produziram nenhum tipo de alteração às estruturas sintetizadas. No entanto, a presença de óxido de germânio amorfo no material AV-7 fez com que a sua estabilidade térmica baixasse e a transformação para Sn-AV-11 acontecesse mais cedo. Outros estudos térmicos revelaram que os silicatos de estanho amorfos quando expostos a alta temperatura se transformam em cassiterite. Essa mesma transformação foi vista para Cu-AV-6 que depois de degradação térmica recristaliza em cassiterite de tamanho nano. Os estudos térmicos também revelaram que a estrutura lamelar (UM-1) aqui produzida transforma-se em Sn-AV-11, e após contínua exposição ao calor começa-se a transformar em Sn-Wadeite.

Table of contents

IV Abbreviations

Å: angstrom

AM-2: Aveiro Manchester – 2, titanium silicate with umbite structure

AV-6: Aveiro – 6, tin silicate with umbite structure

AV-7: Aveiro – 7, tin silicate with sodium and potassium

AV-10: Aveiro – 10, tin silicate with sodium.

AV-15: Aveiro – 15, zirconium silicate

Cu-AV-6: Aveiro – 6 exchanged with copper

cm: centimeters

EDS: Energy dispersive X-ray spectroscopy

ICDD: International Center for Diffraction Data

ITV: Isotropic thermal values

nm: nanometers

PDF: powder diffraction files

SEM: Scanning electron microscopy

Sn-AV-11: Aveiro – 11, tin silicate analogue to AV-11structure

Sn-AV-14: Aveiro – 14, tin silicate analogue to AV-14 structure

Sn-wadeite: tin silicate with the structure of the mineral wadeite

TGA: Thermo gravimetrical analysis

UM-1: University of Minho – 1

UM-2: University of Minho – 2

XRD: X-ray diffraction

Zn-AM-2: Aveiro Manchester – 2 exchanged with zinc ions

Zn-AV-6: Aveiro – 6 exchanged with zinc

Zn-ETS-4: Engelhard titanium silicate – 4 exchanged with zinc ions

Image Index

Table Index

V Introduction

5.1 Microporous Silicates

The history of the microporous materials starts with the discovery of the zeolite minerals. This species were discovered in 1756 by Swedish mineralogist Axel Cronstedt, who gave their common name after upon rapidly heating the material release a steam from absorbed water. Thus, he called the materials zeolites, from the Greek (zéo), meaning "to boil" and (lithos), meaning "stone" [1].

Science advanced and now they are known as hydrated aluminosilicates containing pores of molecular size. The structures of these materials are composed of interconnected SiO_4 and AlO_4 that form a microporous framework. These types of frameworks form negative charged zones in the pores which are compensated by positively charged cations. Along with those cations, the pores also contain structural water molecules. In nature there are large deposits of zeolites but the synthetic ones are more important due to their vast industrial applications. Zeolite A was one of the first widely used commercial zeolites. The success of this material was the trigger point to start the study of new forms and to incorporate these materials in the market [2]. Zeolites are now of vital importance in the fuel industry performing as catalyst to produce gasoline [3] and as molecular sieves used for gas and liquids separations [4]. To date, there are more than 200 framework types of zeolites and the number of hypothetical is still pending a discovery [5].

Recently, the family of the zeolites has been expanded to other silicate molecular sieves obtained by the substitution of AlO_4 tetrahedra by various metals in octahedral coordination. This resulted in new materials (chemically and structurally) with classical zeolitic and new applications in areas such as optoelectronics, nonlinear optics, batteries, magnetic materials and sensors [6].

Within the family of the tetrahedral-octahedral molecular sieves, some of the most important members are the transition metal as titanosilicates, vanadosilicates and zirconosilicates [6]. In the common case, microporous silicates are produced in Teflon-line autoclaves under mild hydrothermal conditions at temperatures from 150 to 230°C during 1 to 10 days [6].

Across the last years many attempts have been made to synthesize new microporous silicates and zeolites with different structures and new potential applications. There is also a

great effort to modify the existing microporous structures in order to infuse them with new properties and improve the known ones. This work focuses on a recent and perspective class of materials as the microporous tin silicates. These solids offer a number of less explored structures and properties that can be an alternative to ones of the zeolites and other tetrahedral-octahedral molecular sieves.

5.2 Previous studies

In number of microporous materials it is common to see the same structures in different chemical forms. These materials are often structural analogues of existing minerals in the nature. Among them one of the most studied is the analogue of the zirconosilicate mineral, umbite, whose tin [6], titanium [7-9] and zirconium [10-12] forms have been prepared in laboratory conditions. Its porous structure is formed by an interconnection of corner sharing SiO_4 tetrahedra and MO_6 octahedra of various elements. In the space of the pores resides a water molecule and K^+ ions that compensate the negative charge of the framework. A model of this molecular sieve can be seen in figure 1. The structure has orthorhombic crystal system with $P2_12_12_1$ space-group and the unit cell dimensions depending on its chemical composition of the octahedral site. These isostructural phases are often called after the institutions where they have been synthesized for the first time. For example the titanium form is called AM-2 (Aveiro Manchester – 2) and the tin form AV-6 (Aveiro – 6).

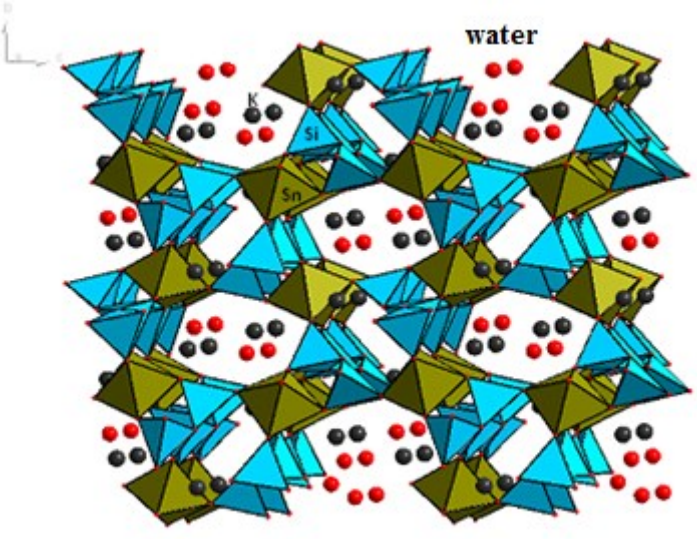

Figure 1. Crystal structure of AV-6, image along a-axis obtained by software Diamond 3.0

The applied properties of different chemical forms of the synthetic umbite have been widely studied. Ion exchange experiments of titanium form showed possibility to uptake Na^+, Cs^+, Mn^{2+}, Sr^{2+}, Ca^{2+} and Rb^{2+}. In these studies the change of the charge compensation cations of AM-2 revealed structural changes and reduction of thermal stability [13-14, 15]. Some ion exchanged forms demonstrated a potential for advanced applications. For example, zirconium umbite exchanged with Zn^{2+} resulted in an antibacterial microporous material [16]. A similar property was discovered on Zn-AM-2 and Zn-ETS-4 (Engelhard titanium

silicate-4). These molecular sieves prove to be effective in the selective elimination of cancer cells [17].

Apart from the ion exchange properties, umbite type structure in its titanium (AM-2) and tin (AV-6) forms shows excellent potential for preparation of membrane for separation of H_2 and N_2. AM-2 shows higher potential and higher thermal stability than AV-6 but the tin microporous framework shows promising potential for the use in CO_2 separation [18]. In terms of structure manipulation, the change of the octahedral site allows finely adjustable lattice dimensions and pore sizes. In this respect, there are reports on synthesis of Ti-V [19], Ti-Zr [20], and Sn-Zr [20] forms of umbite.

Another important microporous ion exchanger tin silicate is EMS-2. Along with AV-6, these materials are the only forms of tin molecular sieves to be studied in terms of ion exchange. Experiments with Mg^{2+}, Ca^{2+}, Sr^{2+} and Ba^{2+} resulted in partly or fully ion exchanged forms. The thermal studies of these ion exchanged forms revealed that all modified frameworks lose stability due to the external ion capture [21].

Thermal properties investigation revealed how structurally different materials AV-6 and AV-7 are transformed into Sn-AV-11 [22]. AV-7(Aveiro – 7) is a microporous tin silicate which is structural analogue of the mineral kostylevite [23]. In spite of different symmetry, AV-7 (monoclinic) and AV-6 (orthorhombic) have the same structural motif. The pore system of both phases is composed of 6-ring and 8-ring channels. With equal occupation on the 6-ring pore, AV-6 and AV-7 differ in the occupation of the 8-ring channel. AV-7 has sodium and potassium ions as charge stabilizers. Despite the resemblances between these two frameworks the ion exchange properties are very different. While AV-6 is easily exchanged to various cation forms, for AV-7 no ion exchange forms have been ever reported.

To date there are no more than 10 known microporous tin silicate structures, AV-6[6], AV-7 [23] and EMS-2 [24] produced by conventional hydrothermal synthesis. Sn-AV-14 [25] and AV-10 [26], two sodium based stannosilicates produced by a two stage synthesis were the synthesis can take more than 10 days. Sn-AV-11 [22] and Sn-wadeite [22] produced by high temperature transformation. All these synthesis of stannosilicates are performed from gels with tin chloride (IV) and sodium metasilicate. As a result they are always synthesized from white gels containing sodium ions. Similar to these frameworks there are chemically different forms of stannosilicates produced by high temperature and high pressure synthesis [27].

A recent study reported the first hydrothermal synthesis of tin silicates using a clear solution as precursor [28]. The new synthesis approach was based on substitution of the tin chloride (IV) by tin chloride (II) in the initial precursor. This work also reported the first ion exchanges with Cu^{2+}. The copper ions in the pores of Cu-AV-6 resulted in decreasing the initial orthorhombic symmetry to monoclinic one. Direct comparison between the powder XRD patterns shows a pronounced peak shift and appearance of new diffraction planes (figure 2) [28].

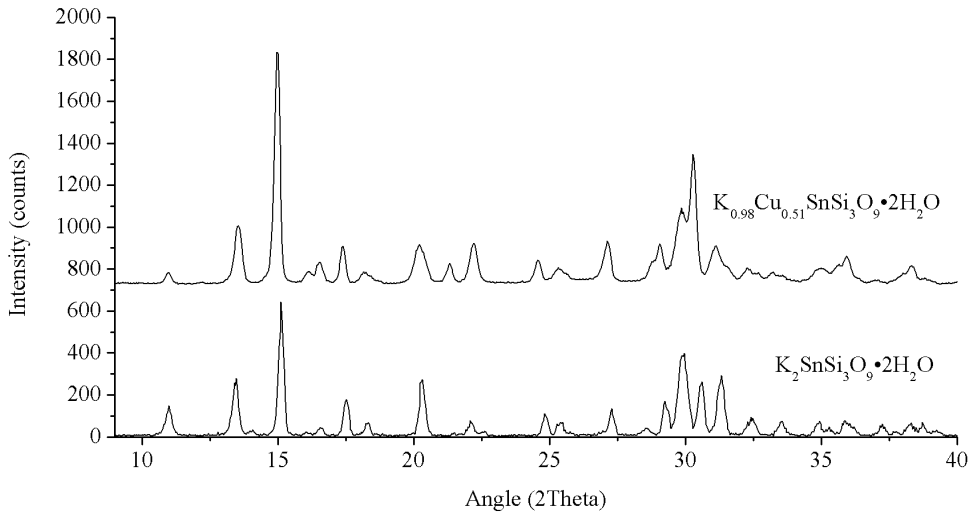

Figure 2. X-Ray diffraction powder patterns of AV-6 and Cu-AV-6.

Cu-AV-6 contains copper ions captured in the 8-ring channels. The occupation is shared with disordered water molecules. The 6-ring pores remain majorly occupied by potassium, as the Rietveld refinement model shows in figure 3 [28]. The same study showed that zinc can also be captured by this framework. In this case the decrease to the monoclinic space-group was complete and the Zn-AV-6 sample turned into a mixed phase material. The exchange with lead on the same material resulted in the framework destruction. The reversed potassium ion exchange to the Zn-AV-6 and Cu-AV-6 showed that these frameworks can return to the original state (orthorhombic). When the copper and zinc ion

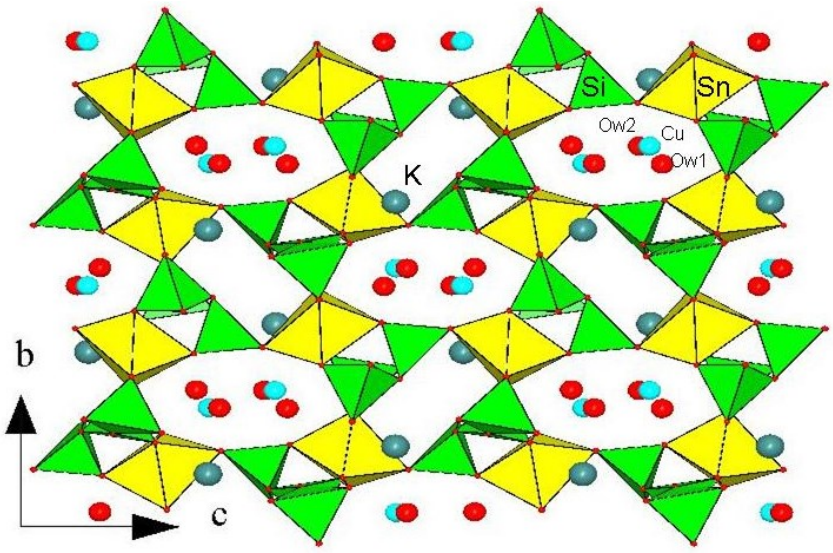

Figure 3. Crystalline structure of Cu-AV-6, cif obtained by Rietveld refinement and image by Diamond 3.0.

exchanged forms of AV-6 are exposed to high concentrated (1Mole) solutions of potassium (KCl) the AV-6 original chemical composition is restored [28].

5.3 Motivation and Objectives

The motivation for this work is driven by the potentially novel and improvement of the known applications of the microporous tin silicates. This motivation is based on the gained experience during the previous work with stannosilicates [28]. The obtained results showed that the stannosilicate system is promising not only for the preparation of new materials but also for the discovery of new ion exchange properties of known molecular sieves. The work performed so far showed the great potential of the synthesis using a transparent precursor. It also showed that there are many possible elements that can be captured in the tin silicate porous framework types. As a result, the obtained materials revealed different properties than the initially synthesized phase. In this respect, the current work is a natural continuation of the previous experience and the objectives include:

a) Development of a new method for the synthesis of tin silicates from a clear solution;
b) Systematic study of the influence of the initial physicochemical conditions on the run product;
c) Optimization of the synthesis conditions;
d) Synthesis and characterization of new stannosilicates;
e) Probing isomorphous substitutions and ion exchange properties with various elements;
f) Study the thermal properties of the obtained materials.

The purpose of this thesis is to extend a previous work in the field of tin silicates. This work intends to establish the optimal physicochemical conditions for synthesis of stannosilicates and to create fields of crystallization where the intended structures can be easily fabricated.

The new synthesis method by clear precursor has unknown outcome in terms of microporous tin silicates formation. In order to understand the full potential of this method this work focus on the behavior of the sodium and potassium as framework stabilizers, their role in the solution and the limitation and advantages of each element in this new method. This work searches for chemical compositions that allow the formation of cheaper materials by the reduction of synthesis time and temperature. The final point of interest in the synthesis procedure is the study of the early physicochemical compositions of the solution and its role in the final product. Precursor pH has been already proven as an important factor on silicate production [29]. However there are many other unstudied factors that can induce structure

formation. This work studies the effects of solution temperature and agitation level and its importance in the production of stannosilicates.

New ion exchanges in tin silicates frameworks were also attempted. As seen before [19] the capture of an external ion can transfer the properties of that element to the silicates material. With that in mind it is possible to think in the doping of stannosilicates to improve its normal capacities. This work attempts the incorporation of antibacterial, magnetic and optical properties by the exchange of the normal alkaline elements present in stannosilicates for Zn^{2+}, Cu^{2+} and Cr^{3+}, respectively. Since the storing of the captured element is very good, a common ion exchange tested is the ability to capture potential radioactive elements. Like in most silicates this work studies the capacity of stannosilicates to capture hazardous but interesting elements like Cs^{+} and Sr^{2+}. These two exchanges serve as direct comparison between these molecular sieves and all other silicates, and a positive result could indicate the eminent application of stannosilicates in nuclear waste disposal.

In this respect there is another great application for these microporous materials, due to the ability of capturing loose ions in a solution this material can work in water purification. The capture of elements like Pb^{2+}, Fe^{2+}, Al^{3+} and some of the previously referred (like Cu^{2+}) can be used for water treatment or recycling of polluted liquids. The use of microporous materials in the recycling and energy harnessing of used fried oil is a common procedure [29], the search for these properties on stannosilicates can result in a new application for this recent material. to understand if the tin silicate frameworks can capture these and other ions this work searches for changes in the materials atomic distribution. These changes must be visible both at a structural level (detected by XRD) and at a chemical composition level (detected by EDS).

To improve and modify the properties of tin silicates isomorphous substitutions were also attempted. These incorporations of new octahedral elements can alter the pores sizes or drastically change the structure shape and properties. The goal was to find and analyze new mixed metal stannosilicates using Zr, Ti, Ge and Bi as substitution elements. Zirconium silicates have great thermal stability however the synthesis of theses microporous materials require higher temperatures or longer time comparing to tin silicates. The incorporation of Zr to tin silicate compositions can result in mixed stannosilicates with higher thermal stability and harder grains. It can also result in zirconosilicates with lower synthesis temperatures and with new transparent precursor synthesis method. Titanium has similar size to tin. When 6 coordinated titanium ion has radii of 0.605 Å [30] and tin one is 0.69 Å [31]. The size difference between the ions is

enough to provoke slightly change in the pore size when one of the ions is substituted by the other. The microporous framework of the mineral umbite can be produced with both ions as octahedral element. The incorporation of both ions in a umbite composition can easily form a mixed octahedral Ti-Sn-umbite material.

The isomorphous substitutions by germanium presents great promise since this element has the ability to form tetrahedra, octahedra and pentahedra; therefore it can substitute both tin and silicon in the framework, creating mixed stannosilicates, mixed germanosilicates or tin germinates. The incorporation of this element can perform several changes and severally distort the stannosilicate structures. The only downsize to its use is the cost of the source; germanium is a very expensive element so only a few tests were performed. The isomorphous substitution by bismuth is interesting due to its valence of $^{3+}$ which differ that of Sn and Si. Successful incorporation of bismuth can seriously affect the whole spectrum of properties. The problem of bismuth is its fast precipitation of its source ($BiCl_3$) in aqueous solutions which requires experiments with different sources.

Finally, thermal study of all the synthesized and modified structures was performed. These tests served to reveal the thermal stability and possible thermal transformations of the obtained phases.

All synthesized and structurally modified phases were characterized by powder X-ray diffraction (XRD).

VI Experimental

6.1 Synthesis

In order to evaluate the potential of this synthesis method the precursor preparation must be fully understood and all possible variables must be eliminated. To understand the effects of composition all syntheses were performed by the same preparation steps. The silica dissolution was performed at 90°C at 240 rpm of magnetic agitation. Silica was dissolved in the alkaline water solution which was always formed from an element in the hydroxide form. The solid alkaline was dissolved in distilled water by the same conditions 90°C and 240 rpm. Separately the tin chloride solution was prepared dissolving the $SnCl_2 \cdot 2H_2O$ in 50% of all the compositional water. The total water in the stannosilicates precursors was fixed at 500 moles and due to maximum capacity of the autoclave all compositions were calculated for 40 grams of water. The mixing of the tin chloride solution and alkaline solutions was performed at 154°C at agitation speed of 240 rpm. The final precursor was then agitated for 15 minutes.

All these steps can be seen in figure 4, schematically showing the solution making process. The precursor was then locked in a Teflon lined stainless steel autoclave and placed in oven for 2 days at 200°C for hydrothermal synthesis. The resulting products came in the form of powder and were washed and dried at room temperature.

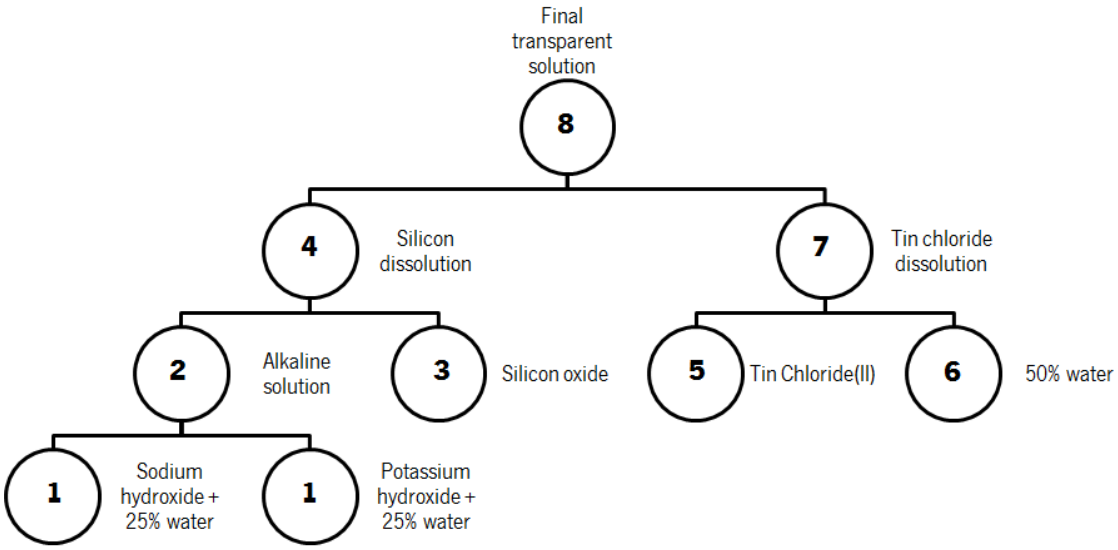

Figure 4. Precursor preparation method, stages 1 to 7 performed at 90°C with 240 rpm agitation and stage 8 performed at 145°C with 240 rpm during 15 minutes.

The sodium based tin silicates were prepared from transparent solutions with varying compositions. The general formula of these compositions was $yNa_2O\text{-}xSnO_2\text{-}5SiO_2 \cdot 500H_2O$,

where silica and water were invariable terms and tin oxide and sodium followed the values shown of figure 5. These 20 compositions were referred as trial C. To produce these precursors the general method, figure 4, was adapted to only one hydroxide that was mixed with 50% of all water. Despite the adjustment all samples were produced at the standard precursor and synthesis parameters.

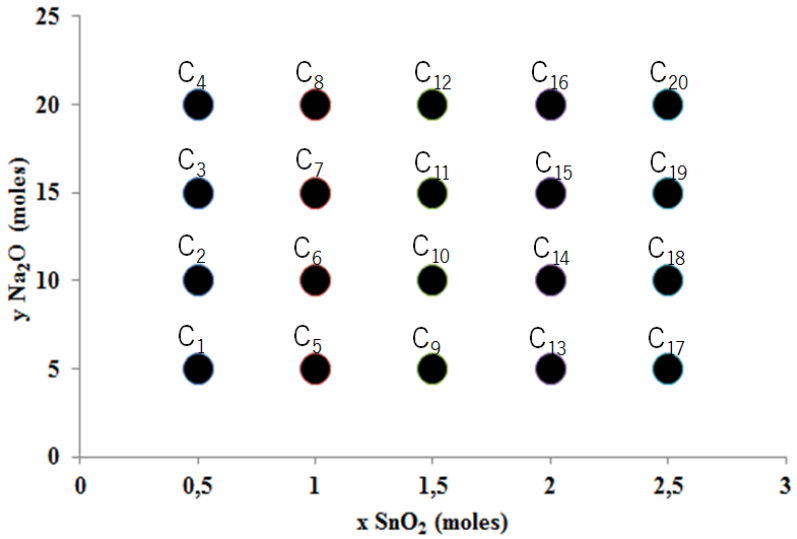

Figure 5. Composition field of the sodium-based stannosilicates (trial C), composition xNa_2O-$ySnO_2$-$5SiO_2$·$500H_2O$.

To study the effects of more balanced solutions, with closer ratios, more sodium based compositions were performed. These 6 compositions (trial E), seen in figure 6, were low concentration alkaline precursors and some of them had a ratio of tin/silicon different from the ones performed on trial C. This test completes the previous composition field and studies the influence of the alkaline material on stannosilicates formation. All compositions included the same synthesis procedure. The precursor preparation steps of figure 4 and a synthesis at 200°C for 2 days, equal to trial C.

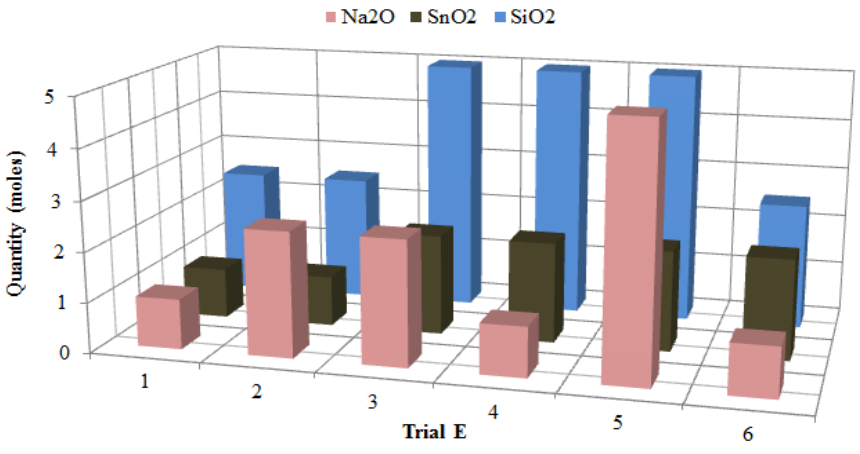

Figure 6. Compositions of trial E. Samples E1 to E6 produced with 500 moles of H_2O.

For the last synthesis with sodium based tin silicates the precursor agitation and synthesis time were changed. The used composition was $15Na_2O$-$5SiO_2$-$1.5SnO_2$·$500H_2O$ (trial C_{11}). The precursor agitation times were 0, 5, 15 and 30 minutes and these different agitation precursors were all heated for 2 and 7 days. The individual parameters of this test, trial T_C, can be seen in table 1. The 0 minutes precursor agitation time represents a manual agitation at room temperature until total dissolution and dispersion. All other variables, temperature, amount of liquid, recipient, magnetic agitator and position on the magnetic plate were kept constant. This ensured a single parameter study.

Table 1. Experimental parameters of trial T_C. Precursor agitation time in minutes and synthesis duration in days.

Trial	Agitation Time (min.)	Time of Synthesis (days)
$\mathbf{T_{C1}}$	0	2
$\mathbf{T_{C2}}$	5	2
$\mathbf{T_{C3}}$	15	2
$\mathbf{T_{C4}}$	30	2
$\mathbf{T_{C5}}$	0	7
$\mathbf{T_{C6}}$	5	7
$\mathbf{T_{C7}}$	15	7
$\mathbf{T_{C8}}$	30	7

In succession to these compositions the sodium and potassium based stannosilicates were studied. The general synthesis used composition was $10(xNa_2O$-$yK_2O)$-$5SiO_2$-$zSnO_2$·$500H_2O$ called trial D. This trial focused on the effects of both sodium and potassium as negative charged compensators on microporous tin silicates.

To perform these compositions the standard precursor preparation parameters of figure 4 were used. In this formula the silicon and water values remained constant and tin, sodium and potassium followed the values given by figure 7. Tin content changed from 0.5 to 2.5 moles (as in trial C) and the ratio between potassium and sodium from 2 to 8 with a total weight of 10 moles in all trials. The trial D was composed of 20 different compositions where sodium and potassium were always present. After precursor preparation the solutions were placed in autoclaves and heated at 200°C during 2 days.

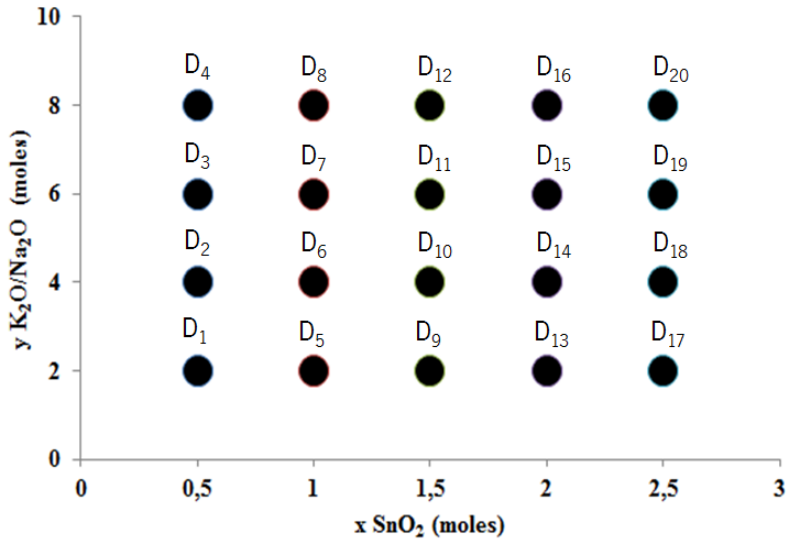

Figure 7. Composition field of potassium- and sodium- based tin silicates. Trial D with a composition of 10(xNa$_2$O-yK$_2$O)-5SiO$_2$-zSnO$_2$·500H$_2$O.

To complete the study on potassium and sodium based stannosilicates the precursor and synthesis parameters were changed. This allowed studying its influence in the resulting materials and structures. The chosen compositions were trial D_1 (3.33Na$_2$O-6.66K$_2$O-5SiO$_2$-0.5SnO$_2$·500H$_2$O) and D_7 (1.43Na$_2$O-8.57K$_2$O-5SiO$_2$-0.5SnO$_2$·500H$_2$O). The variable parameters changed were final the precursor final agitation time and the synthesis duration.

The two compositions were prepared at precursor agitation times of 0, 5, 15 and 30 minutes resulting in 8 different solutions which were heated for a certain time. The D_1 composition solutions were synthesized for 2 days and the D_7 composition solutions for 7 days. This test was called trial T_D and all its individual parameters can be seen in table 2.

Table 2 Experimental parameters of trial T_D. Precursor agitation time in minutes and synthesis duration in days.

Trial	Composition (trial)	Agitation Time (min.)	Time of Synthesis (days)
T_{D1}	D_1	0	2
T_{D2}	D_1	5	2
T_{D3}	D_1	15	2
T_{D4}	D_1	30	2
T_{D5}	D_7	0	7
T_{D6}	D_7	5	7
T_{D7}	D_7	15	7
T_{D8}	D_7	30	7

The next syntheses included potassium based stannosilicates. The explored compositions had the general formula of yK$_2$O-2.5SiO$_2$-xSnO$_2$·500H$_2$O and yK$_2$O-5SiO$_2$-

$xSnO_2 \cdot 500H_2O$. Silicon and water were fixed in each composition and the values of potassium and tin followed the numbers given by figure 8. Potassium had a minimum value of 5 and a maximum of 15 and tin a minimum of 0.5 and a maximum of 1.5 moles. This resulted in 18 different compositions, designated as trial P. It was used the standard synthesis procedure shown in figure 4. Since there was only one hydroxide source, the potassium hydroxide was dissolved in 50% of all compositional water.

All 18 compositions were synthetized at 200°C for 2 days. This test included a change in silicon quantity to test further ratios between the three elements.

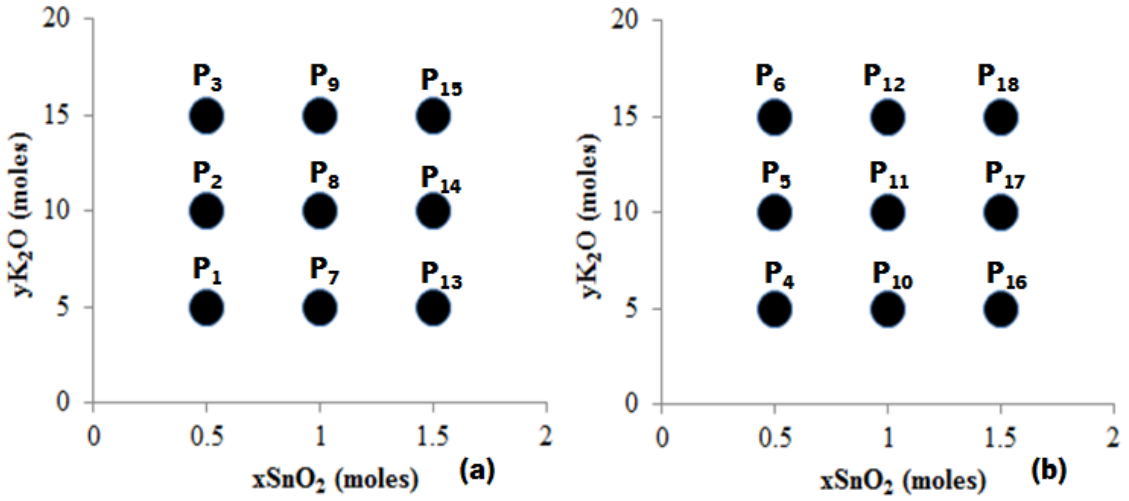

Figure 8. Composition field of trial P. (a) 2.5 moles of SiO_2 (b) 5 moles of SiO_2. All compositions were performed with 500 moles of H_2O.

Synthesis with potassium based tin silicates with different precursor parameters were also carried out. The chosen compositions were $5K_2O\text{-}5SiO_2\text{-}0.5SnO_2 \cdot 500H_2O$ (trial P_4) and $5K_2O\text{-}5SiO_2\text{-}1SnO_2 \cdot 500H_2O$ (trial P_{10}). The changed parameters were once again the final precursor agitation and the synthesis time. Both compositions were performed with 0, 5, 15 and 30 minutes of precursor agitation time and synthesized for different times. P_4 composition solutions were synthesized for 2 days and P_{10} composition solutions for 4 days. The synthesis of all 8 solutions, trial T_P, was performed in autoclaves at 200°C. The individual preparation and synthesis parameters can be seen in table 3.

Table 3. Experimental parameters of trial T_P. Precursor agitation time in minutes and synthesis duration in days.

Trial	Composition (trial)	Agitation Time (min.)	Time of Synthesis (days)
$\mathbf{T_{P1}}$	P_4	0	2
$\mathbf{T_{P2}}$	P_4	5	2
$\mathbf{T_{P3}}$	P_4	15	2
$\mathbf{T_{P4}}$	P_4	30	2
$\mathbf{T_{P5}}$	P_{10}	0	4
$\mathbf{T_{P6}}$	P_{10}	5	4
$\mathbf{T_{P7}}$	P_{10}	15	4
$\mathbf{T_{P8}}$	P_{10}	30	4

To explore the possibility for faster synthesis procedures variable time for agitation for P_{10} composition was tested (figure 8). These time controlled precursors with 10, 15, 20 and 30 minutes of agitation were produced and synthesized at different times, 1 and 2 days at 200°C. The 5 different tests were called trial T_L and its individual preparation parameters can be seen in table 4.

Table 4. Experimental parameters of trial T_L. Precursor agitation time in minutes and synthesis duration in days.

Trial	Agitation Time (min.)	Time of Synthesis (days)
$\mathbf{T_{L1}}$	10	1
$\mathbf{T_{L2}}$	15	1
$\mathbf{T_{L3}}$	20	1
$\mathbf{T_{L4}}$	15	2
$\mathbf{T_{L5}}$	30	2

All syntheses were performed using $SnCl_2{\cdot}2H_2O$ (Sigma – ALDRICH Pu>98%) NaOH (Sigma – ALDRICH), KOH (Sigma – ALDRICH) and SiO_2 (Cab-osil®M-5) has sources of the required elements. To calculate the weights of reagents needed to create each composition it was used the following equation:

$$P_R = \frac{Q_C x\ T_S x M_R}{M_{H2O} x Q_{H2O}}\ (g)$$

Where the Qc was the quantity of the wanted element (in moles), Ts the total weight of the solution (established by the maximum capacity of the autoclave 40 grams), M_R is the atomic weight of the source or reagent, M_{H2O} is the atomic weight of water and Q_{H2O} is the quantity of water in the composition (in moles). By calculating this it is obtained P_R that is the amount of

source needed to execute each composition. For future consult all calculated compositions can be seen in APENDIX 1.

As mentioned before, the autoclave is a Teflon lined stainless steel closed recipient used to accommodate liquid (in this case the stannosilicates solutions) and to prevent gas or liquid escape during the synthesis process.

In this work the volume of solution in autoclave was always controlled and filled near 70% of the total volume which assured auto-generated pressure that do not exceed the autoclave stability. This allowed obtaining the maximum yield of the run product for each precursor. The used autoclave and assembly method can be seen in figure 9.

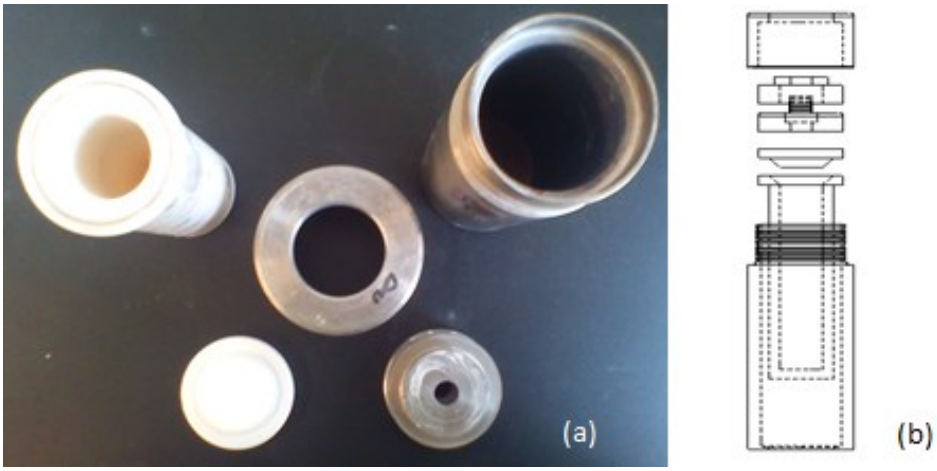

Figure 9. Autoclave used for stannosilicate hydrothermal synthesis; (a) autoclave components (photo) (b) assembly.

6.2 Ion Exchange

The framework of microporous materials is the rigid part of crystal structure that accommodates water molecules and charge compensating cations. These positive charged ions have high mobility and can be replaced by similar ions if the size and coordination allow it [32]. Cation charge can also influence the success of exchange. According to recent studies, if two similar cations have different charge the higher charged cation has higher affinity to the microporous structure [33]. Like any other diffusion process, ion exchange also is improved by the increase of time and temperature. The increase in temperature allows the pores to expand and its occupant and outside cations to vibrate more intensely. This increases the penetration of the external ions and the possibilities of exchange. The time of exchange increases the amount of collisions between cations increasing therefore number of exchanges even in low success rate environments. Time and temperature increase have associated problems. Time of exposure in liquid solutions increases the effects of material dissolution due to aggressive pH. Temperature increase can cause thermal degradation. For all that it is indispensable to fully understand the porous structure and its initial occupancy to be able to manipulate and modify its pore contents by ion exchange.

Because of the required about its structures and the necessity of a continuous perfect production the only to stannosilicates ready for ion exchange were AV-6 and AV-7. These two frameworks have pores occupied by potassium, on AV-6, and by sodium and potassium, on AV-7, and the goal was to fully or partly exchange it for equal and different charge cations. For that the microporous material was placed in liquid solutions containing the exchange cations. These solutions had concentrations with the standard value of 1 Mole. However, due to the low solubility of some cations sources this value was sometimes changed. The amount of stannosilicate used in each exchange was fixed at 0.1 grams. The individual parameters of all the exchanges performed are listed in table 5, where the temperature, time, solution concentration and source of cation can be seen.

*Table 5. Ion exchanges performed on AV-6 and AV-7. Time, temperature solution concentration and type of source. * Sigma ALDRICH ** FLUKA.*

		$CuCl_2$* (1 M)				$ZnCl_2$** (1 M)				$CrN_3O_9 \cdot 9H_2O$* (1 M)			
Phase	**Time →**	**18 h**	**24 h**	**48 h**	**72 h**	**18 h**	**24 h**	**48 h**	**72 h**	**18 h**	**24 h**	**48 h**	**72 h**
AV-6	50°C												
	80°C		X	X	X			X				X	
Av-7	50°C												
	80°C		X	X				X			X	X	X

		$SrCl_2$* (1 M)				$PbCl_2$* (0.01 M)				$AlCl_3$** (1 M)			
Phase	**Time →**	**18 h**	**24 h**	**48 h**	**72 h**	**18 h**	**24 h**	**48 h**	**72 h**	**18 h**	**24 h**	**48 h**	**72 h**
AV-6	50°C					X				X			
	80°C			X									
Av-7	50°C					X				X			
	80°C			X			X				X		

		CsCl* (0.5 M)				$FeCl_3$* (1 M)				NaCl* (1 M)			
Phase	**Time →**	**72 h**	**24 h**	**48 h**	**72 h**	**18 h**	**24 h**	**48 h**	**72 h**	**18 h**	**24 h**	**48 h**	**72 h**
AV-6	50°C												
	80°C			X				X				X	
Av-7	50°C												
	80°C			X				X				X	

For long ion exchange times (over 24 hours) evaporation may change the cations concentration. Therefore more solution was added in 24 hours periods to balance and control cation quantities. To improve the changes of exchange and to increase the materials ability to form suspensions, all stannosilicate samples were milled into a very fine powder. The ion exchanges were performed in glass bowls with adapted cover to reduce evaporation. The recipients were placed in a BINDER oven with digital temperature control with a maximum deviation of 1°C. After exchange all products were washed, filtered and dried at room temperature.

The success of ion exchange was evaluated by XRD where the changes in the crystalline material were detected. The confirmation of the cation capture came from EDS.

6.3 Isomorphous substitution

The doping and partial substitution of structural elements is a common procedure in ceramic materials. This doping needs to be in very small amounts in order to preserve the structure of the original material. In silicates there is another process of doping that does not suffer from that problem. Silicates frameworks can fully substitute the octahedral or tetrahedral element without significant structural changes. This is proven by the amounts of mineral analogues produced in laboratory. The substitution is theoretically possible to all elements that possess the same oxide formations [34]. In stannosilicates the substitution can occur in the octahedral tin and in the tetrahedral silicon atom, each of the elements can be replaced by other metals with the same coordination and similar size. On the contrary to ion exchange the isomorphous substitution is realized during the process of crystallization. When an isomorphous substitution is tried the goal is to use a precursor composition of a determinate structure and infuse it with different elements. This changes the materials properties and pores dimensions without changing the crystal system or the framework type. However, each element has its own chemical and physical behavior and its introduction to the precursor, even in small amounts, can create new reactions that lead to new types of frameworks. The more similar the elements are, chemically, in size, coordination and valance the higher are chances of creating a single phase mixed material.

To perform the isomorphous substitution, this work used the precursor preparation parameters referred in figure 4 with a single modification. The incorporation of tin chloride was done in parallel with the incorporation of the substitution element. The compositions had a gradual increase in the amount of tin substitute. The synthesis parameters were equal to the ones used in the synthesis chapter, 200°C for 2 days. This also served to compare the influence of a new element in the synthesis success and quality. Maintaining the synthesis parameters equal allowed a direct comparison and a better prediction of the resulting structures. The structures obtained during the synthesis trials were again synthesized with substitution elements. The compositions used here were the ones perfected in the synthesis trials. The isomorphous substitutions performed can be seen in table 6 where it is shown the element of substitution, its percentage in relation with tin, the modified composition, its original trial and the precursor preparation and synthesis parameters. The first substitutions were performed with zirconium and titanium. The percentage substituted was 20% and 40% of Zr and 20%, 40% and 60% of Ti. The 60% isomorphous substitutions dictated that more titanium than tin was available for framework construction.

Table 6. Compositions and preparation parameters for the isomorphous substitutions by Zr and Ti.

Trial	Element	Percentage changed (%)	Original Trial	Composition	Time and temperature of agitation (min.-°C)	Time and temperature of synthesis (days.-°C)
I_{S1}	Zr	20	D_1	$6.6K_2O$-$3.3Na_2O$-$5SiO_2$-$0.1ZrO_2$-$0.4SnO_2$·$500H_2O$	15min-145°C	2- 200°C
I_{S2}			P_1	$5K_2O$-$2.5SiO_2$-$0.1ZrO_2$-$0.4SnO_2$·$500H_2O$	15min-145°C	2- 200°C
I_{S3}			C_9	$10Na_2O$-$5SiO_2$-$0.3ZrO_2$-$1.2SnO_2$-$500H_2O$	15min-145°C	2- 200°C
I_{S4}			C_{20}	$20Na_2O$-$5SiO_2$-$0.5ZrO_2$-$2SnO_2$-$500H_2O$	15min-145°C	2- 200°C
I_{S5}		40	D_1	$6.6K_2O$-$3.3Na_2O$-$5SiO_2$-$0.2ZrO_2$-$0.3SnO_2$·$500H_2O$	15min-145°C	2- 200°C
I_{S6}			P_1	$5K_2O$-$2.5SiO_2$-$0.2ZrO_2$-$0.3SnO_2$·$500H_2O$	15min-145°C	2- 200°C
I_{S7}			C_9	$10Na_2O$-$5SiO_2$-$0.6ZrO_2$-$0.9SnO_2$-$500H_2O$	15min-145°C	2- 200°C
I_{S8}			C_{20}	$20Na_2O$-$5SiO_2$-$1ZrO_2$-$1.5SnO_2$-$500H_2O$	15min-145°C	2- 200°C
I_{S9}	Ti	20	D_1	$6.6K_2O$-$3.3Na_2O$-$5SiO_2$-$0.1TiO_2$-$0.4SnO_2$·$500H_2O$	15min-145°C	2- 200°C
I_{S10}			P_1	$5K_2O$-$2.5SiO_2$-$0.1TiO_2$-$0.4SnO_2$·$500H_2O$	15min-145°C	2- 200°C
I_{S11}			C_9	$10Na_2O$-$5SiO_2$-$0.3TiO_2$-$1.2SnO_2$-$500H_2O$	15min-145°C	2- 200°C
I_{S12}			C_{20}	$20Na_2O$-$5SiO_2$-$0.5TiO_2$-$2SnO_2$-$500H_2O$	15min-145°C	2- 200°C
I_{S13}		40	D_1	$6.6K_2O$-$3.3Na_2O$-$5SiO_2$-$0.2TiO_2$-$0.3SnO_2$·$500H_2O$	15min-145°C	2- 200°C
I_{S14}			P_1	$5K_2O$-$2.5SiO_2$-$0.2TiO_2$-$0.3SnO_2$·$500H_2O$	15min-145°C	2- 200°C
I_{S15}			C_9	$10Na_2O$-$5SiO_2$-$0.6TiO_2$-$0.9SnO_2$-$500H_2O$	15min-145°C	2- 200°C
I_{S16}			C_{20}	$20Na_2O$-$5SiO_2$-$1TiO_2$-$1.5SnO_2$-$500H_2O$	15min-145°C	2- 200°C
I_{S17}		60	D_1	$6.6K_2O$-$3.3Na_2O$-$5SiO_2$-$0.3TiO_2$-$0.2SnO_2$·$500H_2O$	15min-145°C	2- 200°C
I_{S18}			P_1	$5K_2O$-$2.5SiO_2$-$0.3TiO_2$-$0.2SnO_2$·$500H_2O$	15min-145°C	2- 200°C
I_{S19}			C_9	$10Na_2O$-$5SiO_2$-$0.9TiO_2$-$0.6SnO_2$-$500H_2O$	15min-145°C	2- 200°C
I_{S20}			C_{20}	$20Na_2O$-$5SiO_2$-$1.5TiO_2$-$1SnO_2$-$500H_2O$	15min-145°C	2- 200°C

Zirconium was provided in the form of $ZrCl_4$ (Sigma-ALDRICH) and titanium in the form of $TiCl_3$ (Sigma-ALDRICH, 10% concentration). $ZrCl_4$ and $TiCl_3$ were dissolved in water and mixed with $SnCl_2$ The first was at its solid state and was dissolved in water and combined with tin.. The necessary reagents quantities were calculated by the use of the previous formula and are listed in APENDIX 1 for future consult. The synthesis products were washed, filtered and dried at room temperature.

After these first zirconium and titanium substitutions, three more were performed where the precursor agitation and the synthesis time was increased. This was done to ensure the production of the more stable structures and to increase the crystallinity of the produced materials. The chosen compositions were the ones of trials IS_7, IS_{17} and IS_{20}. These compositions allowed the test of the different substitution elements and the effect of sodium and potassium. The composition and synthesis parameters of these trials can be seen in table 7. The

solutions were agitated for 30 minutes and synthesis occurred at 200°C for 5 days. These attempts on isomorphous substitutions were called trial I_{SS}.

Table 7. Composition and synthesis parameters for the isomorphous substitution by Zr and Ti at extended synthesis times.

Trial	Element	Percentage changed (%)	Original Trial	Composition	Time and temperature of agitation (min.-°C)	Time and temperature of synthesis (days.-°C)
I_{SS1}	Zr	20	C_9	$10Na_2O$-$5SiO_2$-$0.6ZrO_2$-$0.9SnO_2$-$500H_2O$	30min-145°C	5- 200°C
I_{SS2}	Ti		D_1	$6.6K_2O$-$3.3Na_2O$-$5SiO_2$-$0.3TiO_2$-$0.2SnO_2$·$500H_2O$	30min-145°C	5- 200°C
I_{SS3}	Ti	40	C_{20}	$20Na_2O$-$5SiO_2$-$1.5TiO_2$-$1SnO_2$-$500H_2O$	30min-145°C	5- 200°C

The final isomorphous substitution attempted the incorporation of germanium and bismuth at 2 different compositions. Each element was inserted at sodium and potassium based compositions in order to study these different behavior stannosilicate building units. The four resulting compositions had the same amount of alkaline materials but the sodium based compositions were synthesized for more 2 days than the potassium based compositions. Table 8 shows the trials compositions, precursor and synthesis parameters. These two isomorphic substitutions were only performed to a small trial group due to reagents price.

Table 8. Compositions and synthesis parameters of the isomorphous substitutions by Ge and Bi.

Trial	Element	Percentage changed (%)	Original Trial	Composition	Time and temperature of agitation (min.-°C)	Time and temperature of synthesis (days.-°C)
GeD_2	Ge	20	C_9	$10K_2O$-$5SiO_2$-$0.3GeO_2$-$1.2SnO_2$-$500H_2O$	30min-145°C	2- 200°C
GeD_4	Ge			$10Na_2O$-$5SiO_2$-$0.3GeO_2$-$1.2SnO_2$-$500H_2O$	30min-145°C	4- 200°C
BiD_2	Bi		P_{17}	$10K_2O$-$5SiO_2$-$0.3Bi_2O_3$-$1.2SnO_2$-$500H_2O$	30min-145°C	2- 200°C
BiD_4	Bi			$10Na_2O$-$5SiO_2$-$0.3Bi_2O_3$-$1.2SnO_2$-$500H_2O$	30min-145°C	4- 200°C

The source of germanium was its oxide form, GeO_2 (ALDRICH), and was dissolved in the alkaline water solution formed by water, sodium/potassium and silicon. The source of bismuth was its chloride form, $BiCl_3$ (ALDRICH), and it was dissolved the same way as germanium oxide. The success of isomorphous substitution was also evaluated by XRD and confirmed by EDS.

6.4 Thermal properties

Each framework has its unique quantities of water in pores, therefore, each material has its unique dehydration. This dehydration is most of the times a reversible process. However, there are some cases of deformed frameworks where the loss of water cannot be recovered. In

these cases the structure either collapses turning into a non-silicate material or it gains different pore formation and adapted dimensions. With each modification the frameworks become more sensitive to the thermal effects. The modifications that induce defects to the porous framework lower its thermal stability. The modifications that introduce new elements infuse the framework with the thermal properties of that new occupant. To test the thermal stability of the modified structures it is necessary to known its original synthesized phase. Comparing the two performances it is possible to understand the results of the modification in terms of thermal properties.

The first synthesized and modified materials were exposed to 750°C in an oxidation oven for 4 hours. The oven increased in a linear form and reached 750°C in 1 hour followed by a 3 hours stage at this maximum temperature. Cooling was performed inside oven minimizing the thermic shock. The resulting powders were recovered and analyzed by XRD. In table 7 it can be seen the type of materials exposed to this test, its form of production and initial structure. This group of materials exposed to this temperature was called trial S.

Table 9. Information on the stannosilicates exposed to 750°C for 4 hours.

Trial	Material used	Structure	Obtained by	Temperature and time (hours - °C)
S_1	D_1	AV-7	Synthesis	4 hours -750°C
S_2	Cu-AV-6	Monoclinic Umbite	Ion Exchange	4 hours -750°C
S_3	D_7	AV-6	Synthesis	4 hours -750°C
S_4	Cu-AV-7	Modified AV-7	Ion Exchange	4 hours -750°C
S_5	Cr-AV-7	Modified AV-7	Ion Exchange	4 hours -750°C
S_6	Na-AV-7	Unmodified AV-7	Ion Exchange	4 hours -750°C
S_7	C_{13}	AV-10	Synthesis	4 hours -750°C
S_8	C_{20}	Unknown	Synthesis	4 hours -750°C
S_9	E_6	Amorphous	Synthesis	4 hours -750°C
S_{10}	Zn-AV-7	Modified AV-7	Ion Exchange	4 hours -750°C

After these first trials, the AV-6 and Cu-AV-6 were subjected to even more thermal studies. Both samples were subjected to thermal exposure with in situ XRD analysis for high temperature transformations and dehydration behavior analysis. The samples were exposed to increasing temperatures and XRD was performed at 100°C intervals. After each high temperature XRD the sample was cooled down and analyzed by XRD at room temperature. This procedure was performed for 100, 200, 300, 400, 500, 600 and 700°C. All these studies were performed at ambient atmosphere.

In situ high temperatures measurements were performed in a chamber Anton Paar HTK 1200 N, which assures highly reliable temperature measurements right at the sample and excellent uniformity within the sample. The heating and cooling step in all cases was 30°C per minute.

Concluded the initial tests more modified forms were exposed to even higher temperatures. In this second trial, Trial F, ten samples were exposed to 800°C for 4 hours in an oxidation oven. Temperature increased 13°C per minute and the maximum 800°C stage lasted for 3 hours. The powders were directly exposed to heat placed in a ceramic tile. The amount of powder exposed depended on the sample but all samples had more than 0.2 grams of material. Cooling was performed on oven environment providing uniform drop of temperature and low thermic shock. Table 10 shows all samples exposed in this trial, it also shows tis original material source, the type of structure it possesses and the form of production. In the same table it is also possible to see the thermal exposure parameters.

Table 10. Information on the materials exposed to 800°C for 4 hours.

Trial	Material used	Structure	Obtained by	Temperature and time (hours - °C)
F_1	BiD_4	Sodium phase (Bi)	Isomorphous Substitution	4 hours -800°C
F_2	GeD_4	Sodium phase (Ge)	Isomorphous Substitution	4 hours -800°C
F_3	I_{SS1}	Zirconium tin phase	Isomorphous Substitution	4 hours -800°C
F_4	P_{17}	Lamellar phase	Synthesis	4 hours -800°C
F_5	IS_3	Sodium phase (Zr)	Isomorphous Substitution	4 hours -800°C
F_6	D_{11}	AV-7	Synthesis	4 hours -800°C
F_7	GeD_2	AV-7 (Ge)	Isomorphous Substitution	4 hours -800°C
F_8	Zn-AV-7(24h)	AV-7 zinc form	Ion exchange	4 hours -800°C
F_9	Zn-AV-7(72h)	AV-7 zinc form	Ion exchange	4 hours -800°C
F_{10}	Cu-AV-7(72h)	AV-7 copper form	Ion Exchange	4 hours -800°C

As mentioned before, the high temperature transformation of AV-6 and AV-7 was reported in ranges between 800°C and 1000°C. In order to induce full transformation of these materials this work performed a last thermal study to 1000°C for 5 hours. In this test the heating speed was 17°C per minute and the time of exposure to the maximum temperature of 1000°C was 4 hours. The cooling occurred in oven providing uniform temperature drop and low thermic shock preserving materials integrity. The samples exposed can be seen at table 11 where the structure, source of production and thermal exposure parameters are also shown. The last test reaches the limits of these stannosilicates searching for high temperature irreversible transformations and fusion points.

Table 11. Information on the materials exposed to 1000°C for 5 hours.

Trial	Material used	Structure	Obtained by	Temperature and time (hours - °C)
H_1	E_4	Amorphous material	Synthesis	5 hours -1000°C
H_2	D_7	AV-6	Synthesis	5 hours -1000°C
H_3	P_{10}	Lamellar phase	Synthesis	5 hours -1000°C
H_4	D_{12}	AV-7	Synthesis	5 hours -1000°C
H_5	I_{SS1}	Sodium phase (Zr)	Isomorphous Substitution	5 hours -1000°C
H_6	IS_{11}	Amorphous material	Isomorphous Substitution	5 hours -1000°C
H_7	IS_{11}	Solid block	Isomorphous Substitution	5 hours -1000°C
H_8	GeD_2	Ge-AV-7	Isomorphous Substitution	5 hours -1000°C

The thermal studies were performed from room temperatures until the maximum temperature of 1000°C searching for thermal modifications. These modifications could be dehydration phenomenon, high temperature transformation and thermal limits of these stannosilicates. The resulting samples were analyzed by XRD.

6.5 Structural characterization

Crystalline structures characterization was performed by X-ray diffraction (XRD). As the name says, this technic uses X-rays to interact with mater and determinate its atomic position. X-rays are a form of electromagnetic radiation with a wavelength from 0.01 to 10 nm. This type of radiation can be produced from several methods but for this technique it is produced by electron excitation and recovery. When an atom receives enough energy to excite its intern electrons, the electron leaps into a high energy state. The recovery from that state releases a burst of electromagnetic radiation normally in the form of X-rays. The power of the X-ray released depends on the element that is exited. In this XRD instrument the source is made from copper that releases X-rays with a wavelength of 1.5406 Å. These X-rays are produced, send to the sample and then collected after interaction. Only the sending and collecting of innumerous X-rays in different angles can fully characterize a crystalline structure.

In crystalline materials, atoms form small repetitive cells, called unit cells, which are spread in all the material. Unit cells can be described by 6 fundamental dimensional parameters a, b, c, α, β and γ. The a, b and c parameters are the physical dimensions of the unit cell (height, width and depth). The α, β and γ parameters are the angles between

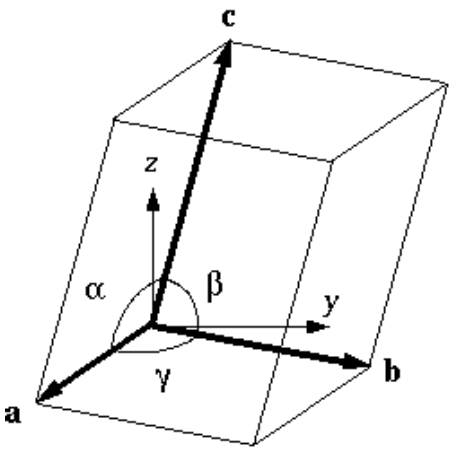

Figure 10. Unit cell representation [35]

them. All these parameters can be seen in figure 10. Within the unit cell, atoms can appear in all type of positions and form several types of planes. To those positions and planes, Miller as given coordinates that allow the tracking of the atoms and the determination of the higher occupied planes. The characterization of the atoms inside the unit cell is enough to identify and identify the materials structure. In crystallography, materials are described by three categories: the type of unit cell, the type of atoms within it (obtained indirectly using physical connections bond distances) and the positions they occupy.

When a series of atoms are hit with X-rays its electrons start to oscillate in the same frequency as the incoming X-ray. That vibration causes interference with the X-ray and in almost all the directions that interaction causes destructive interference. In crystalline materials, that have a regular distribution of atoms, the interaction between X-ray and atoms produce constructive interference. This produces diffracted X-rays that leave the atoms in a specific direction. In this XRD, theta to theta goniometer, the X-ray gun and the detector move simultaneously while the sample remains stationary, creating 2Theta angles between the incident X-ray and the diffracted one, from 0 to 180°. Each time there is a constructive interaction with the atom and the resulting diffracted X-ray hits the detector a count is made. The device counts the number of interactions made at each 2Theta angle, figure 11. The gathering of all angle counts gives the crystal atomic disposition in form of a pattern.

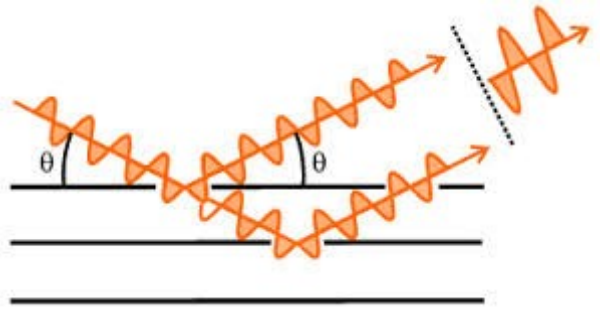

Figure 11. Schematic of X-rays interactions with atomic arrangements.

Using Braggs law, $\lambda=2d\sin\theta$, where λ is the wavelength of the X-ray and θ the diffraction angle (2Theta/2), it is possible to calculate the d-spacing between atoms (atomic planes). That distance (d-spacing) is specific of each pair of atoms and structure, serving as a form of characterization and identification of crystalline materials. This technic can be used in single crystal materials, where the quality of the acquired data is much higher, but also in polycrystalline materials. In multi crystal materials the quality of the data depends on the quality and quantity of the crystals. If all crystals present very similar plane distribution and low number of defects the data will be clear. If the crystals have defects or large amorphous areas the data has variations that could invalidate the identification. To analyze materials in the form of powder the best way is to reduce its grain size and distribute it evenly on the sample older. This increases crystal distribution and helps in the retrieve of more accurate data. As the XRD is

performed, the gathering of counts from each 2Theta angle creates a powder pattern that records the number of X-rays diffracted in that specific angle.

As XRD is performed, the angle variation step determinates the accuracy and precision of the reading. The time per step determinates the amount of X-rays sent at each angle. The angle range limits the minimum and maximum d-spacing's considered. The majority of the crystalline silicates have its primal unit described in the first 50° 2theta. However, when it is necessary to identify the smaller atoms and the full details of the crystalline structure, higher 2theta angles should also be analyzed. The powder pattern is presented in a succession of peaks that are wider or slimmer depending on the crystals size. Small crystals present low number of interactions that lead to a large dispersion of the peak in the 2theta angles. This phenomenon is important since it allows the calculation of the crystal size using Scherrer equation:

$$\beta(2\theta) = \frac{K\lambda}{T cos\ \theta}$$

Where β is the crystallite size contribution to the peak width (integral or full width at half maximum) in radians, K is a constant near unity, T is the average thickness of the crystal in a direction normal to the diffraction plane (h, k, l), λ is the X-ray wavelength and θ is the Bragg angle [36].

This enlargement of the diffraction peak can also be produced by acquisition factors. The step of acquisition and the time per step are responsible for the separation of very close diffraction planes. When these parameters are not carefully defined a multi-diffraction peak may appear. This peak as very wide base, not due to the crystal size but, due to the fact that more than one diffraction plane are described in a single peak. This phenomenon, seen on figure 12, can induce error on crystal size calculation and structure identification. The way to eliminate this multi-diffraction is by decreasing the step of acquisition, refining the quality of the data, and increasing the time per step, sending more X-rays at each angle creating higher and better defined peaks [37].

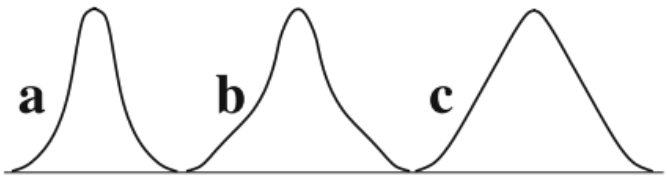

Figure 12. Variation of a primary beam profile caused by multiple scattering. (a) Unaffected diffraction peak. (b) Moderate multiple diffraction. (c) Strong multiple diffraction [37].

XRD analysis has some limitations due to its source of X-rays (usually copper). This technic does not detect light weight atoms like hydrogen. This causes difficulties in the detection of water in porous structures, in the identification of hydroxide groups or even the identification of complete structures due to the nature of the forming elements.

In this work the samples were analyzed using a Bruker D8 Discover diffractometer, figure 13, with copper Kα radiation (λ=1.5406). The standard data collection parameters were a step of 0.04 to 0.06°, a time per step of 1 second and a range going from 6 to 40° 2theta. For full structural refinement and determination, better powder patterns were acquired using a step of 0.04°, a time per step of 20 seconds and a range of 9-90°C 2theta. In in-situ temperature tests the powder XRD patterns were collected in h/2h scan regime for 2h range 9-40°, step of 0.04° and time per step of 1 second.

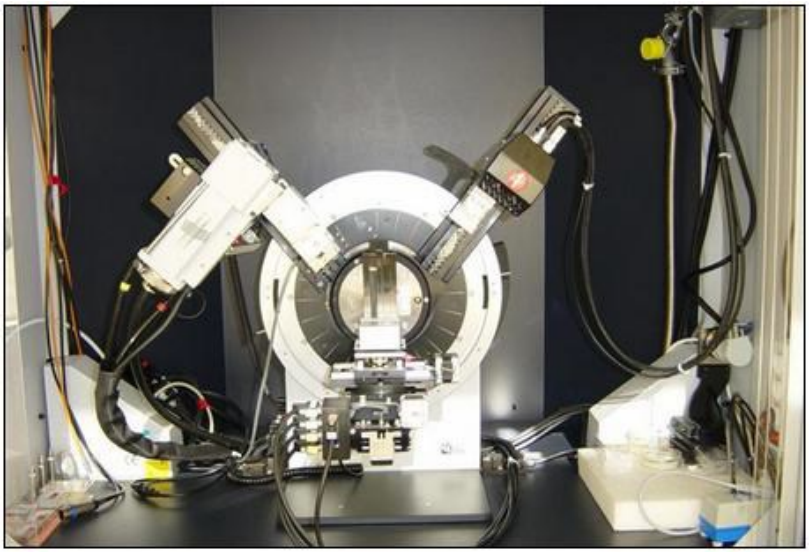

Figure 13. X-ray diffractometer (Bruker D8 Discover) [38].

6.6 Morphology and chemical composition determination

To fully characterize the stannosilicates here produced it is necessary to evaluate other aspects not seen on XRD. Some are visual aspects like morphology, grain size, shape and crystal type. Others are chemical aspects like chemical composition and ratio between elements of the material. Scanning Electron Microscopy (SEM) was used for morphology studies and Energy-Dispersive X-ray Spectroscopy (EDS) was used for chemical composition determination. These analysis technics are performed in simultaneous in the same instrument.

SEM is a technic great for surface studies, to obtain powder shape and crystal growing orientation. To scan the surface electrons are released from the electron beam, accelerated and then pointed to the sample by magnetic lens and anodes. By hitting the surface of the sample

and interacting with the electronic cloud, these electrons are reflected with an angle that depends directly on the surface topography. The reflected electrons are then captured by the detector that analyses and processes the final image of the surface. The electrons course can be seen in figure 13 that represents the electron production, its focus and its retrieval for SEM image processing.

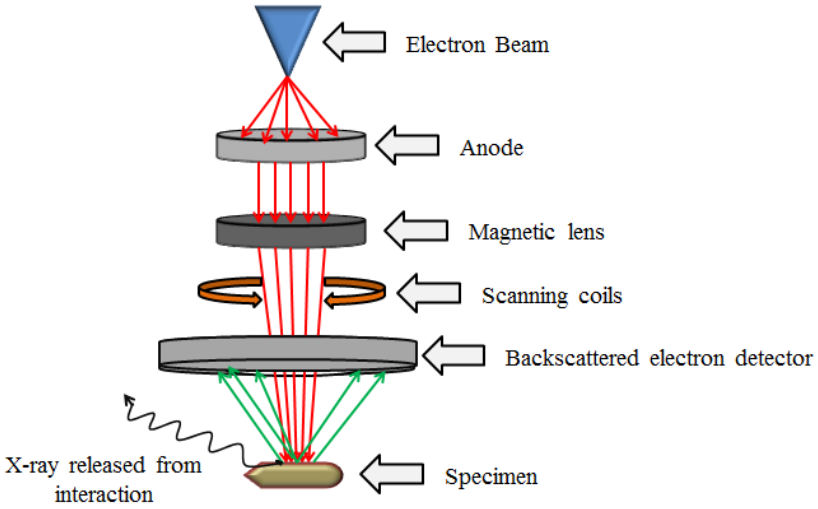

Figure 14. Schematics of SEM set-up.

When electrons interact with the sample surface they can produce several effects. The first is the essential to SEM, the backscattered electrons. The second is the forming of secondary electrons, formed by the interaction with the sample atoms nucleus. These electrons bounce back with specific energies that depend on the type of atom it bounces on. This allows the creation of images with contrast areas of different composition. The third, and last, effect is the excitation and relaxation of the samples electrons. When the electron of the beam interacts with the electron from the sample, this last one jumps to an exited position. The posterior relaxation releases a burst of energy in the form of X-ray. As said before, each element releases a characteristic wavelength of X-rays. By analyzing this wavelength and counting the number of incoming X-rays with the same energy it is possible to calculate a semi-quantitate composition of the sample. This quantification is given in percentages and allows determining element weight relations in the sample.

The technic based on this last effect is EDS, Energy-Dispersive X-ray Spectroscopy. EDS is a high energy analysis technic since it requires electron excitation. Depending on the elements present in the sample the beam electrons must have adequate energy to excite the sample valence electrons. Each element has its specific energies needed to excite its electrons and some of them are very high. Due to its energy, the beam electrons do not interact with the surface

atoms but with the more deep ones located several atomic layers within the sample, figure 15. The majorly of the out coming X-rays comes from the samples bulk making EDS, contrarily to SEM, not fitted for surface analysis.

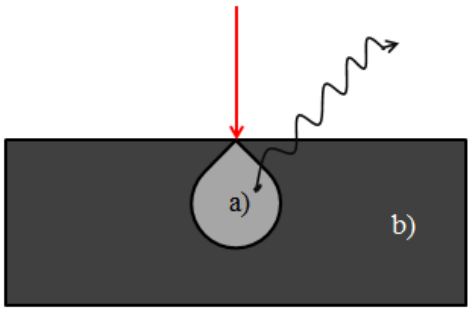

Figure 15. Interaction of electrons and production of X-rays; (a) area of analysis (b) sample.

To other areas this may be a problem but for the study of microporous silicates (in the form of powder) this fact is very helpful. Due to the nature of the synthesis and modification technics these materials usually have contaminations at the powder surface (usually salts forms). By majorly retrieving data from the samples core, EDS decreases the effects of these contaminations being therefore the perfect technic to analyze this kind of materials.

Just like XRD this technic as problems detecting low weight elements. To obtain good quality SEM images the material must be conductive, if not the sample must be coated with a conductive film. The film must be produced of an element not present in the samples composition in order to have a clear identification and ratio quantification on EDS. The main problem with this analysis technic is the need for vacuum and high refrigeration (liquid nitrogen) increasing its cost and time of analysis comparing to XRD.

In this work the images were retrieved by a NanoSEM – FEI Nova 200 (FEG/SEM) and the chemical composition was ascertained by EDAX – PegasusX4M (EDS/EBSD). These instruments can be seen in figure 16.

Figure 16. Photos of EDS and SEM equipment, FEI Nova (FEG/SEM); EDAX - Pegasus X4M (EDS/EBSD) [38]

6.7 Phase identification

All experimental powder patterns, produced by XRD, were compared with existing powder diffraction files (PDF) for identification. These PDF were scanned on EVA, crystallography analysis software with PDF database provided by ICDD (International Center for Diffraction Data) [39]. On EVA software it was possible to perform powder pattern match by raw file analysis. To reduce the amount of possible matches, the database allows for a probable present atoms search. Therefore, to search for stannosilicates only H, O, Si, Sn, Na and K were normally selected. When this produced no results more forms of silicates were selected in order to search for possible analogue structures. There are many octahedral and tetrahedral elements possible but due to the large amount of known structures the elements added were Zr, Ti and V. If none of the database PDF of these forms of silicates matched the experimental powder pattern, all the elements of the periodic table were considered form search. In this case if a match is found, the elements that compose the matching structure should be of possible substitution (charge and coordination) for the ones really present in the material. This match procedure served to identify all the stannosilicate structures that were already reported to other forms of hydrothermal synthesis. Also to find analogue structures to the unknown stannosilicate frameworks. After a visual confirmed match the PDF file was retrieved. On the PDF files are described the material chemical composition, space group, dimensions, powder pattern information (diffraction planes occupied) and the article of discovery. This information helped in the next step of analysis, the dimensions refinement.

The dimensions refinement was a necessary task to understand if the produced materials had the same exact structures of the reported materials or if there were new dimensional differences. These differences result from compositional changes or atom displacement. These differences may be undetectable and unquantifiable on EVA visual match since it only serves as a comparison method. TOPAS 3.0 software package [40] was used to perform Le Bail calculated fits, to refine the unit cell parameters, to determine the crystal dimensions and to produce calculated diffraction planes of the refined powder pattern. Using FPA (Fundamental Parameters Approach) [41], which allows faster and simpler equation solving, the Le Bail allows the fine adjustment of all crystallographic data of the powder pattern. This method was used to confirm if the experimental powder patterns represented pure structures, to calculate the changes produced by ion exchange and isomorphous substitutions. It also served to confirm if a determinate space-group can describe a powder pattern by more than visual analysis. The Le Bail refinement was of vital importance to this work since it was the first

confirmation and analysis toll of all crystalline materials produced by synthesis, modification or thermal degradation.

In addition to this refinement method TOPAS 3.0 also provides Rietveld refinement, which allows structural simulation and phase percentage determination. By introducing the structures Crystallographic Information Framework (CIF) file [42] the Rietveld method allows dimensions refinement and phase percentage calculation. It does this by creating calculated plots in information from the CIF files and adapting it to the experimental powder patterns. The CIF files contain all structural crystallographic information like structure name, composition, space group, dimensions, atoms positions, position occupations, reproduction of the unit cell in space and more. This information is encrypted and can be used in visualization softwares (like Diamond 3.2) and refinement softwares (like TOPAS 3.0 or Fullprof).

The Rietveld refinement TOPAS 3.0 was used to build modified CIF files. When a modification to a known stannosilicate structure was achieved, Rietveld allowed the refinement of the unmodified CIF to the new atomic positions and occupations described in the experimental powder pattern. The refinement produces a new CIF file that is calculated from the start-up CIF and the experimental powder patterns. To reach the modified CIF this work obeyed the standard refinement parameters [43], where the atoms of higher weight were refined first and its connecting oxygen's were refined to the acceptable physical distances. In stannosilicates the heavier atoms are the framework atoms, Sn and Si, so all skeleton was correct first. The Si-O bonds were correct to a medium length of 1.6 Å, with maximum deviation of 0.1 Å, and Sn-O bonds were correct to 2.0 Å, with a maximum deviation of 0.2 Å.

The pore atoms are the last ones to refine in position and occupation. Water molecules inside the channels is represented by a solo oxygen atom (XRD does not detect hydrogen) and its refined occupation must reflect the values of structural water that leaves the structure upon dehydration. To calculate this is commonly used thermo gravimetrical analysis (TGA). The pores stabilizing ions are then refined to optimal position (respecting the angle and bonds) and its occupation and its occupation values must match the values obtained on EDS. After total positional and occupational values refinement the isotropic thermal values (ITV) are obtained and refined to positive levels. The occupation and isotropic thermal factors are good indicators of correct atom placement. When performing atom refinement and occupation shows values superior to 1 it is indicative that the atom in question is not the correct one for that position and a heavier one should be considered. This refinement technic (occupation value) was used to

produce the simulated structures of the ion exchanged forms. In this modified forms the increase of occupation of the pores atoms indicated the presence of the capture element. The ITV are also important to understand if the refinement procedure was correct. Its values must always be positive, low values for the more trapped framework atoms and higher to the looser pore atoms. The framework atoms like Si and Sn should present values from 0.5 to 5, the stabilizing ions (K, Na and others) present higher ITV and the water molecules that are the more loose members of the structure should present the highest ITV.

TOPAS Rietveld refinement can also be used to confirm if CIF's produced by other softwares fully represent the experimental powder pattern. Since it has a very accurate method of producing simulated plots and is well accepted in the scientific community this software allows the confirmation of new CIF by comparing it to the experimental values and producing an error value (Rwp) that the scientific community acknowledges. This Rwp must be as low as possible, for low resolution patterns values near 30 are accepted. For a scientific approved Rietveld refinement, in a high resolution pattern, the Rwp should be inferior to 13.

The required CIF files for any refinement are present in innumerous databases, to this work the CIF's were obtained from the software and database "Find it".

When the ICDD data base does not provide a PDF match to the experimental powder pattern no CIF file is available and the space group is determined by mathematical iteration of the powder pattern data. The software used for this procedure was FullProf Suite, which allowed powder pattern read and individual and automatic peak indexation. By establishing a background function and creating an analyzable peak distribution, FullProf, allowed the search of space-groups and unit cell dimensions by the DICVOL06 or the TREOR mathematical approaches. A solution is then calculated from all possible space-group/dimensions combinations and compared with the experimental powder pattern. The software performs innumerous iterations but the rate of success is normally good. Since FullProf provides more than one solution other software was used to search throw-out the resulting data. Checkcell, the used software, imports the results from FullProf and allows visualization of the found solutions. It also allows comparison in several related space-groups and crystal types. The peaks from the experimental powder pattern are compared with the peaks formed by the solutions. This procedure can be performed manually or automatically. This software performs matching procedures to find the best solution among the ones already provided by FullProf. The combination of these two softwares allowed the phase determination of the unknown powder patterns in this work.

Crystallographic characterization of new or modified structures ends with the creation of the CIF file. The modification of CIF files is and well dominated procedure form of creating new simulated structures. This procedure (done in TOPAS or other Rietveld bases softwares) works well on ion exchange or isomorphic substitution forms. However, when a new form of structure appears and it does not possess any kind of analogue among silicates or any other materials the Rietveld process is no longer an option. This refinement process needs an initial framework to start the refinement, an initial CIF file that must closely resemble the experimental powder pattern. So in cases of unknown phase or new crystalline materials the approach to obtain the final CIF file was performed differently. First unit cell and space-group were determined by FullProf and Checkcell after that EXPO 2009 was used for atom to atom framework build. EXPO 2009 allows structure simulation from powder patterns, unit cell parameters and chemical composition alone.

This software performs atomic position simulation by automatic methods or by constructive methods using Fourier mapping. The construction of correct structures from EXPO 2009 is a very experimental and difficult process since there are no fundamental parameters or standard approaches. It is an atom to atom buildup that requires frequent Rietveld refinement for position confirmation. EXPO 2009 allows atom manipulation within the unit cell making the construction of the unit cell full very dynamic and dependent on the user knowledge of the type of materials in question. After CIF build up, EXPO 2009, internal Rietveld error factor (Rwp) is not very reliable so it is necessary to export the CIF and perform TOPAS Rietveld confirmation. The buildup of CIF files is not current in scientific reports, most of the times structures are obtained by Rietveld of analogue or similar frameworks. Nevertheless, this works used this method to the construction of unknown frameworks and the CIF's produced in EXPO 2009 were then submitted to TOPAS Rietveld for final distances correction and production of the calculated plot and associated Rwp.

During the development of this work, new EXPO software was released, the EXPO2013 had upgraded functions that allowed the restrain of angles and distance of bond more correctly. This new version was used to perfect the angles on all simulated structures, both EXPO2009 and TOPAS 3.0 CIF files.

VII. Results and discussion

7.1 Synthesis

The sodium-based tin silicate compositions (Trial C) showed two distinctive results: run products with solid product and run products without solid product. The resume of these syntheses can be seen at table 12, where the individual synthesis results are shown. It is clear that the increase of the concentration of tin chloride (increase in trial number) increases the possibility for obtaining a solid product.

Table 12. Synthesis results for the sodium-based tin silicates for 2 days synthesis and 15 min. of precursor agitation (Trial C).

Trial	Result of synthesis	Trial	Result of synthesis
C_1	Two kinds of material	C_{11}	White Powder
C_2	White Powder	C_{12}	Yellow solution (no solid product)
C_3	Yellow solution (no solid product)	C_{13}	White Powder
C_4	Yellow solution (no solid product)	C_{14}	Yellow solution (no solid product)
C_5	White Powder	C_{15}	White Powder
C_6	White Powder	C_{16}	White Powder
C_7	Yellow solution (no solid product)	C_{17}	White Powder (great amount of material)
C_8	White Powder	C_{18}	White Powder (great amount of material)
C_9	White Powder	C_{19}	White Powder
C_{10}	White Powder	C_{20}	White Powder

Additionally, the time of agitation as a factor in the hydrothermal synthesis was studied. Four different times were tested – 0, 5, 15 and 30 minutes (Table 13). The 0 agitation time samples (T_{C1} and T_{C5}) did not presented any solid run product. These samples had no magnetic agitation and no exposure to 145°C. The 5 minutes agitation samples (T_{C2} and T_{C6}) revealed a solid run product. These samples were agitated during 5 minutes at 240 rpm at 145°C and this final production step made all the difference in the formation of solid products. The ions dispersed in the solution gained enough energy to connect into the first molecules and then the first precipitates. To confirm this all the other samples with 15 minutes (T_{C3} and T_{C7}) and the 30 minutes (T_{C4} and T_{C8}) of agitation also presented a solid run product. In the sodium-based tin compositions a minimum agitation of 5 is required in order to obtain a solid run product.

Other aspect detected after autoclave opening was that the samples heated for 7 days at 200°C (T_{C6} to T_{C8}) was that the run product was soluble. It is possible that the materials produced in a 2 days synthesis are not stable and at 7 days the run product is composed of other forms. The individual results of the different agitation and synthesis time samples can be seen in table 13.

Table 13. Synthesis results for trial T_C, each composition agitated for 0, 5, 15 and 30 minutes.

Trial	Time of agitation (min)	Synthesis (days)	Result	Trial	Time of agitation (min)	Synthesis (days)	Result
T_{C1}	0	2	Yellow Solution (no solid product)	T_{C5}	0	7	Yellow Solution (no solid product)
T_{C2}	5	2	White Powder	T_{C6}	5	7	White Powder (some soluble solid)
T_{C3}	15	2	White Powder	T_{C7}	15	7	White Powder(some soluble solid)
T_{C4}	30	2	White Powder	T_{C8}	30	7	White Powder (some soluble solid)

The run products of the syntheses performed for two days and 7 days were quite different. Trials T_{C1} and T_{C5} (0 minutes agitation) were completely transparent and had the same appearance of the other precursors. However, the absence of strong agitation and increased temperature made the precursors unfitted for synthesis of tin silicates. It was found that different time for agitation changes the behavior of the solution. It is supposed that when agitated for more time the interaction between the chemical units composing the solution is higher and the formation of nucleus for crystallization is also higher. These nucleuses are then responsible for the formation of a solid run product. The full effect of the time for agitation can be seen by the analysis of the run products crystal structure.

The low sodium stannosilicate compositions (Trial E), presented very different behaviors when compared with trial C. Upon precursor preparation only trial E_2 and E_5 showed transparency and were the only trials to present a white powder as run product. On the remaining trials, transparency was lost and the precursor turned into a yellow gel. This yellow color remained after synthesis in the run product.

The quantity of run product of trials E_2 and E_5 was much more inferior to E_1, E_3 and E_4. Since trial E_5 had the same composition of trial C_{13} and E_2 had a direct element ratio to it (every element except water divided by 2) the production of the same white powder was expected. However, in the remaining trials the yellow colored material indicated that the small amount of sodium present in the precursor was not sufficient to eliminate all the chloride remains. The yellow powders were soft, giving no indication of being crystalline. The white powders were also soft but with a more sandy aspect. The individual results of trial E can be seen at table 14.

Table 14. Synthesis results from trial E. 2 days synthesis and 15 minutes of precursor agitation.

Trial	Result
E_1	Yellow Gel (bad filtration)
E_2	White Powder
E_3	Yellow Gel (good filtration)
E_4	Yellow solids
E_5	White powder
E_6	Yellow Gel (good filtration)

The sodium- and potassium-based stannosilicates (Trial D) presented different shaped powders as run products. All 20 compositions resulted in sandy solid material. Among these compositions, there were also two characteristic results in terms of run product. The majority of the compositions resulted in clear liquids with white sandy powders deposited at the autoclave bottom. The remaining compositions resulted in white milky solution that after filtration formed a fine white powder. The filtration process of the sandy powders was very fast. The milky solutions had a slow filtration. The visual aspects of the obtained powders are described in table 15,

Table 15. Synthesis results for the sodium and potassium based stannosilicates (Trial D). Two days of synthesis and 15 minutes of precursor agitation.

Trial	Result	Trial	Result
D_1	White sandy powder	D_{11}	White sandy powder
D_2	White sandy powder	D_{12}	White Solution (fine white powder)
D_3	White sandy powder	D_{13}	White sandy powder
D_4	White sandy powder	D_{14}	White Solution (fine white powder)
D_5	White sandy powder	D_{15}	White Solution (fine white powder)
D_6	White Solution (fine white powder)	D_{16}	White Solution (fine white powder)
D_7	White Solution (fine white powder)	D_{17}	White sandy powder
D_8	White sandy powder	D_{18}	White sandy powder
D_9	White sandy powder	D_{19}	White Solution (fine white powder)
D_{10}	White Solution (fine white powder)	D_{20}	White sandy powder

Description of the obtained powders from trial T_D is presented in table 16. The variation of the precursor agitation time did not produce significant changes in the samples. All tried agitations, 0 minutes (T_{D1} and T_{D4}), 5 minutes (T_{D2} and T_{D6}), 15 minutes (T_{D3} and T_{D7}) and 30 minutes (T_{D4} and T_{D8}) produced a solid run product. The only visual change detected was between the materials with different compositions (T_{D1} to T_{D4} and T_{D5} to T_{D8}). Trials T_{D1} to T_{D4} that had the composition of trial D_1 showed a white sandy aspect powder. The trials T_{D5} to T_{D8} that had the composition of trial D_7 showed, after filtration of a white solution, a very fine white powder.

Table 16. Synthesis results for Trial T_D. Composition from 1-4 and 5-8 are equal (see in appendix 1). Precursor agitation time for 0, 5, 15 and 30 minutes.

Trial	Time of agitation (min)	Synthesis (days)	Result	Trial	Time of agitation (min)	Synthesis (days)	Result
T_{D1}	0	2	White sandy powder	T_{D5}	0	7	White Solution (fine white powder)
T_{D2}	5	2	White sandy powder	T_{D6}	5	7	White Solution (fine white powder)
T_{D3}	15	2	White sandy powder	T_{D7}	15	7	White Solution (fine white powder)
T_{D4}	30	2	White sandy powder	T_{D8}	30	7	White Solution (fine white powder)

The run products show that the sodium- and potassium- based compositions are more chemically stable than the sodium based. Within this type of compositions it was possible to produce run products in all trials even in solutions with no precursor agitation. The sodium and potassium had great effect on these compositions but these results come also from the fact that the amount of alkaline material was always at 10 moles. This amount of alkaline material was chosen in order to study the influence of the amount of sodium in relation to potassium without changing the alkaline ratio in the composition.

The potassium based stannosilicates, Trial P, showed also a high success in the production of solid run product. It did not present solid run products in all samples like in trial D but it presented much higher amount than the sodium samples (trial C). The main problem about this trial was the size of the powders produced. Most of the trials presented very fine powder as run product making the filtration process impossible. These products were carefully washed and let the rest of solid to precipitate, after that the liquid was removed and the rest (solid material and some remaining water) was dried at 50°C. All samples from the potassium based stannosilicates presented a solid run product with very small grain size. As in trial D, these samples were also dividable by aspect. There were samples with sandy aspect with a grain size that allowed easy filtration and samples that presented itself in the form of a white solution with powders with very fine grain size. Table 17 shows which trial had these larger grains (white powders) and which showed the white solutions (fine white powder).

Not all trials resulted in a solid product after the steps of filtration or evaporation of the run product. In terms of autoclave content all samples of trial P presented some solid run product. However due to the difficulties in the filtration process it was not possible to retrieve solid materials from all samples.

Table 17. Synthesis results for potassium based stannosilicates (Trial P). Syntheses for 2 days at 200°C and precursor agitation of 15 minutes.

Trial	Result	Trial	Result
P_1	fine white powder	P_{10}	white powder (small amount)
P_2	fine white powder	P_{11}	fine white powder
P_3	white powder (impossible to filtrate)	P_{12}	fine white powder
P_4	white powder	P_{13}	fine white powder (small amount)
P_5	white powder	P_{14}	No solid material
P_6	white powder (impossible to filtrate)	P_{15}	White powder
P_7	fine white powder	P_{16}	White powder(impossible to filtrate)
P_8	fine white powder	P_{17}	White powder
P_9	white powder (impossible to filtrate)	P_{18}	White powder

Similar to the sodium- and potassium-based compositions (trial T_D), the variation of the time for agitation did not change the run product of the potassium-based compositions (Trial T_P). The two different compositions (T_{P1} to T_{P4} and T_{P5} to T_{P8}) presented the same type of material, a white powder, and were both of a size that allowed filtration. The samples produced at different agitations, 0 minutes (T_{P1} and T_{P5}), 5 minutes (T_{P2} and T_{P6}), 15 minutes (T_{P3} and T_{P7}) and 30 minutes (T_{P4} and T_{P8}), resulted in run products with the same aspect. The only detected difference was the grain size difference between the two different compositions. The fact that one was synthesized for 2 days and the other for 4 days made them different in grain size. Longer times of synthesis produced a larger grain size. Visually, the effects of a different agitation and composition were not detected but the results from all samples can be seen by table 18.

Table 18. Synthesis results for trial T_P, trials 1-4 composition equal to P_1 trials 5-8 composition equal to P_{10}. Precursor agitation times for 0, 5, 15 and 30 minutes.

Trial	Agitation time (min)	Synthesis (days)	Result	Trial	Agitation time (min)	Synthesis (days)	Result
T_{P1}	0	2	White powder	T_{P5}	0	4	White powder (better powder)
T_{P2}	5	2	White powder	T_{P6}	5	4	White powder (better powder)
T_{P3}	15	2	White powder	T_{P7}	15	4	White powder (better powder)
T_{P4}	30	2	White powder	T_{P8}	30	4	White powder (better powder)

Comparing 4 days synthesis and 2 days synthesis it is possible to say that the extra time allows the grains to grow into easier manipulation size. This was not seen at the other trials (sodium based and sodium/potassium based) indicating that potassium has slower interaction with silicon and tin. Its reactivity in the studied system is lower than sodium ion.

Trial T_L explored the run products of synthesis performed for 1 day. The initial composition was the same as the one of the samples prepared for 2 and 4 days. The agitation time was change to some untested values in order to refine the study of the agitation time effect. The results showed that the run powder aspect seen on trial P_{10} was not repeated in all trials of T_L. Out of the three trials performed with 1 day synthesis only one showed a stable run product. The other two trials dissolved upon filtration. Sample T_{L4} was a reproduction of trial P_{10} and the run powder seemed consistent with the previous production. Sample T_{L5} was an untested combination of parameters that resulted in the same type of run product as T_{L4}. The visual results can be seen in table 19 but the real effects of synthesis time and precursor agitation time can only be seen by XRD analysis.

Table 19. Synthesis results of Trial T_L. All trials performed at the same composition (trial P_{10}).

Trial	Synthesis (days)	Precursor agitation	Result	Trial	Synthesis (days)	Precursor agitation	Result
T_{L1}	1	10 min	Dissolved at filtration	**T_{L4}**	2	15 min	White powder
T_{L2}	1	15 min	White powder	**T_{L5}**	2	30 min	White powder
T_{L3}	1	20 min	Dissolved at filtration				

After analysis of all run products it was possible to understand that sodium and potassium work differently in this clear precursor stannosilicate synthesis method. Potassium stabilizes the precursor and allows the formation of solid run product in all compositions. When alone this element seems to have slow reaction and forms very fine powders after synthesis. On the other hand, sodium is more reactive in the precursor. It speeds up the nucleation process but also makes some compositions unfitted for stannosilicate production when alone as alkaline element. The production of solid run product is clearly favored when sodium and potassium are present in the synthesis composition. All compositions with these two alkaline elements produced a solid run product.

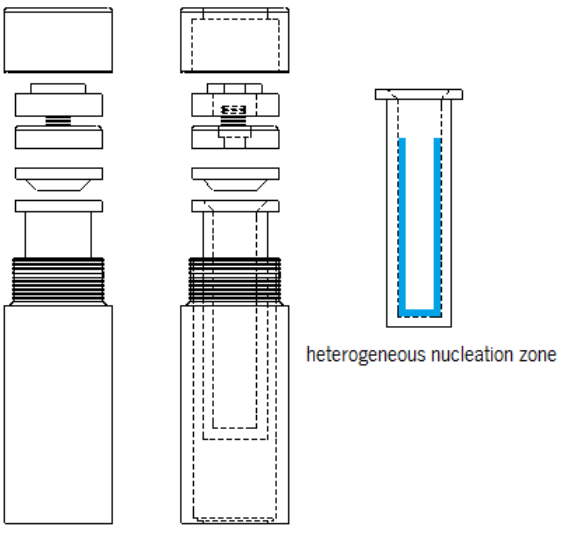

Figure 17. Schematics of the zone of heterogeneous nucleation.

Another interesting observation was that in certain cases (the majority of the sodium/potassium based composition) the nucleation and subsequent crystal growth start from the Teflon walls of

the autoclave (figure 17). Probably the Teflon walls contributed for faster heterogeneous nucleation which led to a shorter synthesis time.

7.2 Characterization of the synthesized materials

After synthesis and drying the materials were stored according to their initial batch composition, time for agitation and crystallization. Additionally, the large grain size samples were milled for better XRD characterization. The obtained powder XRD patterns were analyzed by specialized software (ICDD, EVA and TOPAS) and the samples of particular interest were further characterized by SEM and EDS.

7.2.1 Sodium-based tin silicates

Trial C samples formed materials with sodium as the alkaline stabilizer of the composition. Within these materials the crystalline ones presented powder patterns showing two different phases across the entire composition field. Figure 18 shows the obtained powder patterns. Crystallinity was low in almost every trial but there were clear indications, after EVA analysis, that some trials resulted in a material known as AV-10. The remaining crystalline trials resulted in unknown type of structures characterized by a very high intensity peak at very low 2theta angles, near 7° 2theta. In figure 18 the AV-10 materials are distinguished by the absence of any diffraction peak at 7° 2theta and for the presence of three high intensity peaks between 12 and 17° 2theta. The materials powder patterns had some detectable impurities or defects indicating that the materials formed were not a pure form of AV-10.

The majority of the synthesized materials resulted in materials with the unknown structure. This was an indication that the composition field build favored the formation of this unknown phase. This phase was designated as UM-1 (University of Minho – 1). The formation of AV-10 appeared only in low sodium trials, probably because the sodium available in the compositions was not enough to form the dominant phase of this trial. UM-1 showed broad peaks in all trials indicating either very small crystal size or very low crystallinity. C_9 and C_{13} were the samples that resulted in a powder pattern consistent with AV-10. C_9 presented low crystallinity but C_{13} showed enough diffraction information to try an indexation. From all the samples that resulted in patterns with the distinctive 7° 2theta high intensity peak, C_{11} and C_{20} were the ones with the higher amount of diffraction information and with the lower background contamination. Sample C_1 was identified as a non stannosilicate structure. Within the analyzed materials it was also seen that some samples resulted in amorphous materials (C_{10}, C_{17}, C_{18} and C_{19}).

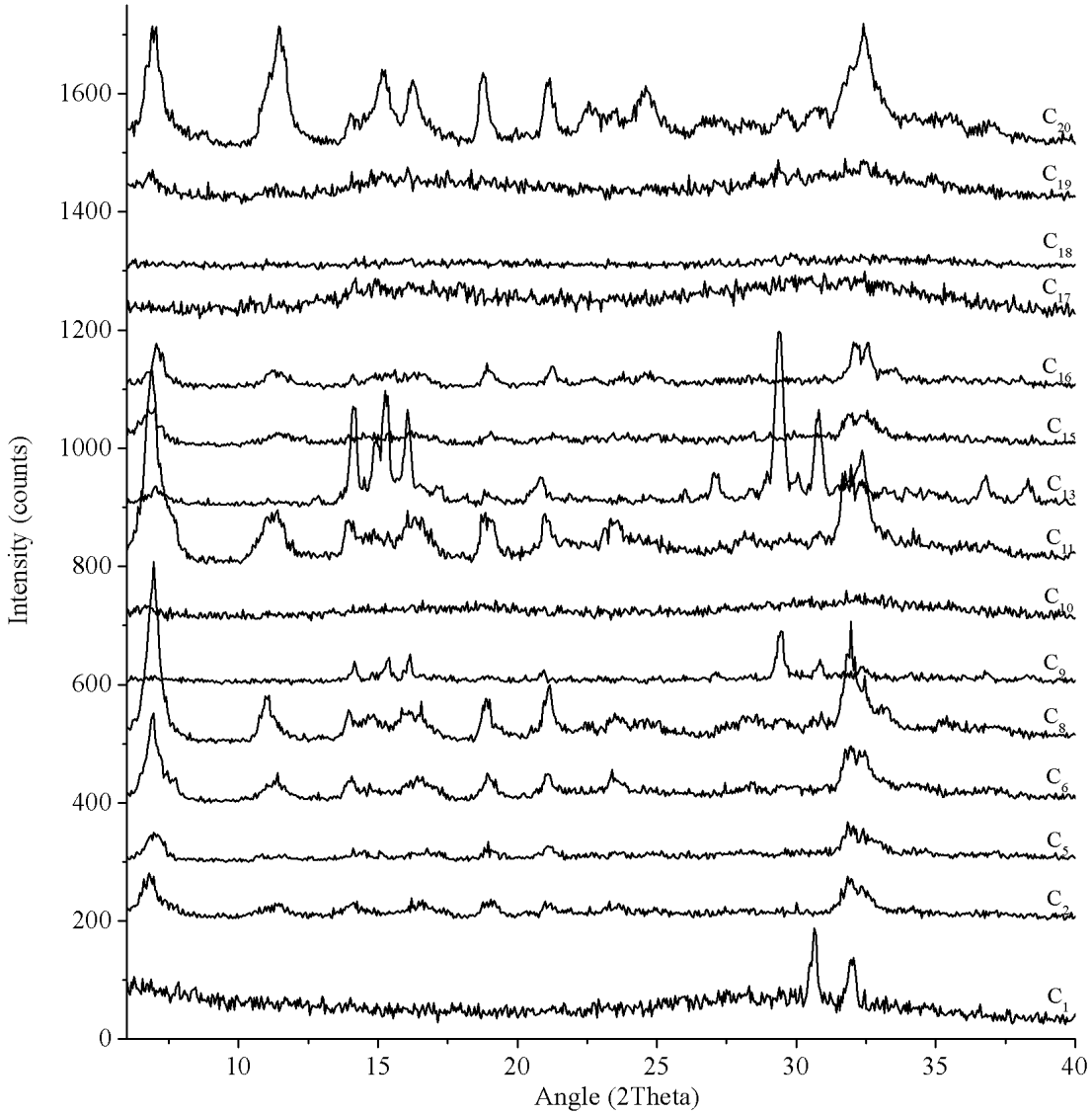

Figure 18. Experimental XRD powder patterns from all the synthesized sodium-based tin silicates (Trial C). Range from 6° to 40° 2theta.

In order to prove that the structures synthesized at C_9 and C_{13} are AV-10, Le Bail refinement procedure was conducted using the crystallographic data from AV-10 (PDF 01-070-9542). Software TOPAS 3.0 was used to refine the parameters of the unit cell (dimensions, angles and volume) and the size of the crystallites. The crystallographic data of the Le Bail fit can be seen in table 20 and the differences between the experimental and calculated curves in figure 19. From that figure, it was possible to see that some impurities (marked with asterisk) were present in the pattern indicating that this was not a pure form of AV-10. The originally reported structure [26] was prepared by two stage synthesis, in long time and with specific procedures not conducted in this work. These differences and the change of tin source may explain the impurities present on C_{13}. Nevertheless, this was a very close result to the pure structure of AV-10 indicating that this structure can be produced from this new synthesis method. In order to do that some chemical composition or preparation parameters must be changed.

Table 20. Crystallographic data of trial C_{13}, performed by Le Bail using hkl data from AV-10.

Cell Type	Orthorhombic
Space Group	$C222_1$
a (Å)	7.9(4)
b (Å)	10.3(3)
c (Å)	11.6(4)
Volume (Å^3)	956.4(1)
Crystal size (nm)	34±1
Rwp	27.5(2)
R-Bragg	4.4(1)

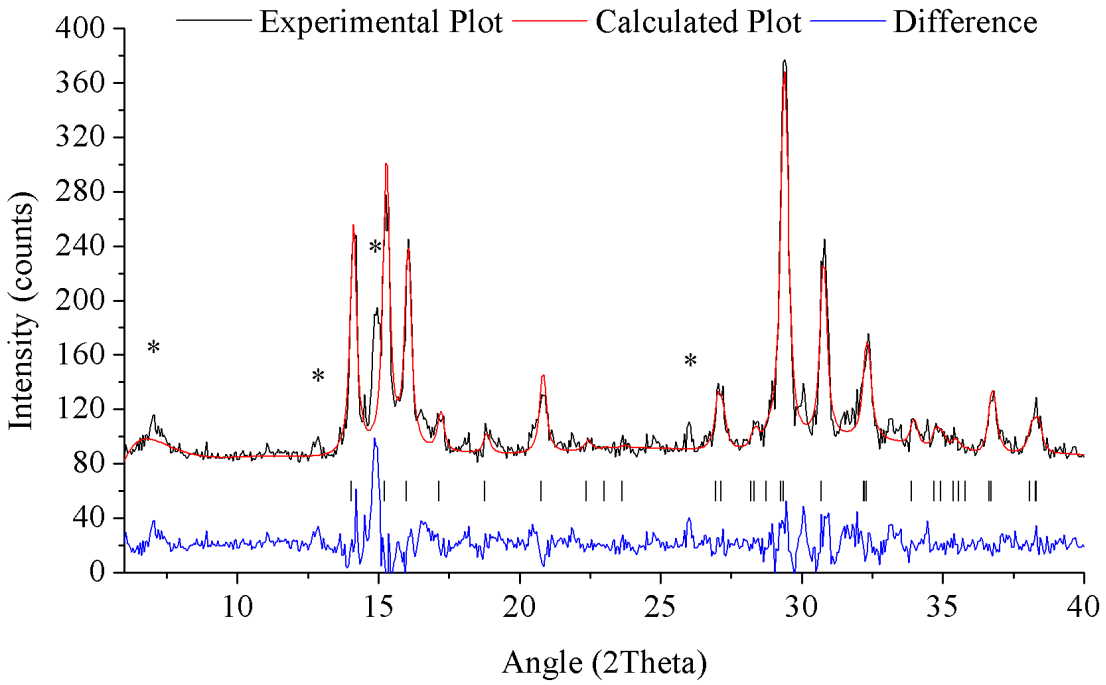

Figure 19. Le Bail refinement of trial C_{13}, experimental and simulated curves. Impurities as asterisk.

In the available literature and ICDD it was not found a structure similar to the synthesized sodium tin silicate. By FullProf and Chekcell, using a high resolution power pattern, a possible set of space-groups and dimensions were found. The attempts to index the powder XRD pattern did not give any reliable space group and further studies with higher resolution data will be necessary. Figure 20 shows one of the attempted indexations. The high number of non-described diffraction planes invalidates the indexation.

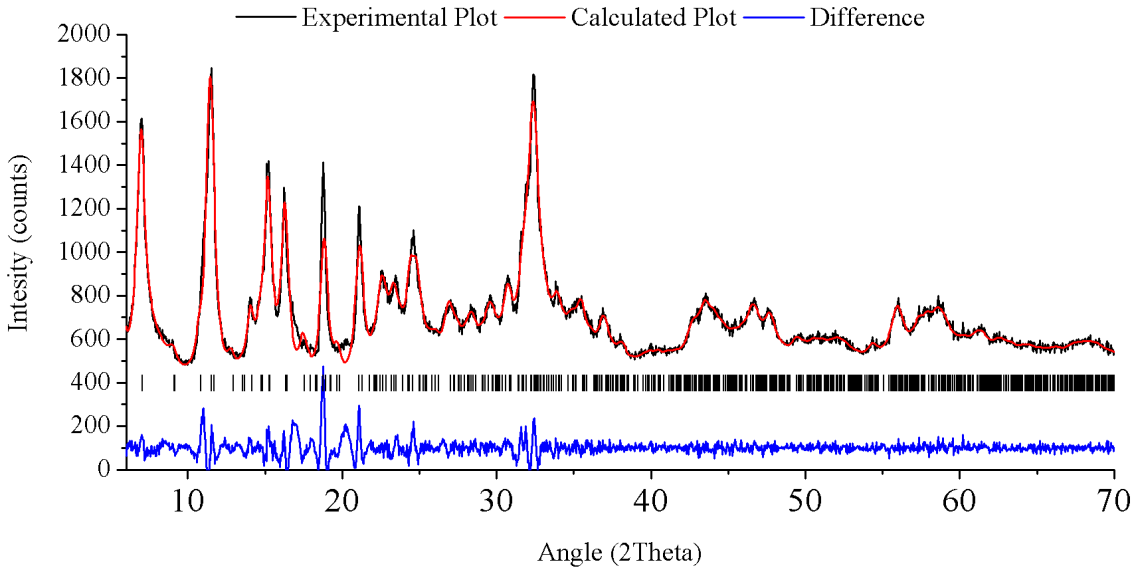

Figure 20. Attempt for Le Bail fit of C_{20} using Pmc21 space-group. Experimental calculated and difference curves well described but with high number of extra diffraction planes.

Trial T_C samples, performed at different precursor agitation times, revealed a very distinctive pattern in terms of crystalline structures formed. In the 2 days synthesis, T_{C1} did not gave product due to the lack of agitation and the 5 minutes agitation trial, T_{C2}, resulted in a very low (near amorphous) crystalline material that had no resemblance to the phases of the samples from trial C. T_{C3}, with 15 minutes agitation, resulted in the same structure as its original trial C_{11}, the UM-1 phase. This repetition proved the stability of the experiments and of the results. T_{C4}, with 30 minutes of precursor agitation, revealed a powder pattern consistent with AV-10. In fact, this AV-10 was with fewer defects than the ones produced on the previous trial C. All these compositions, T_{C1} to T_{C4}, had the same composition and the same synthesis time meaning that all the changes seen in figure 21 were induced by the precursor agitation time. There is no theoretical model that explains this effect therefore the given explanations are just suggestions until further proving. In the precursor (that is mostly composed of water) the positive ions start to interconnect to each other by oxygen bonds. As these bonds start to increase, ions start to form initial building units, these units are then responsible for the solid crystalline material formation. At low agitations, between 0 and 5 minutes, there was no formation of crystalline material. The initial building units in the precursor did not have enough energy and time to form more cohesive units that would last and grew during synthesis in autoclave. At 15 minutes, the agitation of particles started to increase and the building units collided and formed cohesive forms with the structural information of UM-1. These forms grew within the autoclave and formed crystalline material. However, at 30 minutes, where the energy level is higher, the building units stop forming UM-1 and started to form AV-10 structure. This was the first time that a parameter like

precursor agitation time determined the crystalline form of the produced stannosilicates. These results indicated that the determination of the stannosilicates final crystal form starts before synthesis. The type of precursor used and its preparations conditions can have the same effect as a change of chemical composition.

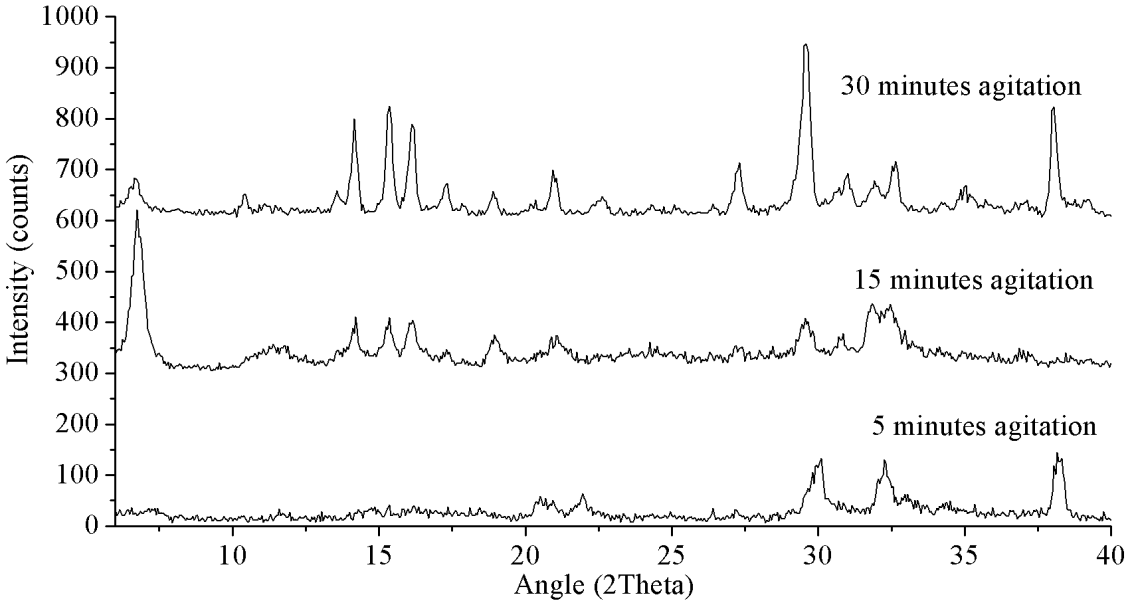

Figure 21. Experimental XRD powder patterns of trial TC2 to TC4. Synthesis at 200°C for 2 days. agitations from 5 to 30 minutes.(5 minutes: unindexed phase, 15 minutes: unknown sodium phase (UM-1) and 30 minutes: AV-10)

The 7 days synthesis test did not showed the same type of results. As seen in the synthesis results, these trials had soluble run products that had no resemblance to other stannosilicates. XRD showed, figure 22, that they were completely different form the 2 days trials, indicating that the phases formed at 2 days cannot withstand a 7 days hydrothermal synthesis procedure. This showed that AV-10 and UM-1 had limited stability in this synthesis environment and that within seven days they dissolve and form new precipitates. The 5 minutes and 15 minutes materials (trials T_{C6} and T_{C7}) were clearly non silicate forms, due to the lack of diffraction peaks. The T_{C8} trial, 30 minutes precursor agitation, presented more diffraction peak, with good resolution, but without any traces of being either AV-10 or UM-1.

The product of trial T_{C8} was a mixture of Na_2SiO_3 and $Na(Sn(OH)_6)$ with some indexed impurities, figure 23. This proved that the sodium based stannosilicate compositions had limited stability and as the time for synthesis increased its structure disintegrate to simpler molecules. Despite the disintegration, this trial was fundamental to understand that in this type of solutions the maximum time of synthesis should be set at 2 days. Any attempt on syntheses longer than that would result in non-silicate materials.

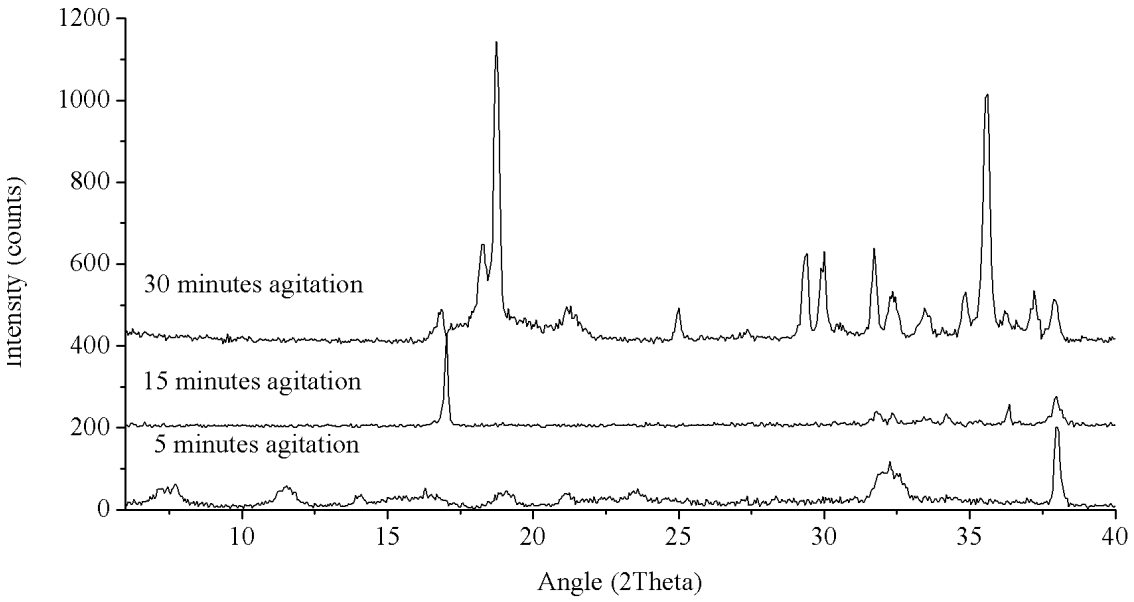

Figure 22. Experimental powder XRD patterns of trials T_{C5} to T_{C8}- 7 days synthesis and precursor agitation going from 5 to 30 minutes (5 minutes: unindexed phase, 15 minutes: unindexed phase and 30 minutes: analyzed bellow).

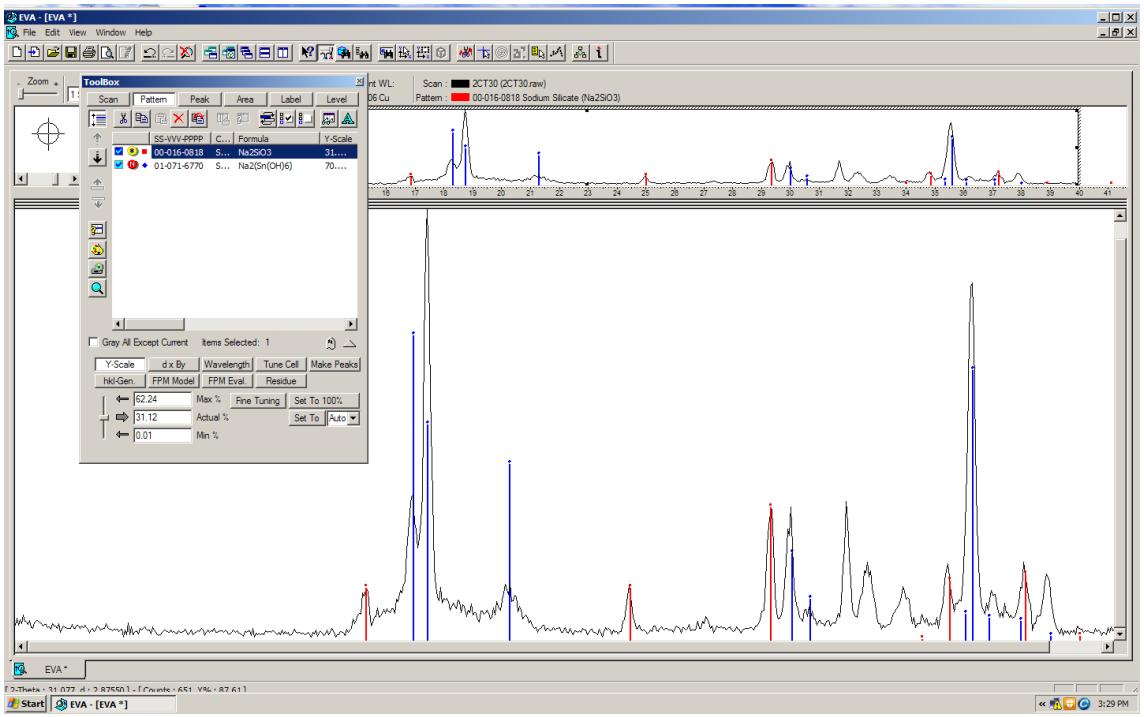

Figure 23. EVA search match for T_{C8}, confirmation of soluble crystalline materials (red: Na_2SiO_3 blue: $Na_2(Sn(OH)_6)$).

These kinds of results did not allow the study of the precursor agitation effect. However, it was possible to see that the hydroxide material has resulted from the excessive synthesis time and not from the change in the time for precursor agitation. The chemical environment produced by sodium was too aggressive to allow any long time synthesis. The building units (nucleus) formed during the precursor agitation did form solid material in the first 2 days of synthesis. However, after this time the solid material started to be dissolved by the remaining solution and only precipitated again in simpler molecules like sodium metasilicate and sodium tin hydroxide.

Trial E, the last sodium based syntheses was performed to test what products would form in low sodium precursors. The drop in sodium concentration in the composition of the precursor (SiO_2+SnO_2+Na_2O+H_2O) is followed by the decreased on pH. With this decrease the ability to dissolve silica was diminished. This type of low pH precursor synthesis was already proven effective in the production of silicate materials [44], but since this synthesis was performed by a different process it was important to understand if the same behavior was possible for stannosilicate precursors. As the synthesis results showed (chapter 7.1), two different products were produced from this trial. The white powders of trials E_2 and E_5 were crystalline, as figure 24 shows, and presented a XRD powder pattern very similar to AV-10. The crystallinity was not the best but the absence of the 7° 2theta diffraction peak clearly indicated that these compositions with the same element ratio resulted in the same crystalline form, AV-10. The remaining colored powders presented amorphous XRD powder patterns proving that no tin silicate was possible to produce from a non-transparent composition with tin chloride (II). These lower pH compositions had no conditions to form crystalline silicates but the amorphous powders may have some interest if tin or silicon are among the amorphous materials.

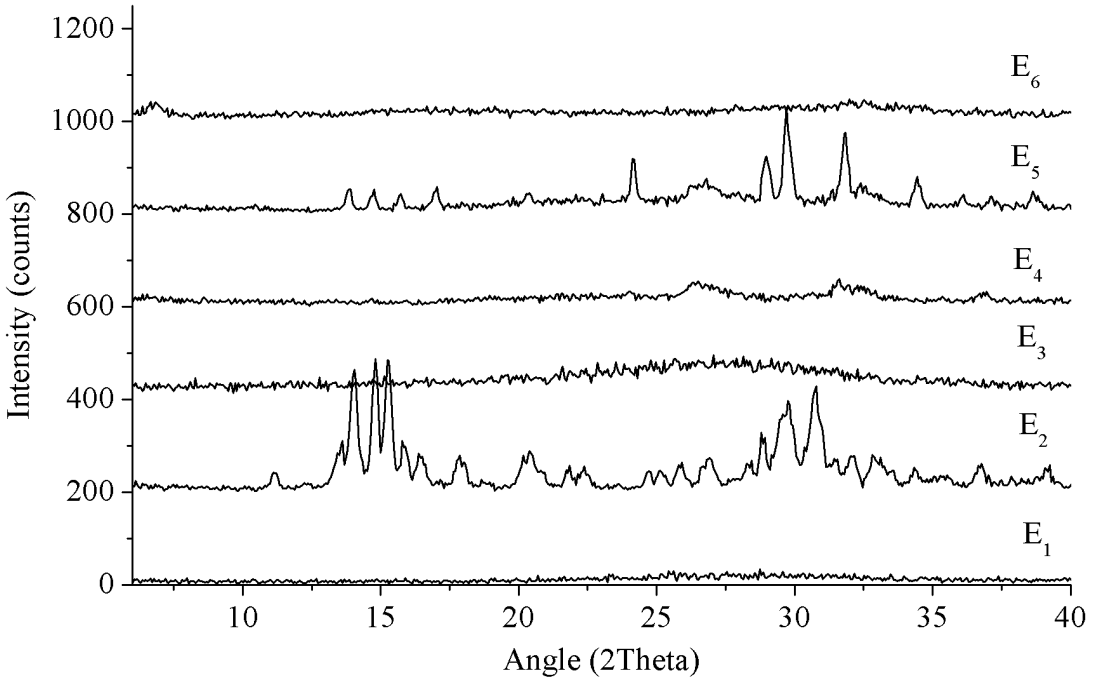

Figure 24. Experimental XRD powder patterns of trial E, 2 days synthesis and 15 minutes of agitation.

7.2.2 Sodium- and potassium- based tin silicates

In trial D the formation of solid run product was achieved for all compositions. In terms of XRD powder patterns all samples of trial D were of high crystalline material, figure 25. The

phases produced were different form the ones seen on trial C. The 20 trials were again dominated by two different structures.

The two structures were identified by EVA as AV-7 (PDF 01-070-4195) and as AV-6, via a zirconium analog (PDF 01-072-1911). Trial D_1 was a clear example of AV-7 and D_7 a pure form of AV-6. From the remaining trials it was possible to see that AV-7 was the most favored structure, even in the mixed phased compositions. This was an expected behavior since AV-7 has been reported as a sodium and potassium tin silicate with a composition of $Na_{0.5}K_{1.5}Si_3Sn_1O_9{\cdot}H_2O$. The precursor ratio of sodium and potassium favored the formation of this structure because potassium was always present in higher quantities. As for AV-6, a potassium tin silicate with a composition of $K_2Si_3Sn_1O_9{\cdot}H_2O$, these were not the ideal compositions for crystallization. However, just like in the previous reported papers [6, 28] its formation can happen in a sodium and potassium chemical environment since sodium often stays out of the silicate nucleus and therefore out of the structure. In fact the amount of sodium present in the precursor was not decisive for the AV-6 formation. The lowest sodium trials produced mainly AV-7, and AV-6 was produced in medium (K_2O/Na_2O=4 or 6 moles) potassium/sodium ratios (check compositions on figure 7).

These two structures, AV-6 and AV-7, have a very similar formation mechanism since the majority of the trials resulted in materials with mixed phases of these structures. Another detected behavior was that as samples with lower crystallinity levels were the ones produced with composition with the wither amounts of SnO_2 (amounts superior to 1.5 moles). This happened due to the pH decrease, caused by $SnCl_2$ addition. This fact helped to understand that these two structures were favored by a high pH environment.

The described synthesis of AV-6 and AV-7 are with 50% faster than the reported synthesis approaches which is a significant step towards the optimization of their production at lower cost.

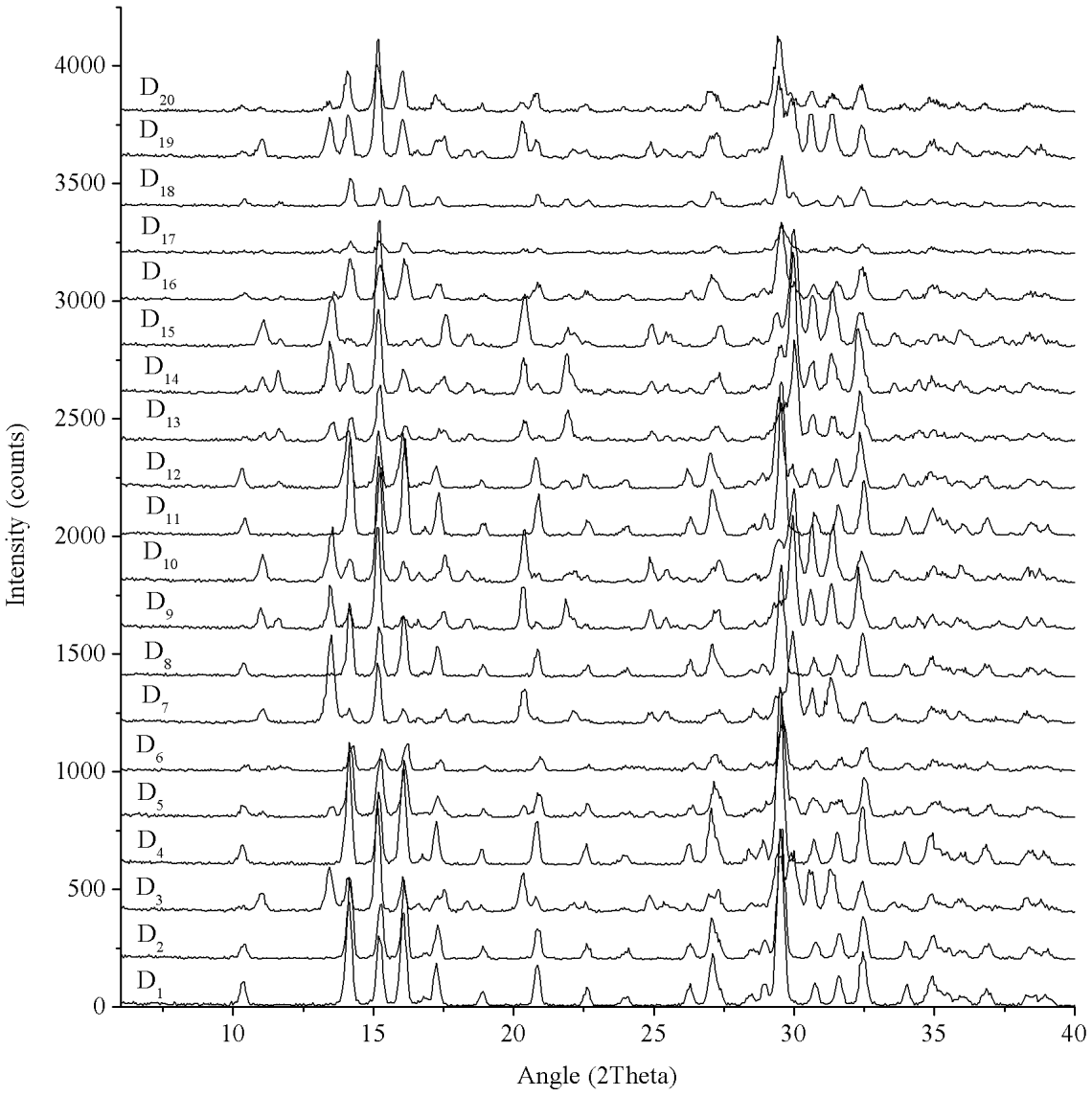

Figure 25. Experimental XRD powder patterns of trial D, 2 days synthesis and 15 minutes of precursor agitation.

AV-6 and AV-7 are chemically and structurally different. The first has orthorhombic structure with potassium as negative charge compensator. The second has monoclinic structure with sodium and potassium as negative charge compensator. Le Bail refinement was used to confirm the lattice parameters and the purity of the two phases. Table 21 shows the obtained dimensions. The refined unit cells were very similar to the reported ones and the simulated curve described the experimental powder patterns with low Rwp factors (for a low resolution powder pattern), figure 26 and table 21. The difference in powder visual aspect described in the synthesis chapter (chapter 7.1) was caused by the difference in crystal size.

Table 21. Refinement results of trial D1 and D7. Obtained by Le Bail with hkl data from AV-7 and AV-6.

Trial D_1 represents AV-7		**Trial D_7 represents AV-6**	
Cell Type	Monoclinic	**Cell Type**	Orthorhombic
Space Group	$P2_1/c$	**Space Group**	$P2_12_12_1$
a (Å)	6.45(2)	**a (Å)**	10.14(9)
b (Å)	11.60(3)	**b (Å)**	13.14 (9)
c (Å)	12.93(9)	**c (Å)**	7.15(2)
β(º)	105.00(3)	**β(º)**	90
Volume (Å^3)	935.79(1)	**Volume (Å^3)**	954.60(8)
Crystal size (nm)	60±1	**Crystal size (nm)**	37±1
Rwp	19.4(3)	**Rwp**	26.2(9)
R-Bragg	3.6(6)	**R-Bragg**	5.21(5)

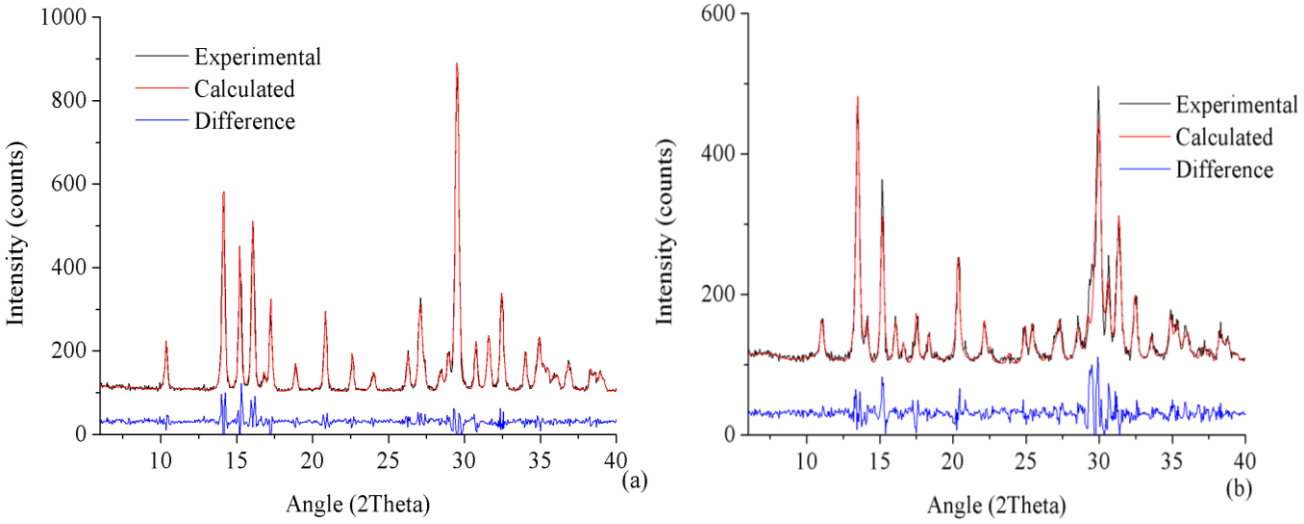

Figure 26. Experimental and simulated curves of trials D_1 (a) and D_7 (b) extracted by Le Bail refinement.

SEM images of both crystalline materials, figure 27, showed ~~the~~ crystal morphology of AV-6 and AV-7. In this case, AV-7 as composed of large crystal that grew in different directions forming ~~crosses~~ cross-like and prismatic crystals and AV-6 grew as needle shaped crystals stacked in every direction forming large agglomerates.

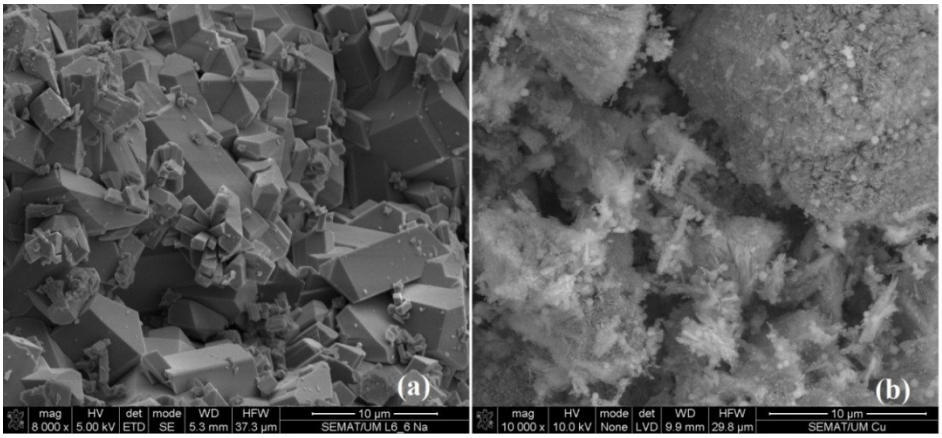

Figure 27. SEM images of AV-7 (a) and AV-6 (b). AV-6 sample with some copper chloride contaminations (confirmed by EDS).

Trial T_D, focus on the precursor agitation time effect, which helped to understand the formation of AV-6 and AV-7. The trials performed on an AV-7 composition (trial D), T_{D1} to T_{D4}, indicated that the formation of AV-7 was only achieved when some precursor agitation was given, figure 28a. In fact the increase of the time of precursor agitation allowed different trials with the same chemical composition to produce materials with two phases with different percentages of AV-7. These variations in time of agitation made possible the formation of AV-7 with 100 % purity after 15 minutes. The material with zero minutes of agitation started as a mixed phase composed of AV-6 (56%) and AV-7 (47%) and with the increase of time for agitation the run product transformed to pure AV-7. The same phenomena was not observed in the trials with the composition of AV-6 (found at trial D), T_{D5} to T_{D8} (Figure 28b). In these compositions the increase of the precursor agitation time increased the crystallinity and produced minor structural changes but did not perform any purification of AV-6 or AV-7 as agitation increased.

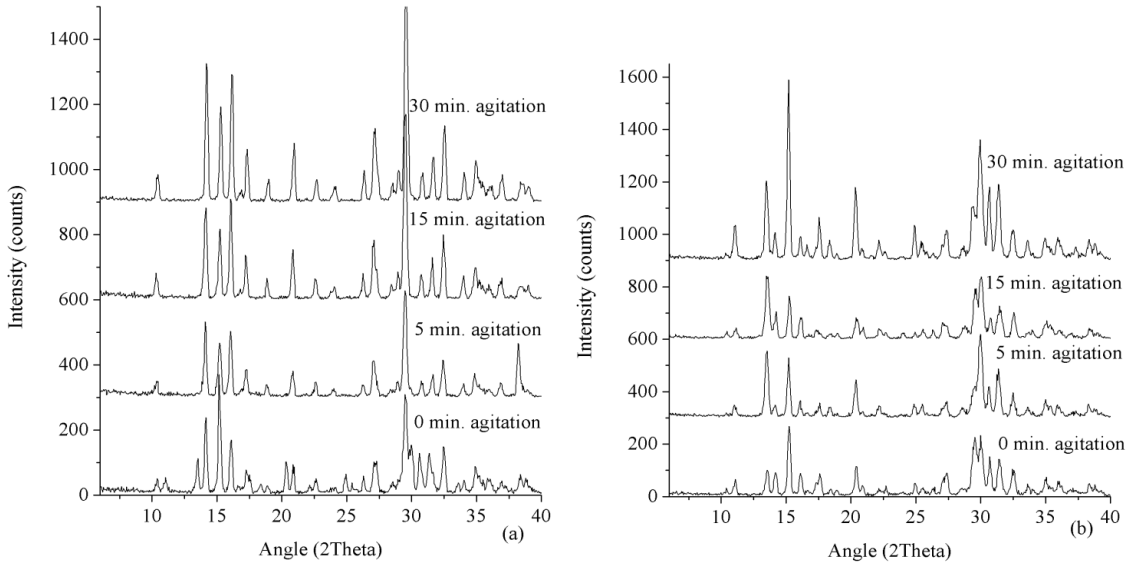

Figure 28. Experimental powder patterns from trials: T_{D1}-T_{D4} for 2 days of synthesis (a); trials T_{D5}-T_{D8} with 4 days synthesis (b).

The effect of the precursor agitation time was even more evident after Rietveld refinement showing the gradual disappearance of AV-6 with increasing of the time for agitation. In the samples with an AV-7 composition (trial T_{D1} to T_{D5}) the effect of the agitation time was very effective in the increase of AV-7 purity. After 5 minutes agitation the materials formed were 96% composed of AV-7. This purity kept increasing as agitation time increased. At 15 the material had 99% of AV-7 and at 30 minutes the material was a pure form of AV-7. This proved that for AV-7 synthesis the best way to assure pure production is to ally a favorable composition with a long precursor agitation. In the AV-6 composition (trial T_{D5} to T_{D8}) the precursor agitation time had no significant effect. The material was at all agitation times dominated by the AV-6 framework but with some impurities of AV-7 were never eliminated, not even at 30 minutes of precursor agitation time. The phase percentage variation showed on figure 29a describes a increase of AV-7 percentage as precursor agitation time increases. Figure 29b shows a stable percentage of AV-6 in all the agitation times.

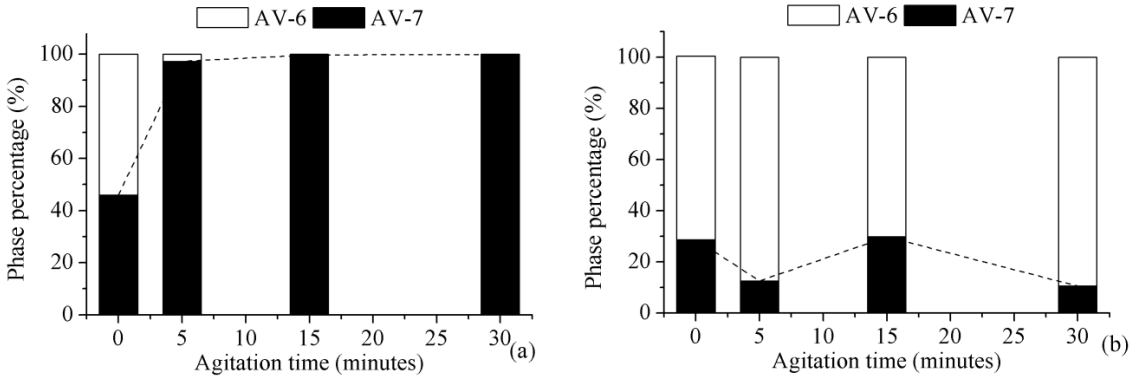

Figure 29. Phase percentage evolution: trial T_{D1} to T_{D4} (a); trial T_{D5} to T_{D8} (b). Data calculated by Rietveld refinement.

This behavior has never been described for tin silicates and therefore there were no physical or chemical models that could explain it. Nevertheless it was possible to say that inside the precursor form of the first building units (nucleus), small segments of octahedral and tetrahedral units. Those nucleuses were possibly influenced by the agitation of the precursor that dictates the molecules speed and rate of collision. Speed and rate of collision are determined by the time of agitation given to the precursor that, in fact, can direct the nucleation towards one or another phase. A similar phenomenon was already seen in other zeolitic structures, where kinetic factors of the nucleus influenced the type of resulting microporous structure [45].

The reason for the observed time dependent behavior can be a matter of speculations but for solid evidence it is necessary a further specialized analyses. Nevertheless this was the

first structural manipulation of tin silicates using a physical pre-synthesis factor like precursor agitation.

7.2.3 Potassium-based tin silicates

All samples produced in trial P were sodium free so from all the already seen phases the most probable to appear was AV-6. The synthesis results showed that not only AV-6 but also AV-7 can appear in sodium free conditions. In fact, this trial resulted in three different frameworks: the expected AV-6, AV-7 and an unknown crystalline structure, figure 30.

The first remarkable result of this trial was the synthesis of AV-7. (trial P_5). To date it is known that the preparation of AV-7 requires sodium and potassium ions as these elements are part of its structure. In this work AV-7 was produced for the first time in sodium free conditions which resulted in chemically new stannosilicate. This result was not an exception and it was repeated in several compositions of trial P, in a pure form or in a mixed phase form material sharing crystalline presence with AV-6. The second remarkable result was the multiple production of a new, unknown, tin silicate phase. This material was called UM-2 (University of Minho – 2). UM-2 had a powder pattern very distinct from the other AV structures and it was successfully indexed as a pure phase.

This phase was successfully synthesized in trials P_{10}, P_{16}, P_{17} and P_{18}. Analyzing the compositions that resulted in this phase it is possible to say that this structure is favored by an increased presence of tin oxide. It is to believe that if the tin concentration were even higher the formation of this phase would occur in even more compositions.

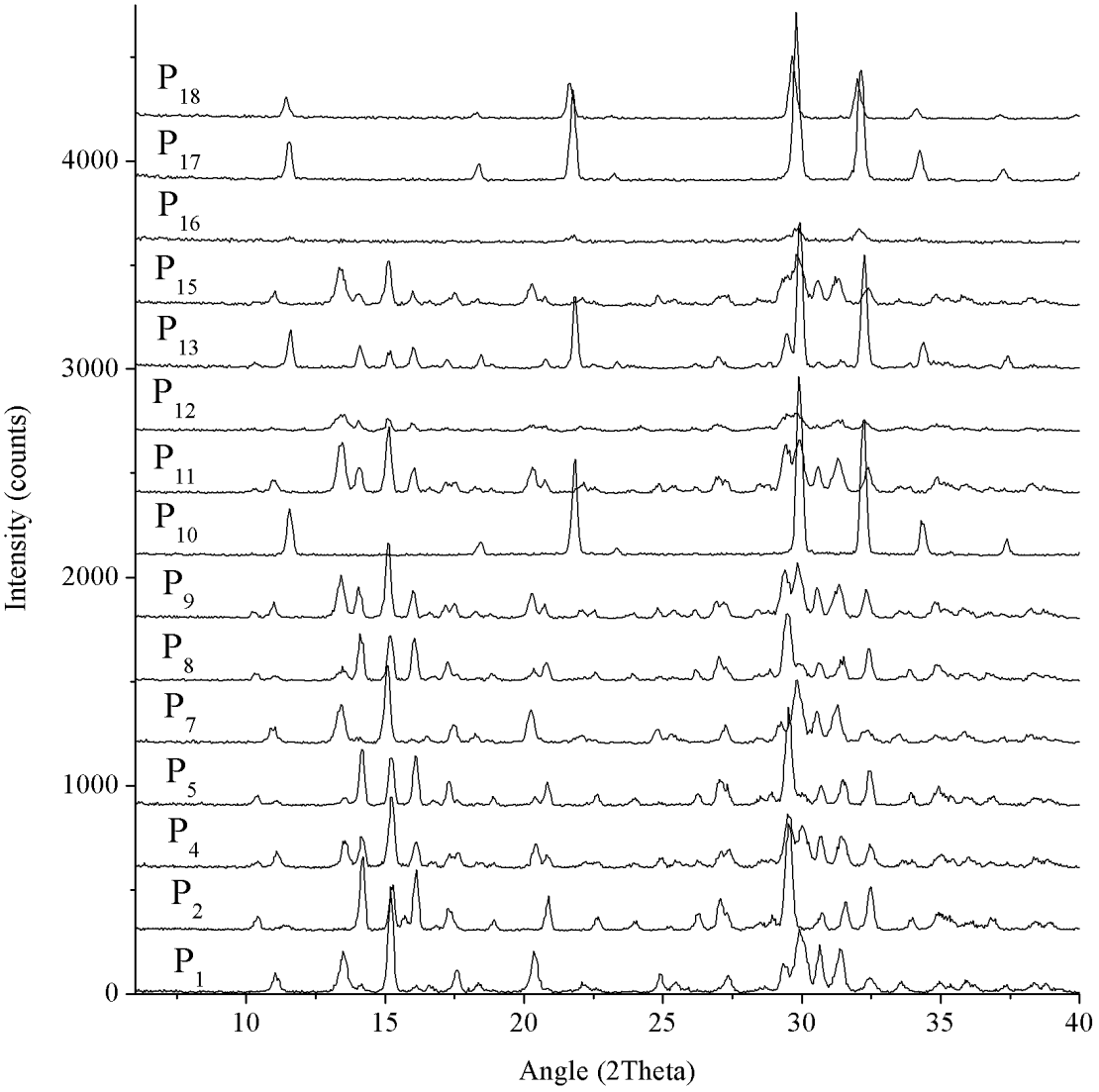

Figure 30. Experimental powder XRD patterns of trial P, 2 days synthesis and 15 minutes of precursor agitation.

After analyzing all the trials from trial P it was possible to see a clear dominance of AV-6 production. This was expected since the chemical composition of the precursors tested was in very similar to the chemical composition of this stannosilicate. Even in these favored conditions the majority of the samples resulted in a material with mixed crystalline structures. This may have happened due to the agitation time chosen to do these experiments.

As seen in the previous chapter (7.2.1 figure 29) time of agitation of 15 minutes favors the formation of AV-7 in certain compositions. Nevertheless, as seen in figure 29b not all compositions are influenced by the time of agitation. Some chemical preference for AV-7 must be established in order to obtain high purity materials. This is seen in sample P_5 where the result of synthesis was a nearly pure AV-7 structure.

The UM-2 had more difficult analysis. To understand phase formation it was necessary to characterize the sample, in terms of structural and chemical composition.

At the first identification tests, this phase shared many diffraction similarities with a potassium lutetium phosphate (PDF 01-085-1586). Using this material unit cell dimensions (a=9.601 and c=7.725) and space group (P-3) it was possible to get to the real lattice dimension of the new stannosilicate. These dimensions came from a related space-group and were significantly smaller, seen at table 22. Obtained by Le Bail method and by the use of a high resolution powder pattern, these dimensions and space-group rigorously respected the experimental powder pattern, figure 31, proving that this data represented a single crystalline formation.

Table 22. Crystallographic data from the Le Bail refinement performed to trial P_{10}.

Cell Type	Trigonal
Space Group	P-31m
a (Å)	5.55(1)
c (Å)	7.61(1)
Volume (Å^3)	203.05(2)
Crystal size (nm)	103±1
Rwp	9.6(3)

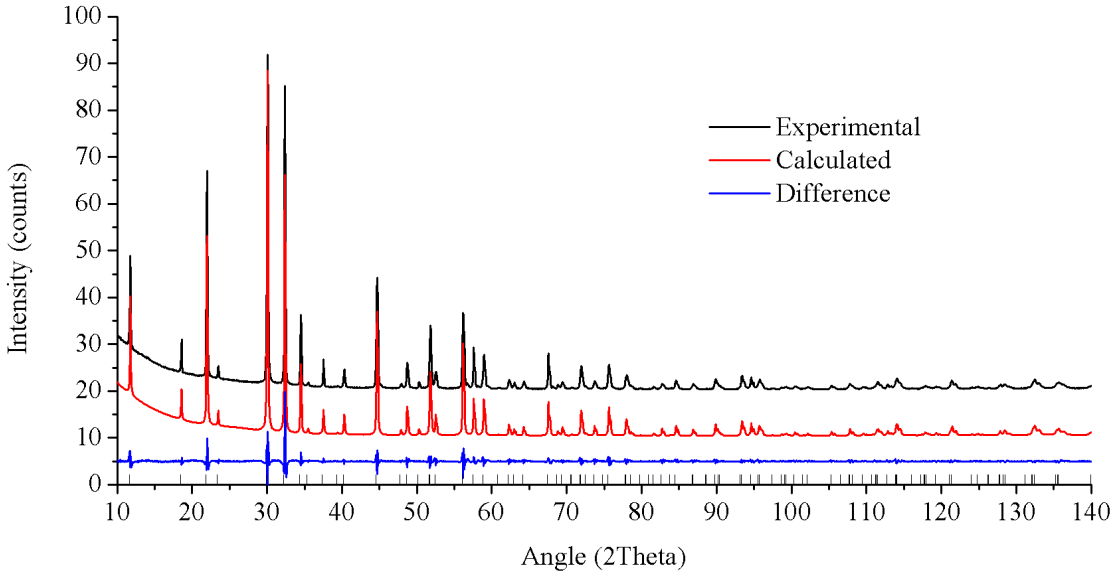

Figure 31. Experimental and simulated XRD patterns produced by Le Bail method of TOPAS 3.0.

With the true cell dimensions and supposed space-group the next step was the construction of this phase atomic distribution. The procedure that leads to the determination of the atomic distribution is still a not well defined process. The results come from many trial/error approaches but a successful result makes the material ready for any time of study. Normally the new structures are refined using similar frameworks. Those frameworks are changed into the new forms, by changing the chemical content and atomic positions by Rietveld refinement. In this case there was no available starting framework model to perform the Rietveld refinement so it

was necessary to create a framework from other atomic simulation procedures. To perform these procedures along with a high resolution powder pattern it was also necessary to have detailed information of the materials (unknown phase) chemical composition. Since the first was already assured, EDS was performed to obtain the chemical composition of this new phase. The results, seen in figure 32 and table 23, indicated that this material was composed of potassium, tin and silicon in equal atomic weight. The carbon detected was provided by the adhesive tape needed for the analysis and the oxygen values were discarded since this EDS was not accurate for these low weight atoms. This 1 to 1 to 1 element ratio is uncommon for synthesized stannosilicates, on AV-10, AV-6 and AV-7 the ratio is in all 1 Sn to 3 Si. In fact, the only stannosilicate structure to present a 1 to 1 ratio in Sn and Si is Sn-AV-11 [22], a structure produced from high temperature transformation.

Table 23. Chemical composition of trial P_{10}, obtained by EDS.

	Weight percentage (%)	**Atomic percentage (%)**	**Error (%)**
Sn	44.57	13.10	0.83
Si	12.03	14.95	0.84
K	17.64	15.74	0.78
O	22.77	56.21	1.16

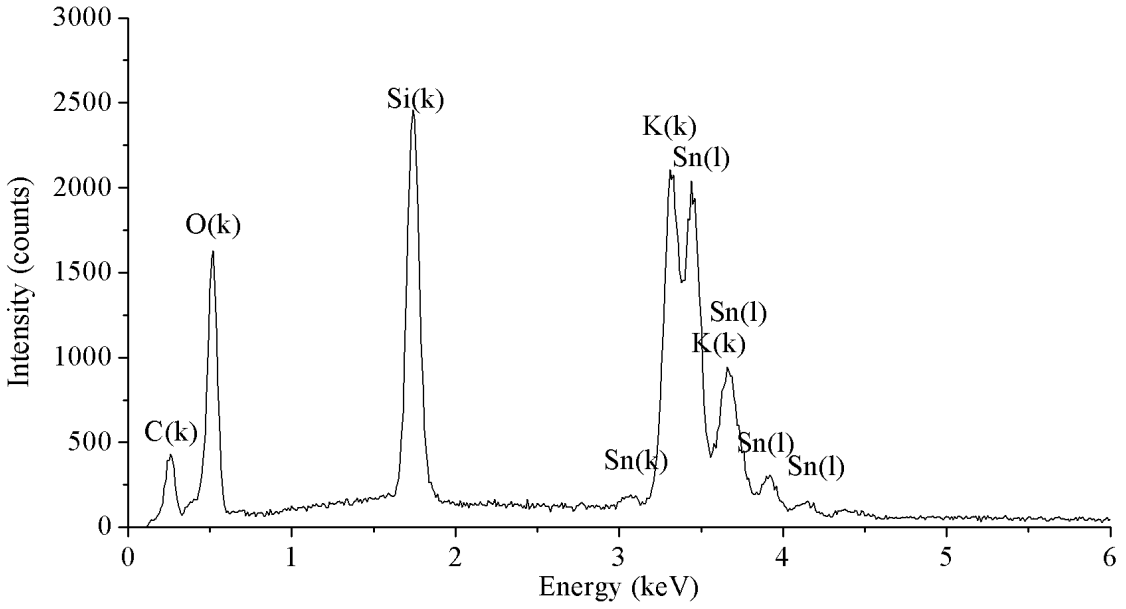

Figure 32. EDS spectrum of trial P_{10}.

After obtaining this vital information the simulation parameters were set and the structure search has started. At first, the simulation was performed on EXPO2009 and even in the early attempts the structure showed a layered nature with potassium as layer separator. During the simulation, potassium was always inside a ring formed by 6 tetrahedral elements and forming VIII coordination. After several attempts to simulate the missing octahedral tin and tetrahedral silicon a good and solid structure was produced. This structure respected the physical bonds between Sn-O (1.8Å to 2.2Å) and Si-O (1.5Å to 1.7Å) but after Rietveld refinement revealed some missing diffractions. This was enough to invalidate the simulation result and the simulation approach method performed. A new approach using EXPO2013 was performed next. The new structure software had new algorithms that produced different results. The layered form of the unit cell and the potassium position was preserved but the framework was produced in a different distribution. The 6-ring was now made from octahedral tin bonded to tetrahedral silicon. This structure had high density layers and small space between them, figure 32. All bonds and distances were in the correct physical values (data confirmed on Appendix 2) and the number of atoms corresponded to the one determined by EDS, a ratio of 1 to 1 to 1 in Si, Sn and K.

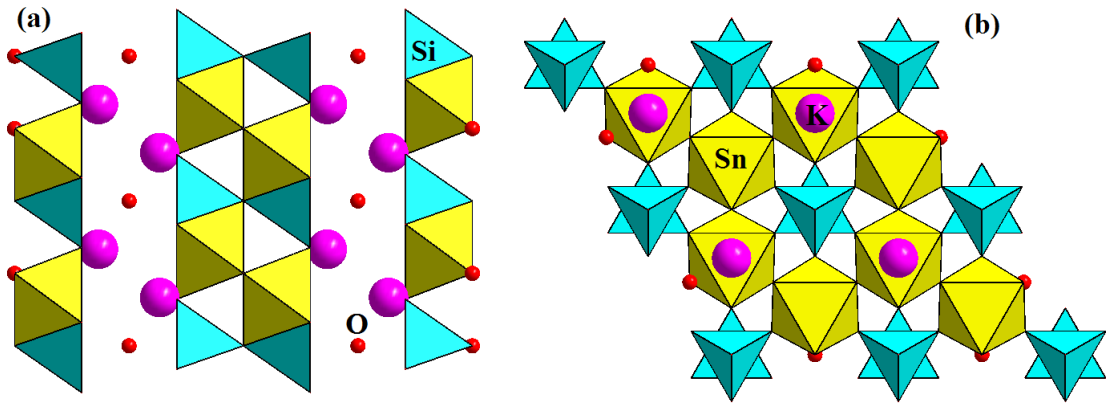

Figure 33. Representation of the developed structure for trial P_{10} (UM-2). Visualization in direction a (a) and direction b (b).

After Rietveld refinement, this structure revealed no missing diffraction peaks and no major deviations from the experimental powder pattern. Figure 33 shows the result from the Rietveld refinement and proves that the simulation work was well performed and this framework and atomic positions are the ones that represent this new stannosilicate.

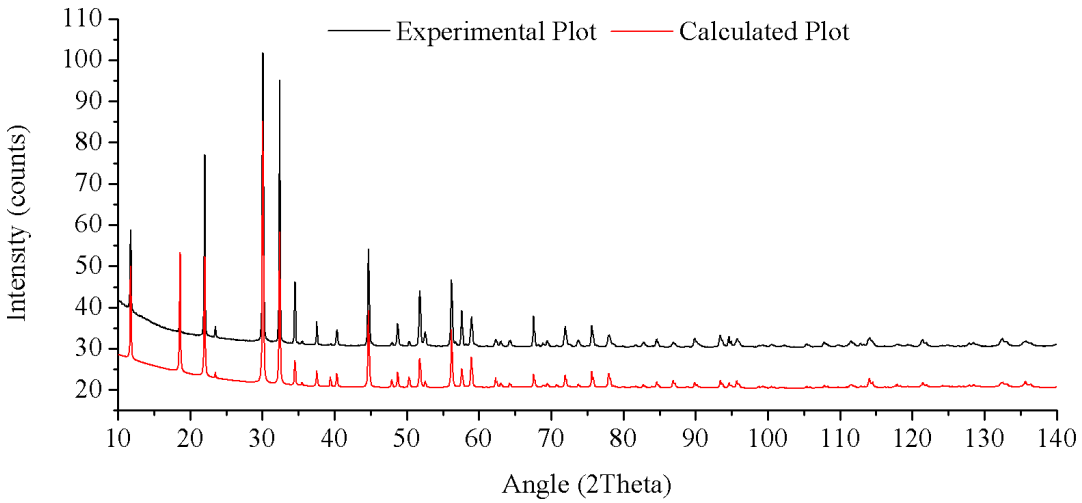

Figure 34. Experimental and simulated curve produced from Rietveld refinement procedure to trial P_{10}.

In terms of crystallographic data this simulation still needed some work, but the results reached here left no doubt about the structure of this new material.

This structure also presented some unique aspects in terms of powder shape. The SEM analysis showed morphology very different from the ones seen on the other discovered tin silicates. The material grew into cylindrical shaped grains, figure 35, connecting very closely into one another.

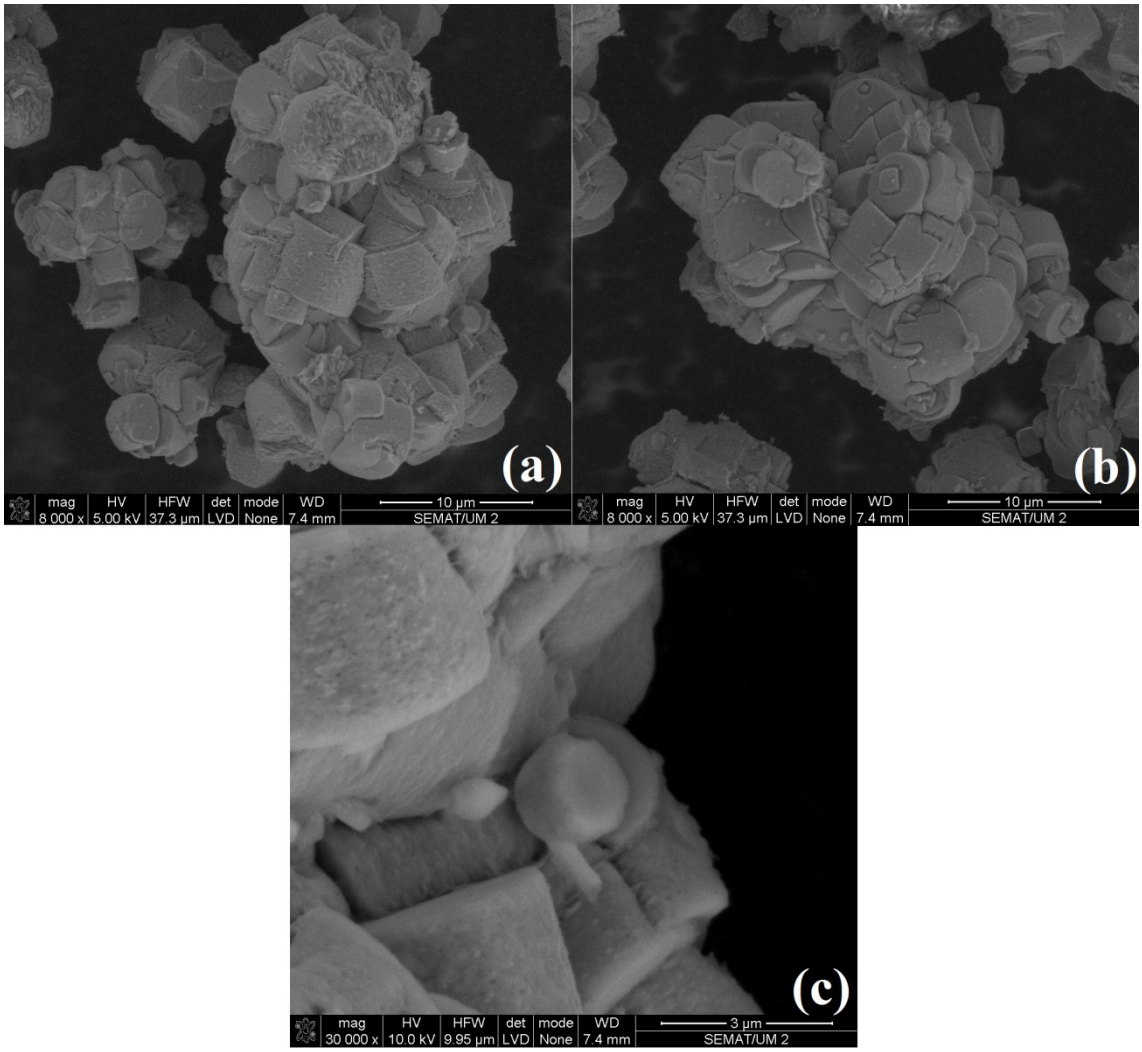

Figure 35. SEM images of the tin silicate layered phase (UM-2) (a) and (b) are different zones from the material and (c) a detailed image of the cylinders like particles.

The SEM images confirmed that this tin silicate was formed by a single phase. This phase was different from all the others seen in this work or any stannosilicate article.

Trial T_P, that served to study the influence of the precursor agitation time in two potassium-based tin silicate compositions that produced three distinct phases: AV-6, AV-7 and mixed phase AV-6 and AV-7. The first composition tested (TP_1 to TP_4), figure 36a, presented a nearly pure AV-6 powder pattern when at zero precursor agitation time (TP_1). As precursor agitation increased to 5 minutes (TP_2) the resulting powder pattern showed more AV-7 diffraction peaks and at 15 minutes (TP_3) the powder pattern was almost fully composted of AV-7. At 30 minutes agitation (TP_4) the amount of AV-7 in the material decreased. This meant that for the potassium compositions the maximum precursor agitation for the production of AV-7 is close to 15 minutes. Any increase after this time induced the nucleation of AV-6. Even without sodium this composition favored the formation of AV-7 nucleus. This allowed continued purification of the

material, showing at 15 minutes a nearly pure AV-7 phase. In this potassium-based composition the formation of AV-7 nucleus was slower. This was due to the chemical difference, the need for adaptation to a single potassium composition. Nevertheless, with the right precursor agitation time the nucleuses of the analyzed composition formed AV-7.

The second composition tested (T_{P5} to T_{P8}), on figure 36b, resulted in a mixed phase material with diffraction peaks of AV-6 more intense that AV-7 (T_{P5}). The same composition produced with 5 minutes (T_{P6}) of agitation resulted in a low crystallinity material. The 15 and 30 minutes samples (T_{P7} and T_{P8}) resulted in a material were both AV-6 and AV-7 structures were present. This indicated that the precursor agitation time had no effect on this composition. This was already seen in trial T_D; however, this time the initial composition did not favored any of the resulting phases (AV-6 or AV-7). In the first test with this chemical composition (P_{10}), the time of synthesis was 2 days and the resulting structure was the new layered phase. Synthesis carried out for four days resulted in a run product different than the new layered phase. This indicated that the hydrothermal phase stability is time dependent. It is clear that after a certain time the phase dissolves and transforms to a new stable product.

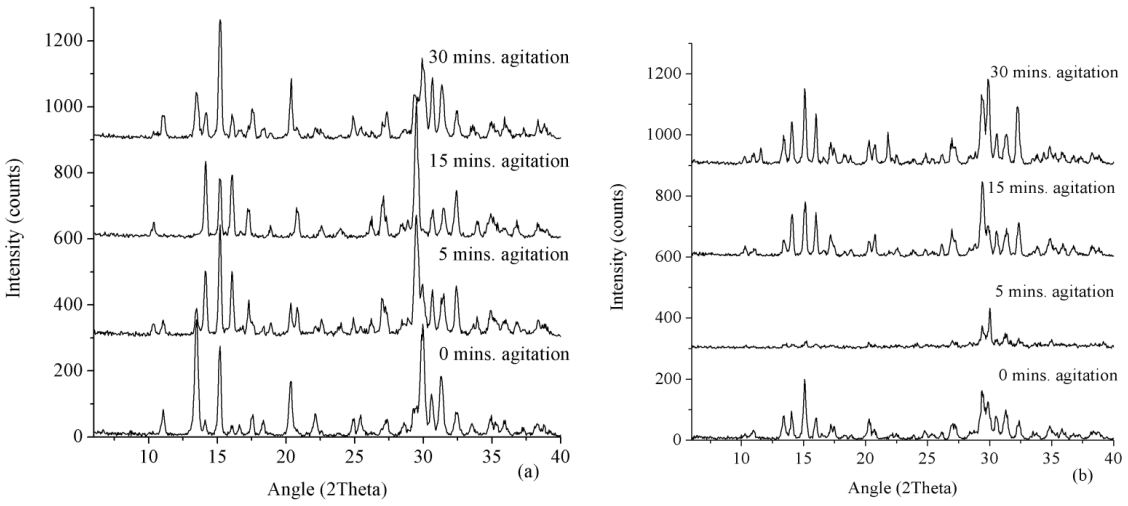

Figure 36. Experimental XRD powder patterns from trial T_P, 2 days of synthesis (a) and 4 days of synthesis (b).

Trial T_P showed once again the importance of the precursor agitation for the formation of the stannosilicate structures. In short time syntheses this parameter can influence the resulting structure. It was also seen that in situations where the structures formed collapse and then recrystallize from the collapsed products the change in agitation time has no influence in the final structure formed. To better understand the time of agitation effect on the formation of AV-6 or AV-7 Rietveld refinement was performed. The refinement gave the percentage of AV-6 and AV-7 in all the produced materials. These values show an increase in AV-7 percentage has time of agitation

increases. It also shows that after 15 minutes that amount of AV-7 phase starts again to decrease, figure 37a. This was the only difference between the potassium composition (Trial T_P) and the sodium - potassium composition (trial T_D). Figure 37b shows the phase percentage of the run product that started as the new layered potassium stannosilicate. As seen above this layered phase is time dependent and after four days the run product is composed from AV-6 and AV-7. It is not possible to see any dependence on the time of agitation since the AV-6 and AV-7 phases were formed after the dissolution the layered phase and therefore had all the same ion distribution.

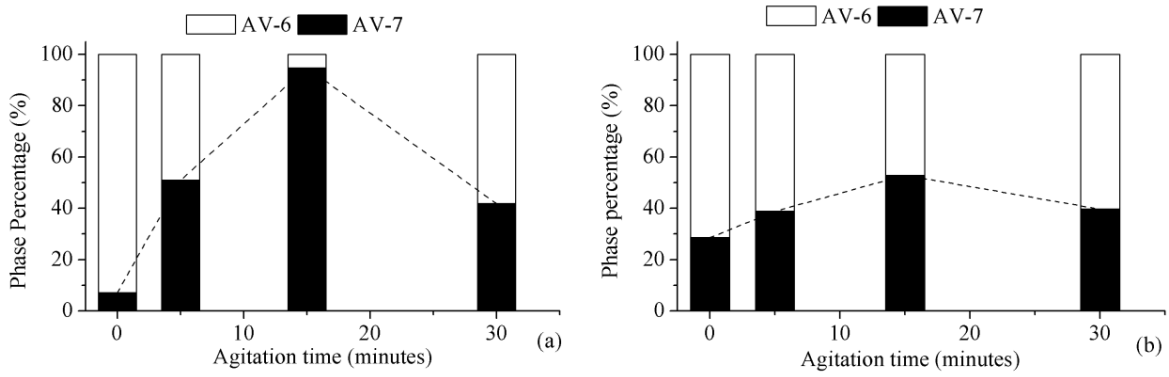

Figure 37. Phase percentage evolution for trial T_{P1} to T_{P4} (a) and trial T_{P5} to T_{P8} (b) (Values calculated by Rietveld refinement).

The formation of sodium free AV-7 was confirmed by EDS. In the analyzed sample, trial T_{P3}, it were only detected Si, Sn and K The obtained Sn:Si (1:3) ratio corresponds to the one reported in the literature (23). Table 24 shows all the atoms detected by EDS. Oxygen and carbon that have large associated error and were not important for the analysis.

Table 24. Chemical composition of trial T_{P3} obtained by EDS.

	Weight Percentage (%)	**Atomic Percentage (%)**	**Internal error**	**Atoms ratio**
Si	17.91	17.69	0.66	2.9
K	18.16	12.89	0.79	2.1
Sn	28.41	6.64	1.09	1.1
Others (O and C)	35.52	62.78	5.41	———

The SEM images showed two different shaped grains. This was consistent with the information from XRD that indicated that the material was formed from AV-7 and small amounts of AV-6. Figure 38 shows large amounts of typical shaped AV-7 crystals (seen in figure 27a) surrounded by small amounts of different shaped grains. These grains are the small amounts of

AV-6 detected on the XRD powder pattern. The AV-7 material was composed of large and small well defined crystals and the AV-6 material of small spherical particles.

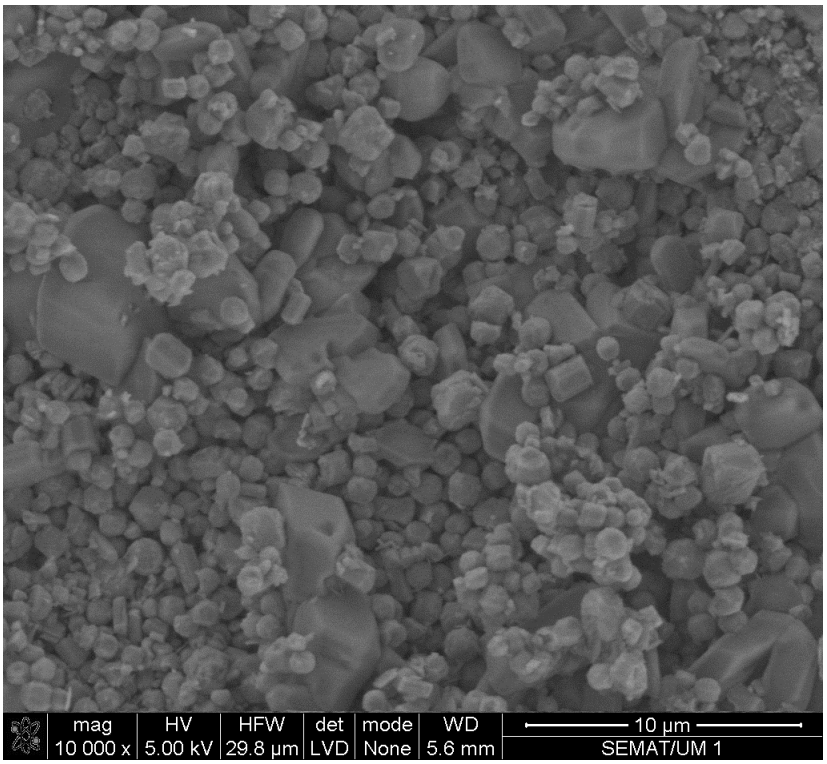

Figure 38. SEM image of Trial T_{P3}.

Trial T_P showed that the layered phase was not stable for 4 days synthesis, showing therefore a very high sensibility to the synthesis parameters. This was confirmed on trial T_L, where the same P_{10} composition was performed in different synthesis conditions. The precursor agitation time was changed and the synthesis time was 1 and 2 days in order to test the same conditions as the first successful try. The results, figure 39, showed that this phase (in this composition) could only be synthesized in 2 days and for 15 minutes agitation. Any variation of these conditions and the result was a low crystallinity material or a material with mixed phases, AV-6 and AV-7. As seen before this structure has a 1 to 1 ratio between tin and silicon explaining the difficulty of its production in a composition that as 1 to 5 ratio. Due to the chemical instability and the small amount of tin available this structure only managed to grew in very restricted synthesis conditions. However, these are just suggestions about the synthesis behavior of this new phase. Only more experiments with different compositions and with different parameters can explain the mechanism of production of the new layered potassium stannosilicate.

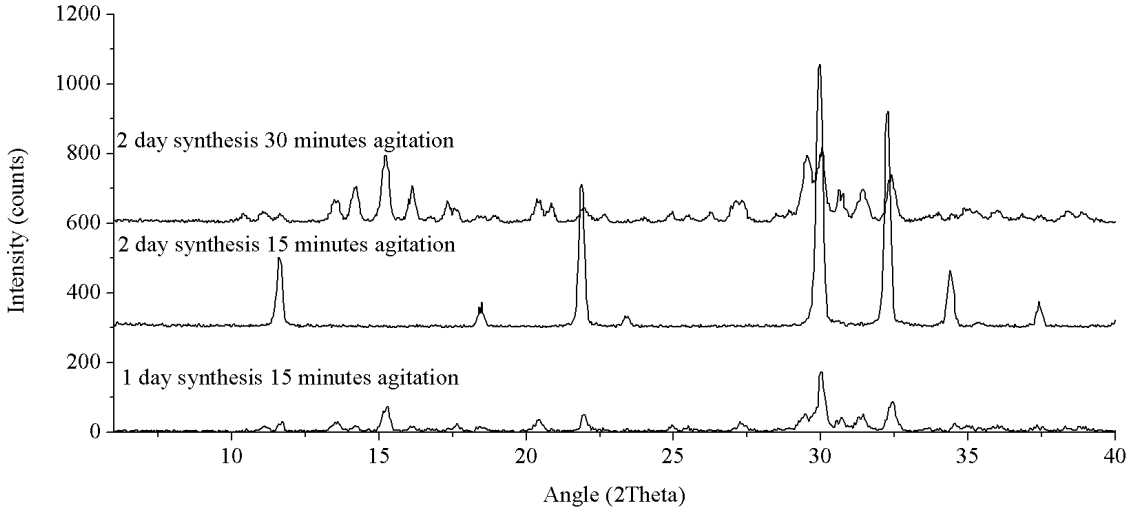

Figure 39. Experimental powder XRD pattern of trial T_L. Synthesized with P_{10} composition at various conditions.

Only three out of the five experiments resulted in solid material but it was interesting to see that in 24 hours some crystalline material is already formed. The run product of the 24 hours sample had very low crystallinity but the main diffraction peaks of AV-6 were already identifiable.

7.3 Crystallization fields

The systematic syntheses performed here helped the discovery of unknown phases and established new optimized conditions for hydrothermal synthesis of various tin silicates. The characterization of the run product from different chemical compositions resulted in creation of fields of crystallization that can serve for phase prediction and starting point for further studies.

7.3.1 Sodium-based Stannosilicates

The sodium-based tin silicates crystallization field, presented in figure 40, shows the dominance of the UM-1 (seen in Trial C_{20}). Along with the results from the tested compositions, the field also allows the result prediction of compositions with similar values to the ones tested. UM-1 can be seen at all the compositions marked with its symbol (new phase) and at all the untested compositions that were compressed in the dashed line. In this field it is also possible to see the compositions that resulted in AV-10. This phase is located at the bottom of the field in compositions with equal amount of sodium. This indicates that for tin values between 1.5 and 2 moles and with sodium and silicon at 5 moles the resulting composition (to these synthesis parameters) would most likely be AV-10.

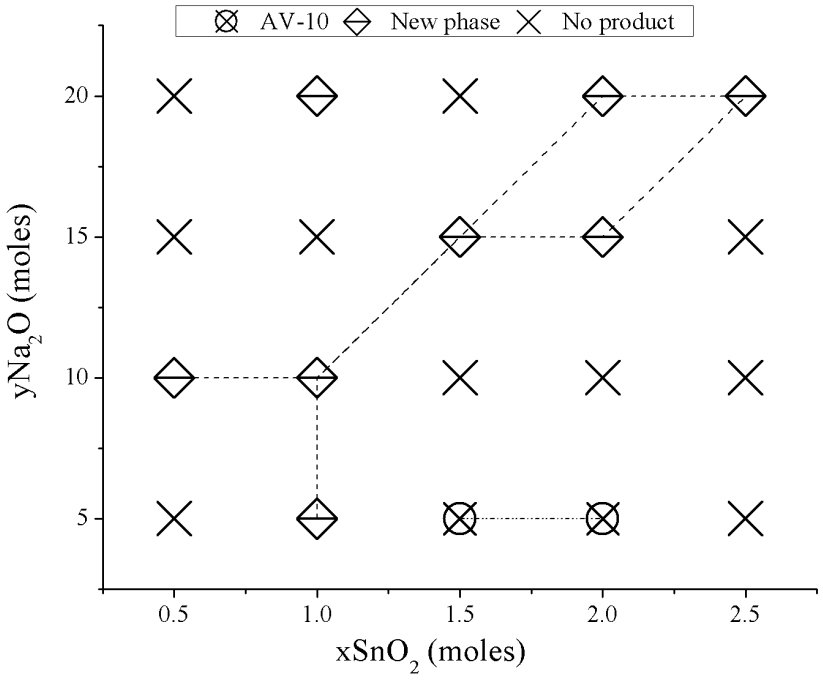

Figure 40. Crystallization field of the sodium-based stannosilicates. Produced for 2 days of synthesis and 15 minutes of precursor agitation, based on trial C.

The diagonal lines represent compositions with the same ratio between ions. The diagonal lines closer to the origin of the field were proven to be the best compositions to perform the unknown sodium phase (figure 20). There were some deviations but they only proved the

higher stability and dominance of UM-1. AV-10 appeared in a horizontal line but tests performed at different compositions with the same element ratio (Trial E) revealed that this phase also followed diagonal lines of crystallization. The field also showed many compositions without successful synthesis. These no product points were one of the reasons to create this crystallization fields. By the identification of the non-productive compositions this work is providing great help for future investigations.

On chemical aspects this field proved that the ratio between sodium and tin was very important. The majority of the formed structures were produced in medium ratios of $NaOH/SnCl_2$. The extreme ratios, high and low, located at the field's superior left corner and inferior right corner, respectably, were non-productive zones. This ratio also influenced the structures stability after crystallization. The high reactive environment produced by sodium resulted in fast degradation of the formed crystals. Even in a low synthesis time, 2 days, the productive compositions already presented large signs of amorphization. This was the main obstacle in this composition field, due to the material degradation the new sodium phase was not possible to identify and the AV-10 produced was not of a pure nature. Despite that low crystallinity this was the first time that AV-10 was produced in a single step hydrothermal synthesis and in a time much sorter then the one of its publication. Is not yet been proved that pure AV-10 can be produced from a single step synthesis with sort time.in oven. Nevertheless, this work has showed promising results in this aspect.

7.3.2 Sodium- and Potassium- based Stannosilicates

The sodium- and potassium-based crystallization field, figure 41, revealed even more information: the compositions where AV-6 and AV-7 the mixed phases are. These two phases dominated the entire crystallization field but AV-7 showed more pure forms and a larger average percentage in the mixed phase compositions. Several compositions, following diagonal, horizontal and vertical lines, revealed to be very effective in the production of AV-7. This indicated the great stability of this structure in solutions with sodium and potassium even in a new hydrothermal synthesis procedure. AV-6 appeared more scattered and with lower purity and inferior stability. The number of compositions that resulted in a crystalline run product was superior to the ones seen in other fields This shows that sodium and potassium were not direct substitutes but complementary ions that performed different functions within the solution.

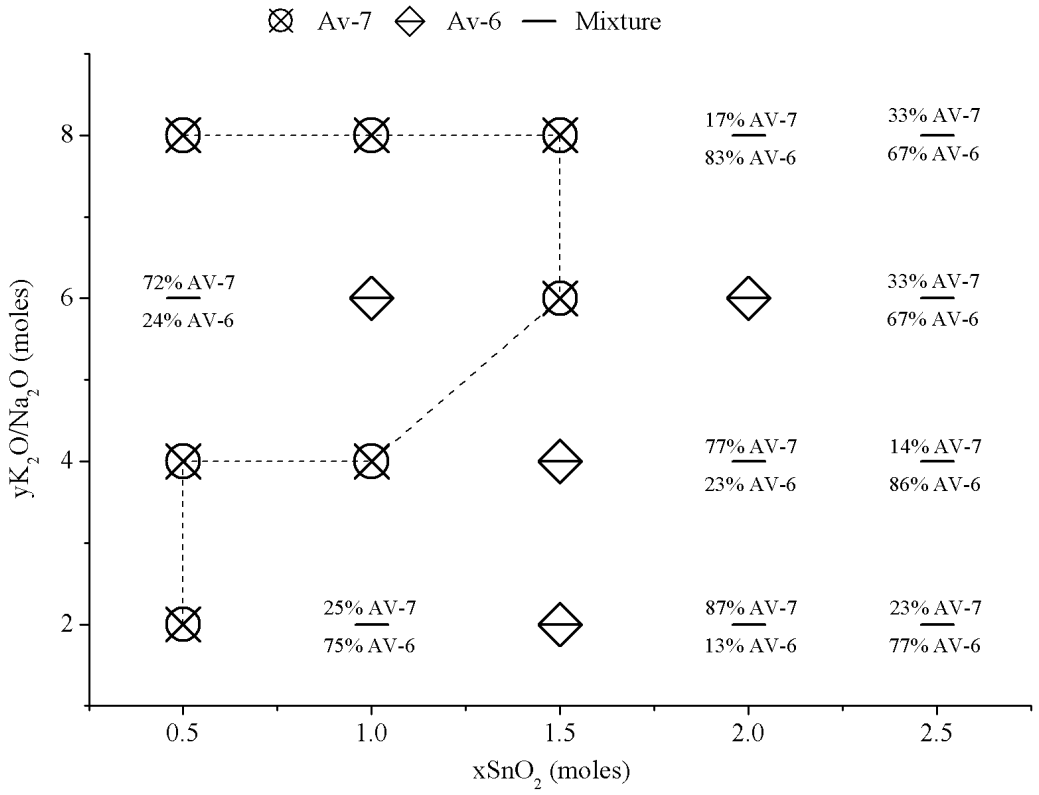

Figure 41. Crystallization field of the mixed sodium- and potassium- based stannosilicates. Performed for 2 days of synthesis and 15 minutes of precursor agitation, based on trial D.

The formation of AV-6, in this crystallization field, was very difficult due to the continuous formation of AV-7 nucleus at very early stages. Those nucleuses were induced to grow by the precursor agitation time, 15 minutes. As seen before, the nucleus AV-6 and AV-7 appeared with higher or lower concentration depending on the precursor chemical composition. However, due to the precursor agitation time effect on the formation of AV-7, the synthesis conditions of this crystallization field eventually favored the formation of AV-7. If no agitation was provided this crystallization field would certainly be dominated by AV-6. This assumption was based on the results from trial T_D that revealed this untested behavior in a transparent precursor hydrothermal synthesis. The combine effects of sodium and potassium ensure that every composition had a solid tin silicate as final result.

7.3.3 Potassium-based stannosilicates

This last crystallization field showed fewer compositions crystalline run product when compared with the previous one. As seen before sodium and potassium are complementary in synthesis. A single alkaline composition has less changes of producing high crystalline run products. This effect depends on the chemical stability created by the alkaline ions (when single or together) but in sodium and potassium compositions the formation of solid run products seems favored. The materials produced here had lower grain size and lower crystallinity. Despite that, this field presented two important results. The first was the formation of AV-7 without the presence of sodium. The second was the formation of a layered phase (UM-2), stable in several compositions. The crystallization tendencies of AV-6, AV-7 and UM-2 are described in figure 42. The field maps each phase and allows the understanding of the parameters that influenced the formation of each one.

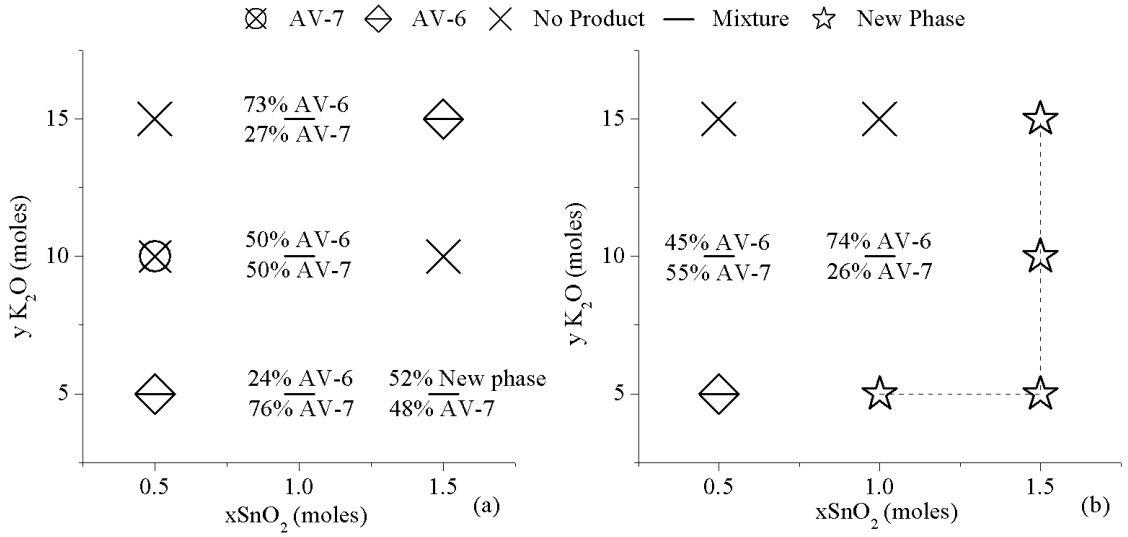

Figure 42. Crystallization field for the potassium- based stannosilicates. The synthesis was performed for 2 days and 15 minutes of precursor agitation, based on trial P.

Very few compositions produced AV-7. Even within the compositions that produced materials with mixed phases AV-7 was in the majority of cases in inferior percentage. It is to believe that these compositions presented some AV-7 due to the agitation time given to the precursor. A crystallization field performed with shorter agitation times would probably have lower presence of AV-7. This field shows the compositions to obtain a pure AV-6 material without the use of sodium. This is also a new form of synthesis proved in this work. In fact, in this work, the production of AV-6 using a single alkaline ion in the precursor (K^+) proved to be more efficient than the common production using sodium and potassium. The field also shows the compositions to produce the new UM-2 material. These compositions were the ones that had a

closer ratio of tin, silicon and potassium. These results are concurrent with the material chemical composition since UM-2 as a 1 to 1 to 1 ratio in Sn, Si and K. Along with this relation in ratio the best compositions to form the layer phase where also the ones that had 5 moles of SiO_2. With only 2.5 moles of SiO_2 the only thing achieved was a mixed phase material with 52% of UM-2.

The studies performed to the P_{10} composition showed that this was a sensitive point of crystallization. However, it is to believe that the other points of the layer phase (P_{16}, P_{17} and P_{18}) formation would have larger tolerance for the synthesis parameters. This would happen due to the closer resemblance between composition and structure chemical composition. This was the crystallization field more influenced by the precursor agitation time. This parameter lowered the production of AV-6 but also allowed the formation of a chemically modified AV-7 and the production of an undiscovered tin silicate, the layered phase.

7.4 Ion exchange properties

Due to the good crystal quality the ion exchange experiments were directed to AV-6 and AV-7. The crystal quality of AV-10 was not sufficient for ion exchange and the new sodium and potassium phases are still under structural characterization and the ion exchange experiments will be a matter of future works.

7.4.1 Ion Exchanges on AV-6

In order to get a complete ion exchange high concentration (1Mole) solutions of selected metal ions were used. Ion exchanges with Na^{+}, Cu^{2+}, Zn^{2+} and Cr^{3+} at 80°C for 48 hours were performed. The XRD patterns, in figure 43, show that copper and zinc ions result in changes similar to the ones reported in literature [28]. The other ions (Na^{+} and Cr^{3+}) showed no alterations in relation with the original powder pattern of AV-6. These results indicated that copper and zinc ions are incorporated in the pores of AV-6 structure and that chromium and sodium have no detectable influence on the structure. These two elements were washed away by the filtration process.

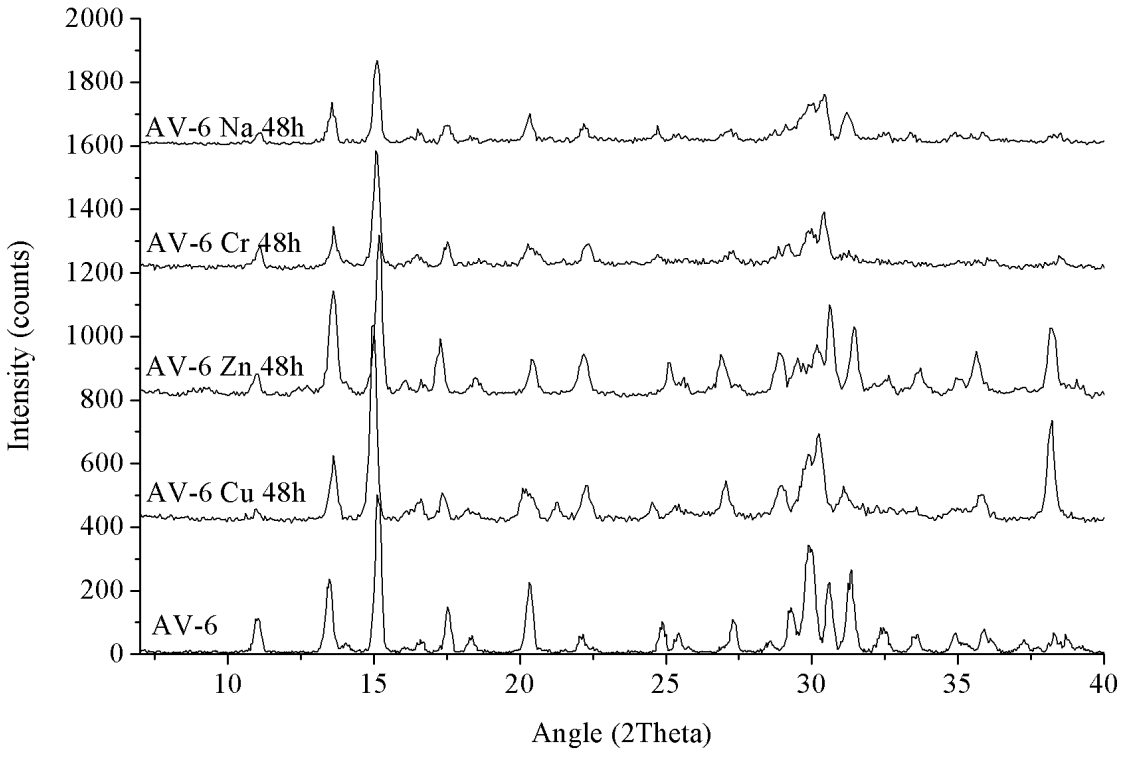

Figure 43. Experimental powder XRD patterns from the ion exchanges of AV-6. Performed at 80°C during 48 hours.

Sodium and chromium exchanges only revealed a general decrease on crystallinity and no of its diffraction peaks suffered any displacement. Considering that sodium ion exchange has been previously realized on titanium silicate with AV-6 (umbite) structure (AM-2 [13] the obtained results indicate that structurally equivalent and chemically different materials show different ion

exchange properties. This finding could allow selective targeting of selected elements by changing the structure forming metal elements.

In spite of some studies that, within a certain size resemblance, higher charged ions have higher affinity to be exchanged in a microporous framework [33] the attempt for heterovalent ion exchange of K^+ by Cr^{3+} showed that the ionic radius difference is of main importance. Chromium (Cr^{3+}) has an ionic radius of 0.615Å [46] for a VI coordination and potassium (K^+) 1.38Å [47] for the same coordination. This difference is the main reason for lack of affinity of AV-6 to the chromium ion.

Copper and zinc ion exchange were already successfully realized for AV-6 [28]. In this work the ion exchange was performed at higher temperature than in the reported success [28] producing therefore a more reactive exchange environment. The purpose of the ion exchange with copper was to study the structural changes and possible use of AV-6 as a material for capture of polluting agents. Le Bail refinement showed that the ion exchange with Cu^{2+} change the initial orthorhombic *($P2_12_12_1$)* structure of AV-6 to monoclinic one *($P2_1/c$)*. This result was confirmed when the ion exchange is carried out for 24, 48 and 72 hours. The details of the refinement are shown in table 25 and the obtained powder patterns in figure 44.

Table 25. Crystallographic data from AV-6 ion exchanges with copper. Exchanged for 24, 48 and 72 hours.

	AV-6 Cu form (24h)	**AV-6 Cu form (48h)**	**AV-6 Cu form (72h)**
Rwp	10.4(6)	10.1(5)	8.9(1)
GOF	2.6(5)	2.4(8)	2.2(2)
R-Bragg	1.9(2)	1.7(9)	1.5(8)
Space group	$P2_1/c$	$P2_1/c$	$P2_1/c$
Volume (Å^3)	955.81(8)	952.45(2)	952.42(4)
Crystal size (nm)	52.5±0.1	47.4±0.1	47.7±0.1
a (Å)	7.22(8)	7.22(1)	7.22(1)
b (Å)	10.15(6)	10.14(4)	10.15(1)
c (Å)	13.02(1)	13.00(2)	12.99(5)
Beta (◦)	90.91(1)	90.88(1)	90.83(2)

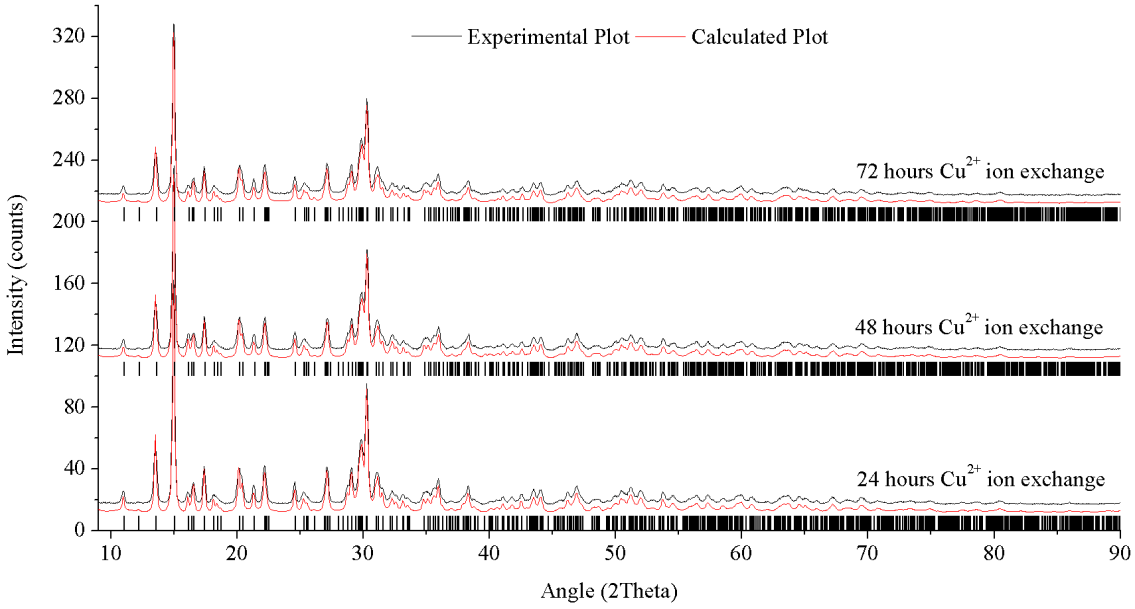

Figure 44. Experimental and simulated powder XRD patterns form the Le Bail refinement on the ion exchanged Sn-umbite. Exchange with copper for 24, 48 and 72 hours.

The change from orthorhombic to monoclinic space group was followed in three steps - 24, 48 and 72 hours. In these three steps the monoclinic symmetry is preserved and only small variation in the lattice metrics were detected. Over the time, the amount of copper in pores was also unchanged. This means that within 24 hours the copper accommodates in the pore of AV-6. Increasing the temperature of ion exchange (from 50°C to 80°C) allowed the production of almost fully exchanged ($K_{0.98}Cu_{0.51}Si_3Sn_1 \cdot 2H_2O$) Cu-AV-6 materials at 24 hours.

The observed ion exchange and the structural characterization of Cu-AV-6 was published in Journal of Porous Materials [48]. In conclusion, it is shown the detailed structural characterization of Cu-AV-6 and affinity of AV-6 to capture copper ions in water solutions.

Despite the close resemblance to copper, zinc ion behaved slightly differently. Both ions have oxidation state of two and very similar radii 0.73Å to copper [49] and 0.74Å to zinc [50], but in water solutions their affinity to the pore space of AV-6 is different. The XRD pattern of zinc treated AV-6 show reflections typical for the original orthorhombic and distorted monoclinic symmetry. Thus, after 48 hours, a mixture of two different phases was observed: one with the typical structure of AV-6 and one with a monoclinic space-group and undetermined amounts of zinc. The Rietveld refinement, figure 45 and table 26, show that the zinc ion exchange (48 hours) resulted in 40% of orthorhombic and 60% of monoclinic phase.

Table 26. Crystallographic data from Rietveld refinement of the exchanged form of AV-6, exchange with zinc at 80°C during 48 hours.

	Modified AV-6 (Monoclinic)	**AV-6 (Orthorhombic)**
GOF	2.4(9)	
Rwp	33.0(9)	
Phase percentage (%)	59.9(1)	40.0(9)
space-group	$P12_1/c$	$P2_12_12_1$
a(Å)	7.08(3)	7.07(7)
b(Å)	10.23(2)	10.28(5)
c(Å)	12.99(2)	12.98(7)
β(°)	90.67(6)	90
Volume	941.61(5)	945.50(1)
crystal size	55.2±0.1	63±0.1

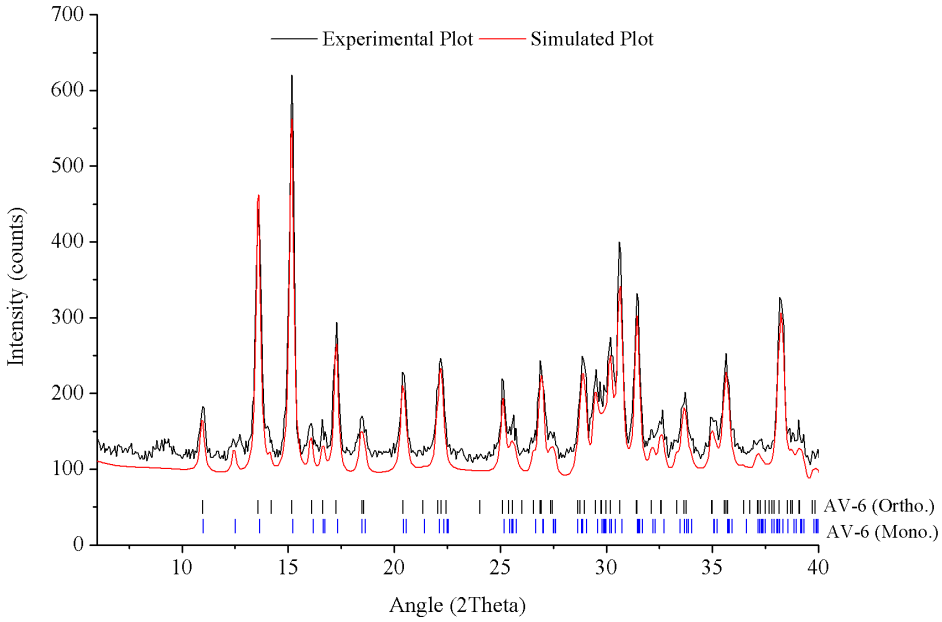

Figure 45. Experimental and simulated curves from the exchange with zinc. Simulation done using TOPAS 3.0.

This proved that the space-group transformation was again uncompleted even at elevated temperatures for ion exchange. Therefore the framework selectivity of AV-6 goes beyond size and charge of the element.

Due to the higher reactivity of the selected ions the other exchanges on AV-6, with Al and Pb, were performed at lower temperatures and shorter times. In previous studies [28] the attempts to exchange AV-6 with these ions led to the material amorphization. However, as shown in figure 46, at lower temperatures AV-6 easily withstand the presence of aluminum and also keeps some of its crystallinity when it is in contact with Pb ions. The exchange with Pb^{2+}, that forms several types of coordination [51], was performed at lower concentrations than the other

exchanges. Despite that, this was the element that caused more destruction to the microporous structure. The sensibility to this particular element was very high and even at lower temperatures or shorter times the result is partial amorphization.

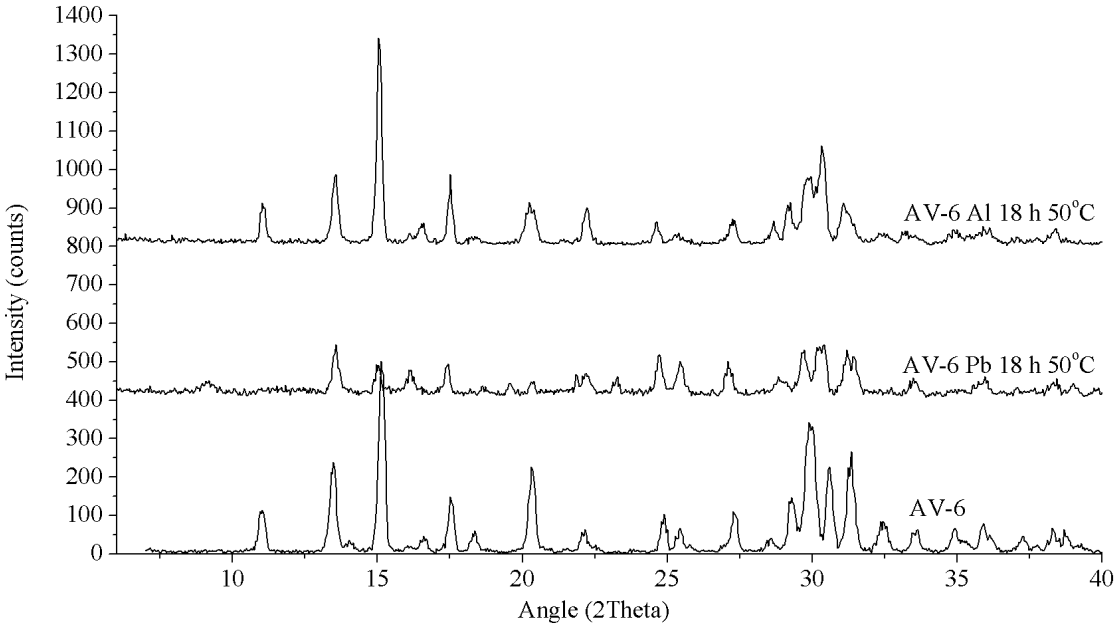

Figure 46. Experimental powder XRD patterns of the AV-6 ion exchanges with Pb^{2+} and Al^{3+}. performed for 18 hours at 50°C.

The exchange with Al^{3+} showed no signs of structural destruction. The experimental powder pattern show great similarity to the copper exchanged phase. The Rietveld refinement (TOPAS), table 27 and figure 47, revealed that the exchange with aluminum may have changed the orthorhombic structure of AV-6 to monoclinic one. The low resolution powder pattern indicated that this trivalent ion may have entered the pores of this microporous material. The fact that aluminum has the same IV coordination [52] as the copper has suggested that the exchange was possible.

Table 27. Crystallographic data from the Rietveld refinement. AV-6 ion exchange with aluminum.

	Modified AV-6 (Monoclinic)	**AV-6 (Orthorhombic)**
GOF	1.5(1)	
Rwp	31.1(1)	
Phase percentage (%)	96.3(9)	3.6(1)
space-group	$P12_1/c$	$P2_12_12_1$
a(Å)	7.24(3)	7.21(2)
b(Å)	10.15(1)	10.09(8)
c(Å)	13.09(9)	13.01(3)
β(°)	90.71(8)	90
Volume	963.2(1)	947.89(5)
crystal size	58.9±0.1	65.1±0.1

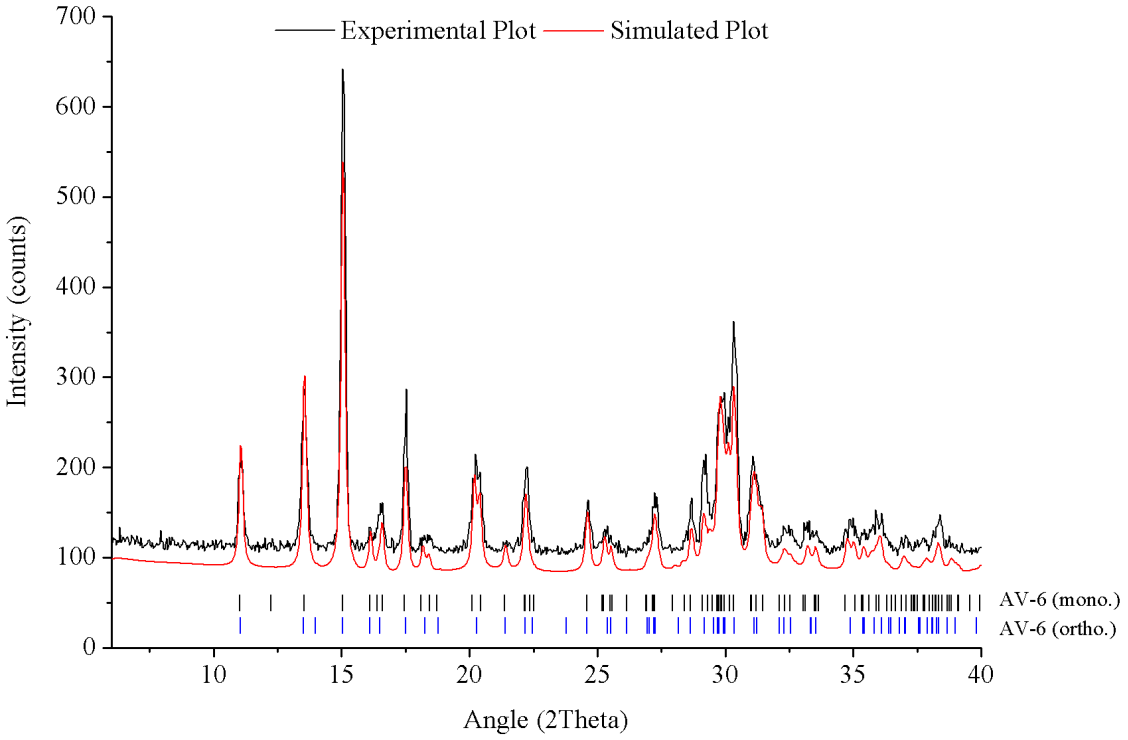

Figure 47. Experimental and simulated curves from the TOPAS 3.0 Rietveld refinement. AV-6 ion exchange with aluminum for 18 hours at 50°C.

However, the EDS analysis seen at table 28, showed no presence of aluminum. The changes on the low resolution powder pattern may have been done by the aluminum chloride solution but the ion had not entered the porous structure. Clearly the differences seen in this powder pattern were misleading since the AV-6 material remained chemically unchanged after the attempted exchange in aluminum ions.

Table 28. EDS results of AV-6 exchanged with aluminum.

	Weight Percentage (%)	**Atomic Percentage (%)**	**Internal error**	**Atoms ratio**
Al	0.38	0.34	12.35	0.068
Si	17.49	15.42	0.81	3.084
K	9.64	6.1	1.34	1.22
Sn	26.85	5.6	1.36	1.12
Others (O and C)	45.64	72.53	4.74	———

Despite the absence of aluminum, this AV-6 sample presented upon SEM analysis a unique powder shape. Its morphologic aspect was very different from the one seen on the copper exchange [48]. This material presented much more gaps between the crystallites, figure 48, agglomerates of prismatic/needle like particles. These changes in morphology did not come from the ion exchange procedure, but probably from the synthesis parameters. The first AV-6 SEM

image seen was from a 4 days synthesis this one was produced in a two days synthesis procedure. Any change on synthesis time or chemical composition could have changed the crystals growth method. This also proved that the new hydrothermal synthesis method was capable of producing unique shaped materials, different from the ones produced with a white gel precursor.

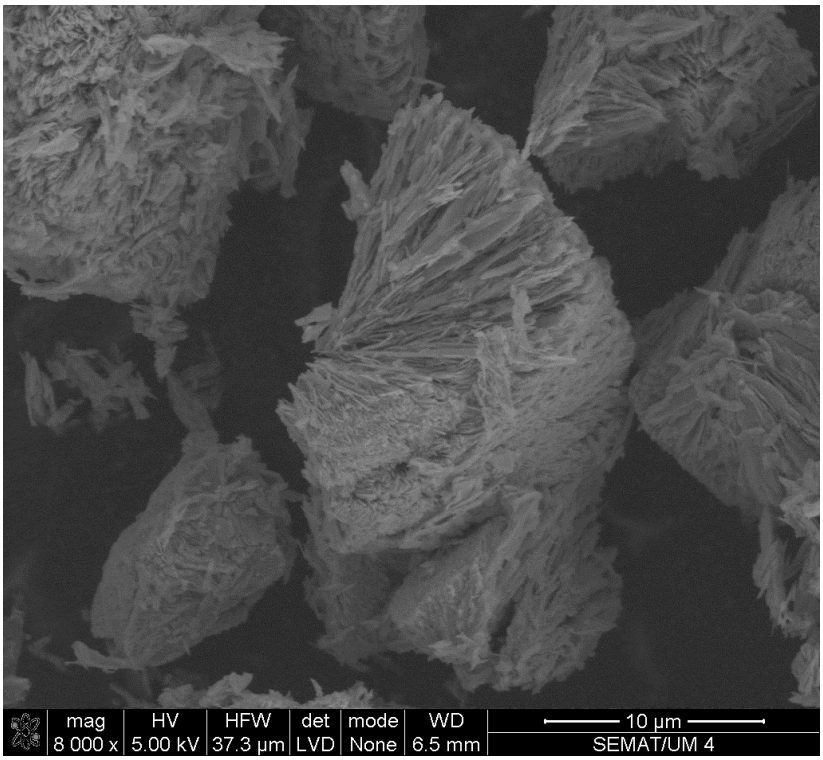

Figure 48. SEM image of Av-6 produced by a clear precursor. Attempt of ion exchange with aluminum.

The ion exchanges on AV-6 revealed structural affinity to Cu and Zn ions. In the tested conditions this stannosilicate showed no affinity to uptake ions as Na, Al, Cr or Pb. This means that AV-6 can be used for selective capture of Cu and Zn in the presence of certain concentrations of the mentioned elements.

7.4.2 Ion Exchanges on AV-7

This untested structure revealed a different behavior when exposed to ion exchanges. The XRD powder patterns, figure 49, showed significant changes after different ion exchange. Copper and zinc ions, that had similar behavior in AV-6, showed different interactions with AV-7. The coordination number of charge compensation cations (K^+ and Na^+) in the pores of AV-7 is eight. Since the copper cannot form this type of coordination [46] its capture resulted in a distortion of one of the diffraction planes (located at 15.3° 2Theta). Zinc ion, however, can perform eight coordination [47] so when captured there was no significant distortion. These distortions were later on quantified by Rietveld analysis.

Chromium ion, that had no effect on AV-6, resulted in distortion of AV-7 that is similar to the one observed by the copper ion in the same structure. Sodium and cesium ion exchanges produced no changes in the powder XRD patterns. These ions can have coordination 8 [50-51] but the powder XRD pattern shows that there was no located loss of intensity. This suggested that the exchange was not successful. The other ion exchanges, with strontium and iron, destroyed the crystal structure.

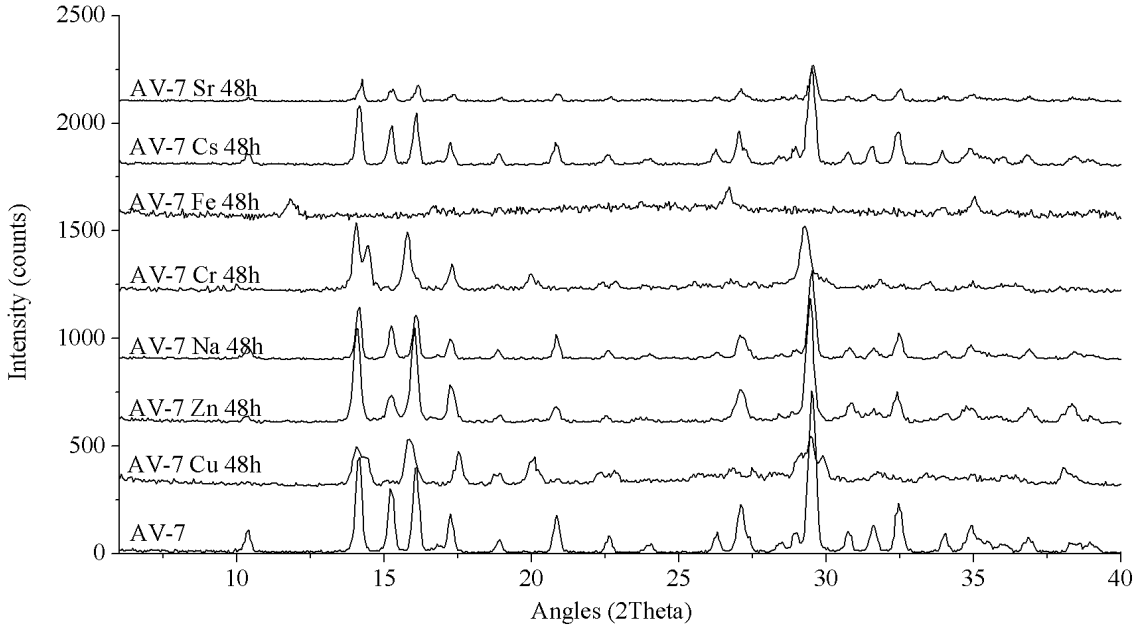

Figure 49 Experimental powder patterns of the ion exchanges of AV-7. Performed at 80°C during 48 hours.

The pH of the solutions for ion exchange varied between 3 and 7. Aluminum, chromium and iron solutions had pH lower than 3. Lead, zinc and copper had a pH of 5 and sodium and strontium a pH near to 7. The results showed that Pb and Sr caused much more destruction than Al or Cr. This indicated that the nature of the ion exchange element was clearly more important than the pH of the used solution.

The ion exchange kinetic of chromium was studied for 3 different times: 24, 48 and 72 hours. The XRD patterns from those samples were analyzed by TOPAS 3.0 (figure 50). The obtained results showed that the exchanged material can be described by the same space-group (monoclinic $P2_1/c$). Nevertheless, the initial monoclinic structure had changed in some characteristic planes. The low resolution curves did not give the full details of the ion exchange sample powder patterns but using this basic information it was possible to retrieve the materials crystal dimensions. Table 29 shows these dimensions and the crystallographic data of the Le Bail refinement indicating a large increase in the b-axis of the unit cell. Figure 50 shows that the peak

situated at 15.3 2Theta and corresponding to atomic plane (020) is clearly shifted to the lower 2Theta angles.

Table 29. Crystallographic data of the AV-7 ion exchanges with chromium. Exchanges performed during 24, 48 and 72 hours at 80°C.

	AV-7 Cr form (24h)	AV-7 Cr form (48h)	AV-7 Cr form (72h)
Rwp	14.9(3)	14.8(5)	18.6(1)
GOF	1.0(1)	1.1(4)	1.0(4)
Space group	$P2_1/c$	$P2_1/c$	$P2_1/c$
Volume (Å^3)	1003.25(5)	998.38(4)	1012.21(3)
Crystal size (nm)	37.2±0.1	45.8±0.1	30.9±0.1
a (Å)	6.36(5)	6.34(5)	6.38(5)
b (Å)	12.52(7)	12.51(8)	12.55(2)
c (Å)	13.06(7)	13.03(8)	13.10(1)
β(°)	105.6(7)	105.4(4)	105.4(4)

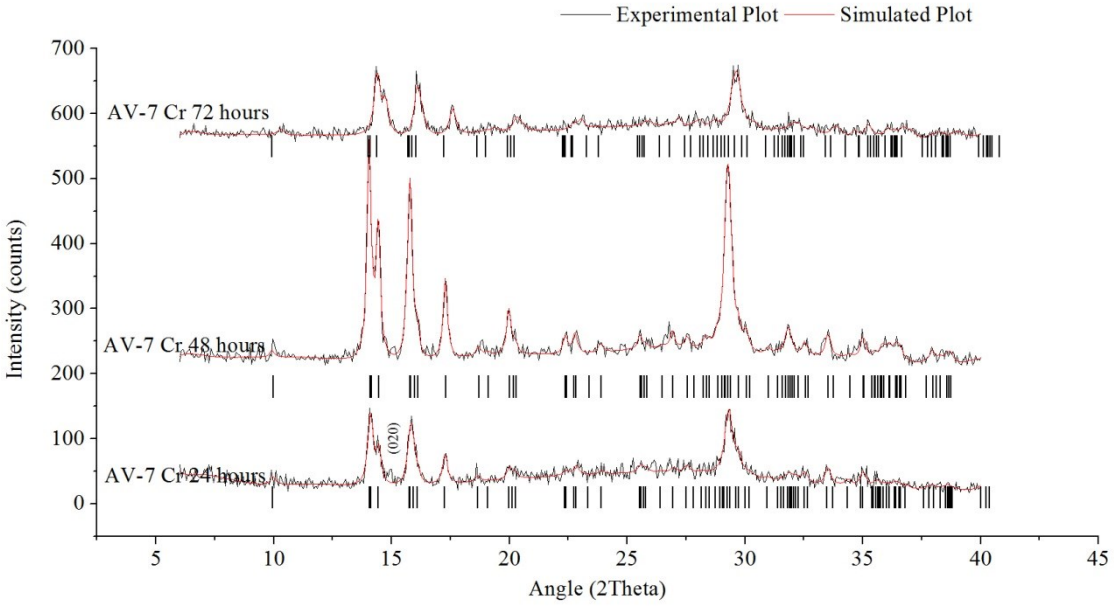

Figure 50. Experimental and simulated powder patterns from Le bail refinement on AV-7 ion exchanged with chromium. Exchanges during 24, 48 and 72 hours at 80°C.

The shift in the (020) plane was clear in all cases for ion exchange. The unit cell of AV-7 had expanded from a volume of 935Å^3 to a mean volume of 1000Å^3. This was a clear indication that the chromium was in the pores of AV-7. However, as the time of ion exchange is increased the material also started to lose crystallinity. To perform a structural characterization, with a simulated structure, it was necessary to perform more ion exchange experiments. These experiments produced greater amounts of the same material, enough for a better analysis. The new ion exchange materials were analyzed by SEM/EDS and the results, table 30, showed very small amounts of chromium present in the exchanged material. The chemical analysis also

showed a low percentage of sodium and potassium. This indicated that all the present chromium was inside the structure compensating the framework negative charge.

Table 30. Chemical composition of AV-7 ion exchange with chromium.

	Weight Percentage (%)	Atomic Percentage (%)	Atoms ratio
Na	0.43(5)	0.34(1)	0.17
Si	12.22(5)	7.78(5)	3.89
K	0.68(5)	0.31(1)	0.15
Sn	14.88(5)	2.24(1)	1.12
Cr	0.58(5)	0.20(5)	0.10
Others (O and C)	71.18	89.12	——

SEM images showed the successful preparation of AV-7 with unique morphology (figure 51). The material is composed of nanorods, figure 51, with a length of several microns and a diameter close to 100 nanometers. Since the ion exchange procedure does not affect the materials shape, this type of growth came from the synthesis conditions. The trial that produced these AV-7 crystals was D_{12}. This particular material was synthesized out of a composition with high concentration of tin and potassium. It is possible that the composition used in D12 was responsible for this crystals shape, that composition can be seen at figure 51. The needle-shaped material was the only form present in the material. These needles presented several diameters and the larger ones had well defined edges.

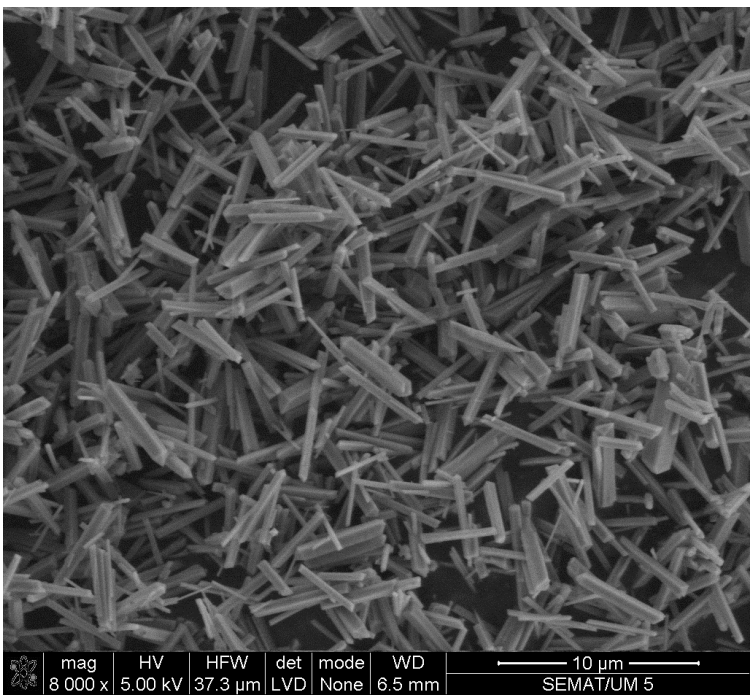

Figure 51. SEM image of AV-7 ion exchanged with Chromium. AV-7 produced on trial D12.

A high resolution PXRD was collected and more accurate hkl data was obtained. That data was used for Rietveld refinement of Cr-AV-7, figure 52 and table 31. This procedure allowed the modification of AV-7 original simulated structure to the chemically changed Cr-AV-7. The obtained results indicated that Cr^{+3} ions entered the 8-ring pores substituting the potassium ion. The structure was not completely solved and there are still some issues with atoms occupation. However, the values of error reached here clearly indicated that the refinement is correct.

Table 31 Crystallographic data from the Rietveld refinement to the AV-7 chromium exchanged material. Exchange at 80°C during 72 hours.

	AV-7 Cr form
Rwp	5.08
GOF	1.31
R-Bragg	1.775
Space group	P2$_1$/c
Volume (Å^3)	998.1047
Crystal size (nm)	39.4
a (Å)	6.482886
b (Å)	12.57638
c (Å)	12.70776
β(°)	105.5605

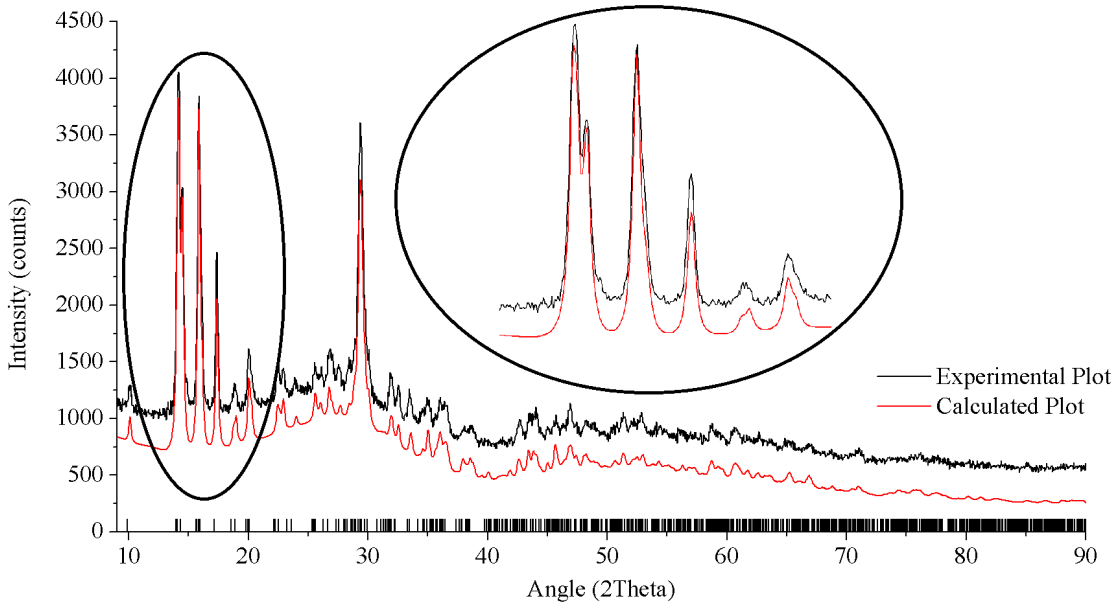

Figure 52 Experimental and simulated powder patterns of AV-7 Chromium exchange obtained by Rietveld refinement.

The presence Cr^{3+} in the 8-ring channel made the smaller one (6-ring) to expand, figure 53. This small channel had only potassium as charge stabilizer and due to the higher charge of chromium the structure was distorted. This distortion resulted in increase of lattice volume with 6%. Additionally, changes in the atomic positions were also detected (table 32). The pore occupants' positions are completely different from the ones on AV-7. The framework atoms

suffered also some minor adjustments but the framework type, as it can be seen on figure 53, remained very similar.

Table 32. Atomic coordinates for AV-7 Cr-form.

Site	x	y	Z
Sn1	0.102(5)	0.705(3)	0.232(4)
K1/Ow2	0.190(1)	0.997(6)	0.570(2)
Si1	0.171(5)	0.952(6)	0.268(7)
Si2	0.200(2)	0.703(4)	-0.015(1)
Si3	0.616(9)	0.660(8)	0.183(3)
Cr1/Ow2	0.694(2)	0.860(8)	-0.005(5)
O1	0.054(1)	0.532(8)	0.260(1)
O2	0.053(1)	0.699(2)	0.069(8)
O3	0.806(9)	0.738(1)	0.187(5)
O4	0.072(4)	0.851(7)	0.204(49
O5	0.148(6)	0.705(5)	0.390(8)
O6	0.454(4)	0.693(4)	0.249(6)
O7	0.194(5)	0.891(5)	0.388(7)
O8	0.704(4)	0.550(3)	0.194(6)
O9	0.448(7)	0.665(2)	0.056(1)
Ow1	0.671(5)	1.055(7)	-0.079(3)

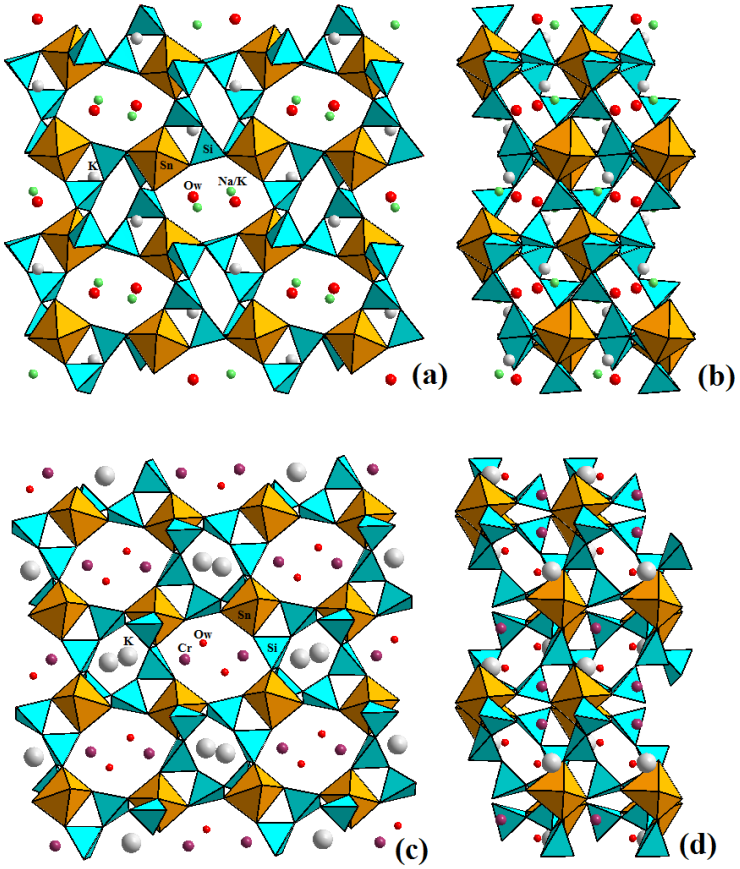

Figure 53. Simulated structures from AV-7 and Cr-AV-7. Direction a-axis of AV-7. (a) Direction c-axis of AV-7 (b). Direction a-axis of AV-7 Cr form (c). Direction c-axis of AV-7 Cr form (d).

The ion exchange with copper during 48 hours presented the same type of changes seen in the chromium ion exchange. Copper ion also has a coordination limit of 6 suggesting that it can also be accommodated in the pores system of AV-7. Ion exchange experiments performed at 24 and 48 hours revealed that the shift in the (020) plane was slower on the chromium exchange. At 24 hours the amount of intensity lost in the plane (020) was not total and the increase in the (002) was minimal, figure 54. This indicated that very small amount of copper could have entered the structure. At 48 hours the (020) plane had completely disappeared and the (002) was perfectly formed. From the Le Bail refinements, table 33 and figure 54, it was revealed that the 24 hours exchanged phase had a minor expansion of 1%. However, the 48 hours exchanged phase showed an increase in volume of 6.5%, very close to the expansion presented on the chromium exchange.

Table 33. Crystallographic data for AV-7-ion exchange with copper. Refinement by Le Bail method.

	AV-7 Cu form (24h)	**AV-7 Cu form (48h)**
Rwp	15.7(4)	17.1(5)
GOF	1.4(8)	1.2(6)
Space group	$P2_1/c$	$P2_1/c$
Volume (Å^3)	945.94(1)	995.76(4)
Crystal size (nm)	25.4±0.1	34.4±0.1
a (Å)	6.47(5)	6.33(5)
b (Å)	11.64(2)	12.48(5)
c (Å)	12.95(7)	12.99(2)
β(°)	104.4(4)	104.4(8)

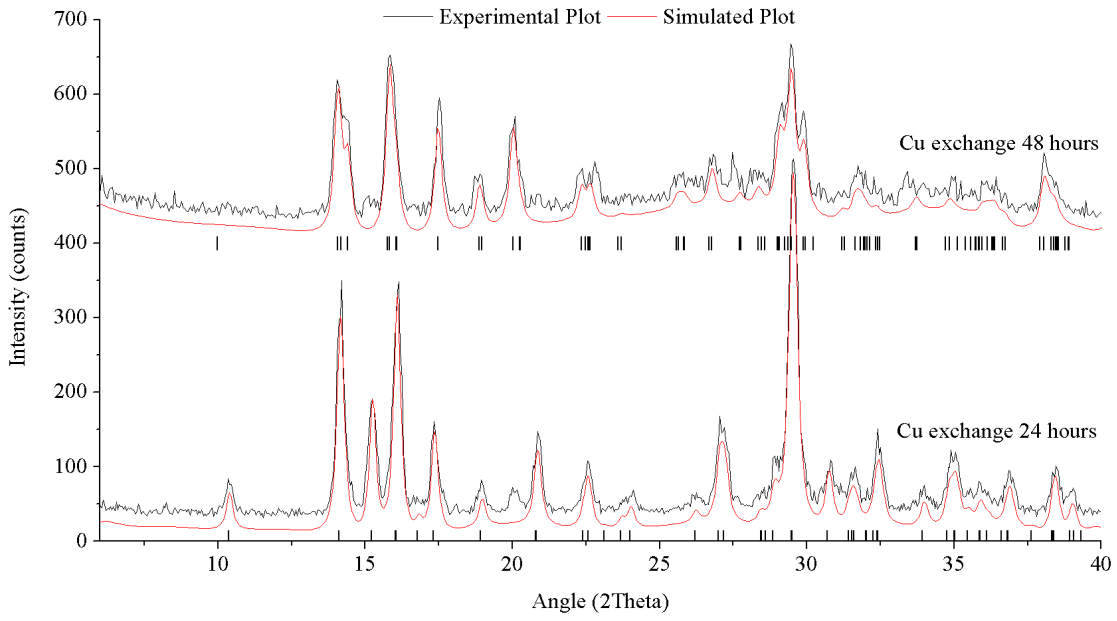

Figure 54. Experimental and simulated curves of AV-7 ion exchange with copper.

This result showed that for Cu^{2+} the structural transformation happens in the same way but much slower than in Cr-AV-7. Comparing with chromium, copper had lower affinity to AV-7

channels. Following the ion exchange behavior that Fewox proved in his thesis, higher charge ions have higher affinity to be captured by ion exchange [33]. The EDS results confirmed the presence of copper in the material exchanged for 48 hours. These results, table 34, showed, like the chromium ion exchange, a low percentage of pore stabilizers. On normal AV-7 sodium and potassium represent 2 moles in the materials chemical composition. However, it appears that when ion exchanged this structure loses chemical ratio and the amount of stabilizers decreases. Even with the higher charge compensation, in the copper case $^{2+}$, the total amount of positive charge in the porous structure is insufficient for charge compensation. It seems that the ion exchanged forms of AV-7 have unbalanced pores, indicating that some amounts of potassium were expelled and not exchanged.

Table 34. Chemical composition of the AV-7 ion exchange with copper for 48 hours.

	Weight Percentage (%)	**Atomic Percentage (%)**	**Error (%)**	**Atoms ratio**	**Corrected ratio**
Si	19.38	17.575	0.18	2.92	2.92
Cl	0.6	0.43	0.01	0.07	0
K	2.135	1.41	0.685	0.23	0.23
Sn	28.49	6.145	2.38	1.02	1.02
Cu	6.01	2.41	0.08	0.40	0.36
Other elements	43.38	72.03	2.81	-	-

The chlorine detected by the chemical analysis was superficial $CuCl_2$. This material resisted filtration process but did not interfere with the Rietveld refinement. The EDS results were recalculated after chloride removal and the correct ratio is presented at table 34. The corrected ratios give a total presence of charge stabilizers of 1. The missing charge may have come from OH^- compensation. The framework atoms Si and Sn may have change some of the Si-O and Sn-O bonds to Si-OH and Sn-OH bonds, like in other reported works [12]. By doing this the total amount of charge needed for compensation decreases and therefore the occupancy of positive charge elements in the channels must be inferior to the normal of AV-7. These connections to OH^- are reflected in the bonds length, the hydroxide connections are longer and weaker. The more hydroxide groups present in the structure the more disordered it gets.

The SEM analysis of this ion exchanged material revealed an already seen shape of AV-7 crystals, figure 55. This time however, the crystals had irregular surface, the material presented the typical large crystals shape but the surface was covered by fine powders. It was also visible

small agglomerates of different material. This material was the copper chloride detected in the chemical analysis.

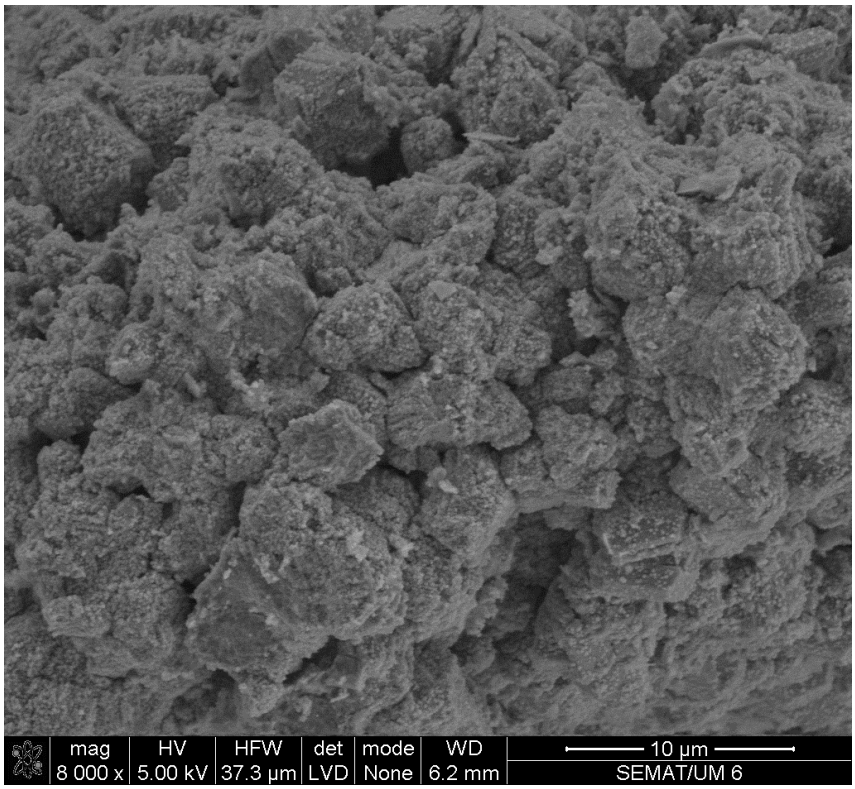

Figure 55. SEM image of AV-7 ion exchanged with copper. Exchange during 48 hours at 80°C.

The ion exchange experiments with zinc revealed no shifts of the diffraction peaks. Nevertheless, the intensity loss of a single peak, plane (020) (figure 56) gave indications that the AV-7 framework may have captured the VIII coordination ion. After performing Le Bail refinement of samples exchanged for two different times: 24 and 48 hours, it was possible to see that the cell volume did not change as drastically as in other experiments with this microporous stannosilicate, table 35.

Table 35. Crystallographic data from the Le Bail refinement to the AV-7 ion exchanges with zinc.

	AV-7 ion exchange with zinc	
Time of exchange	**24 hours**	**48 hours**
Space-group	$P2_1/c$	$P2_1/c$
Volume (Å^3)	942.97(2)	943.00(1)
Crystal size (nm)	42.7±0.1	50.6±0.1
a	6.48(4)	6.46(9)
b	11.57(1)	11.58(4)
c	12.96(9)	12.98(2)
β(º)	104.30(7)	104.25(2)

The unit cell dimensions remained very similar with a volume change of 0.85% for both times. However the refined powder XRD patterns showed the same intensity loss in the same

diffraction plane, figure 56. Since there was no shift like in the other ion exchanges experiments, zinc may have not entered or produced a different type of modification. It is possible that it occupied a different position that allowed the formation of 8 coordination bonds.

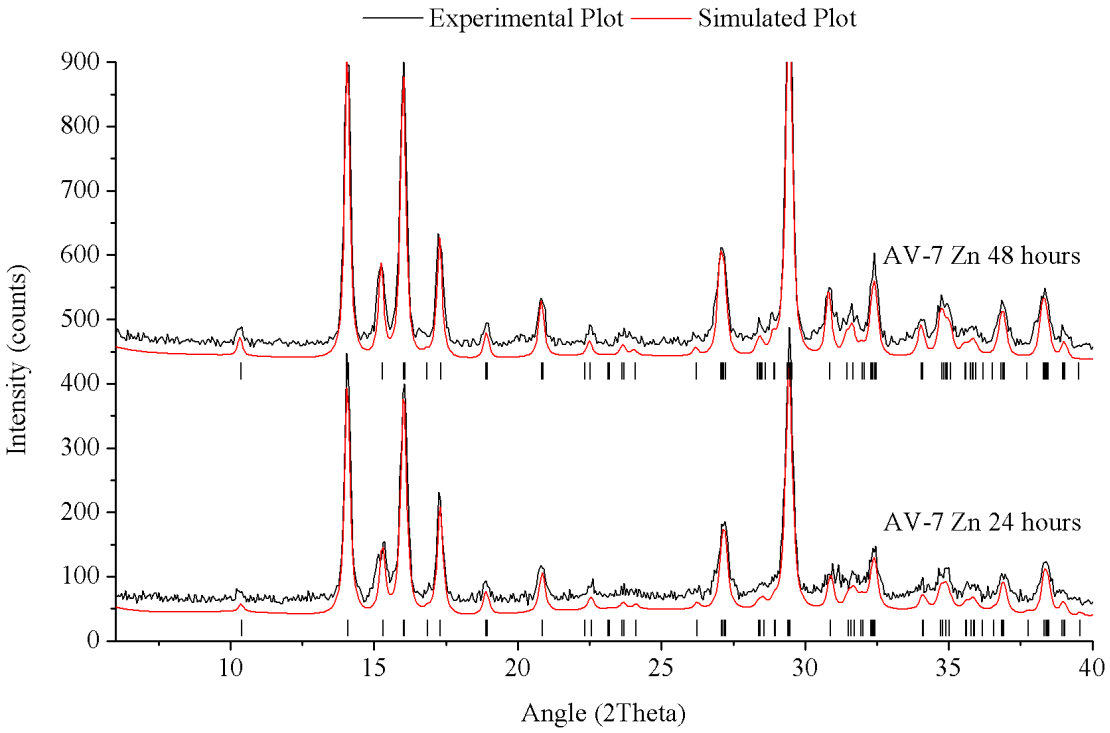

Figure 56. Experimental and calculated curves from the Le Bail refinement of AV-7 ion exchanged with zinc.

The EDS analysis confirmed that the ion exchange was successful. In fact this was the exchange with higher percentage of captured element. The chemical composition, table 36, showed a ratio of zinc of 0.5 representing the maximum possible occupation of Zn in the AV-7 unit cell. Potassium also showed the same ratio indicating that this ion is placed in other pore position also with mixed occupancy. To balance this occupancy these ions share its position with water molecules. The ratio of Si and Sn were in the typical framework relations, 3 to 1, and there were no traces of sodium or chloride.

Table 36. Chemical composition of AV-7 ion exchanged with zinc for 24 hours.

	Weight Percentage (%)	**Atomic Percentage (%)**	**Error (%)**	**Element ratio**
Si	18.81	18.08	0.21	3.01
K	5.085	3.52	0.395	0.58
Sn	27.81	6.335	1.14	1.05
Zn	8.305	3.43	0.115	0.57
other elements	39.99	68.64	1.44	

The SEM images confirmed the typical shape of AV-7. The large shaped like crystal particles were very well defined and there was no presence of any contaminant or any

amorphous phase. On figure 57 it is possible to see large agglomerates of crystal with well-defined faces.

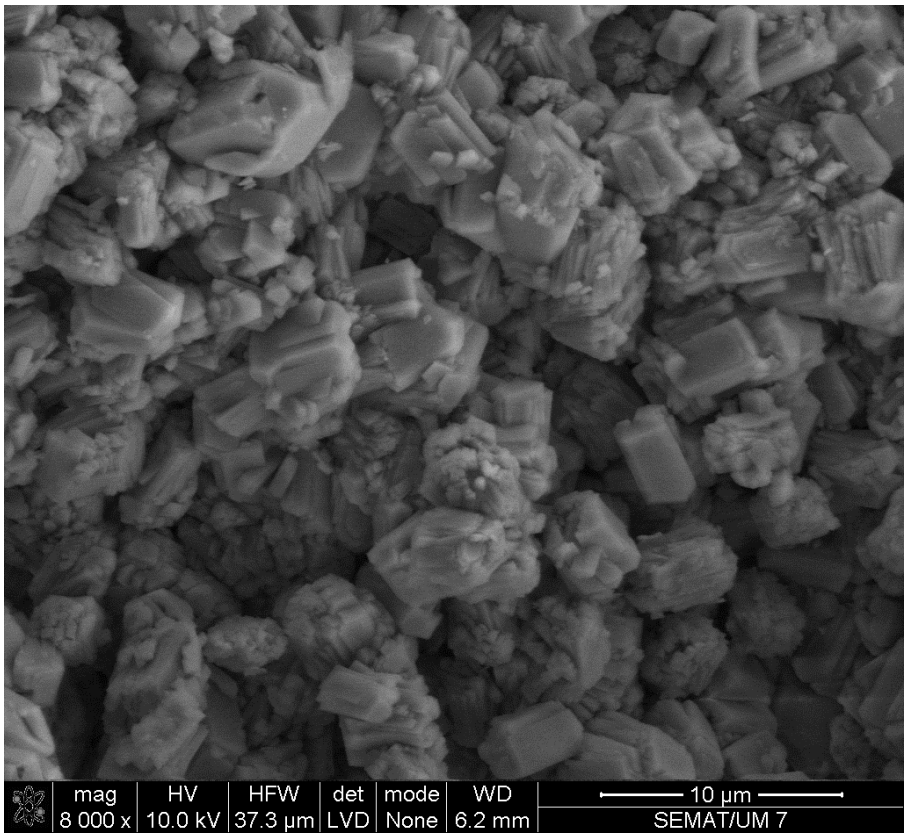

Figure 57. SEM image of AV-7 ion exchanged with zinc for 24 hours at 80°C.

Ion exchange experiments with aluminum and lead ions were performed at shorter times and lower temperatures due to their tendency to damage the crystal structure of AV-6. Within 18 hours at 50 °C the solution of Pb^{2+} ions resulted in almost complete amorphization of AV-6. When AV-6 is placed in a solution of Al^{3+} (18 hours at 50 °C) the result is only a slight loss of crystallinity. The same solutions applied on AV-7 for the same time and temperature had a significantly different result. No evident signs of ion exchange or structural destruction were observed, figure 58. As the time and temperature of ion exchange increase the material degradation is also slowly increased. However at 24 hours at 80°C of exchange with aluminum the AV-7 material still had all its crystalline features unchanged. The lead ion exchange experiment showed a different behavior. In addition to the resistance to amorphization, the ion exchange sample structure had loss intensity in the (020) plane indicating that Pb^{2+} may have entered the porous framework. Just like zinc, this ion can form a VIII coordination. As figure 58 shows the sample exposed to Pb also revealed a slight loss of intensity in the (020) plane. This may indicate that Pb can also be captured by this microporous stannosilicate (AV-7). This ion

exchange is detectable within 18 hours but it is even more enhanced when the reaction is performed for 24.

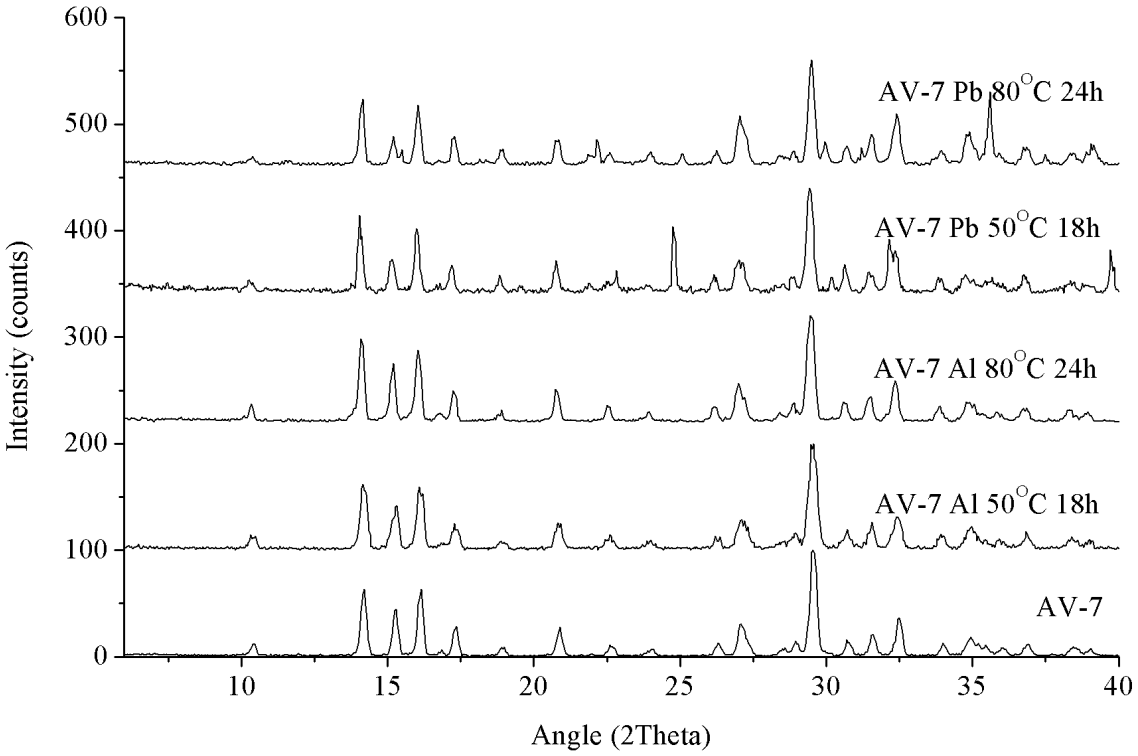

Figure 58. Experimental powder XRD patterns of AV-7 ion exchanged with lead and aluminum.

After Le Bail refinement it was visible that all the powder patterns had the same unit cell volume, table 37. Despite the contaminations of lead chloride detected, figure 59, the analysis was accurate and unaffected. By the volume and unit cell dimensions analysis there was no evident change on the different AV-7 powder patterns.

Table 37. Crystallographic data from Le Bail refinement of AV-7 ion exchanged with Pb and Al.

Material	**AV-7**			
Ion exchanged	**Al^{2+}**		**Pb^{2+}**	
Time	18 hours	24 hours	18 hours	24 hours
Rwp	28.4(4)	23.4(4)	24.4(5)	24.6(6)
GOF	1.3(1)	1.3(4)	1.1(4)	1.4(6)
Space-group	**P21/c**			
Volume ($Å^3$)	947.94(5)	944.43(9)	943.34(8)	943.85(1)
Crystal size (nm)	53.8±0.1	64.3±0.1	68.8±0.1	77.9±0.1
a (Å)	6.46(1)	6.45(7)	6.45(8)	6.45(9)
b (Å)	11.65(6)	11.64(9)	11.63(3)	11.63(4)
c (Å)	13.01(9)	12.98(2)	12.98(7)	12.98(9)
β(º)	104.79(5)	104.76(5)	104.82(6)	104.77(5)

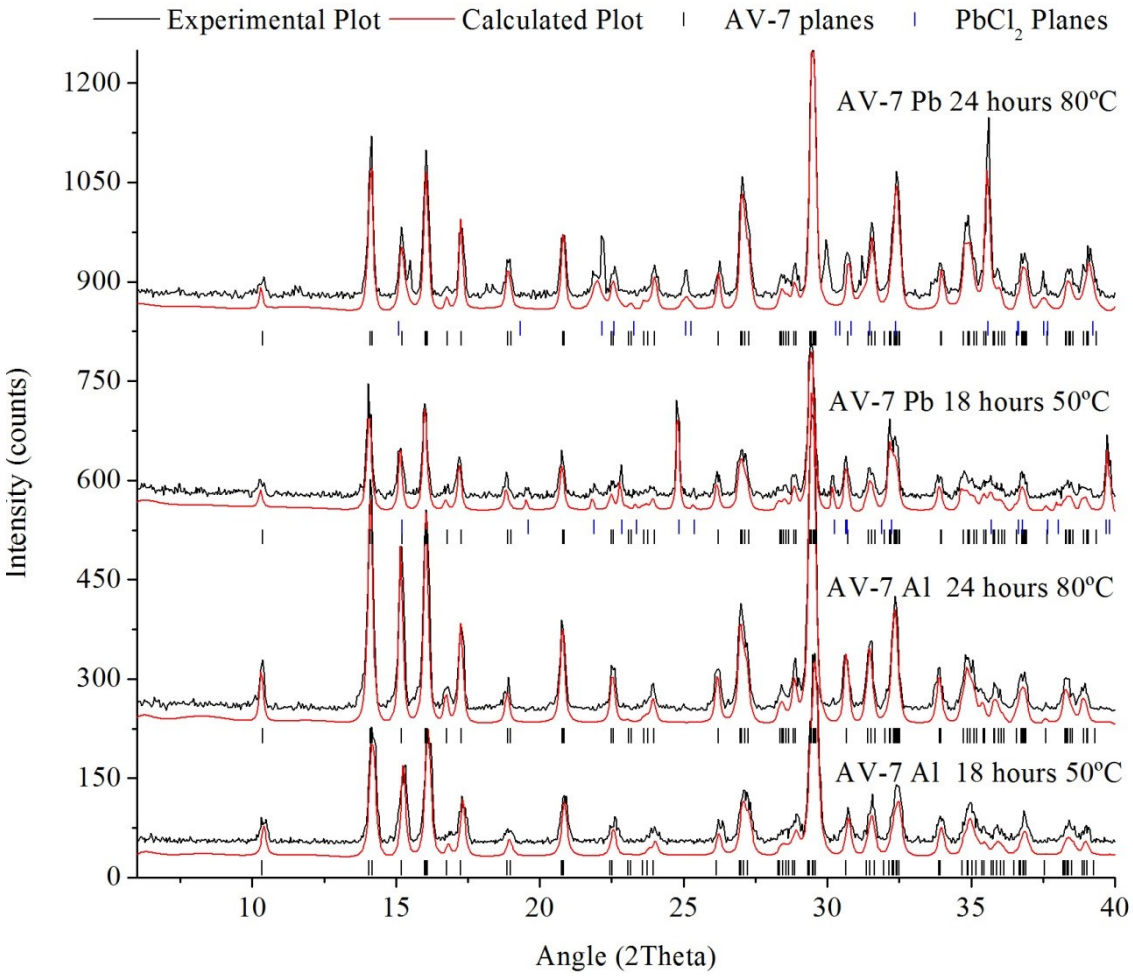

Figure 59. Experimental and simulated curves of the Le Bail refinement of AV-7 ion exchanged with Pb and Al.

Since the Le Bail procedures gave no clues about the success of exchange a different type of analysis was performed to the powder patterns. Only the ion exchange experiments with divalent ions with coordination 8 were compared since only these ion exchange samples performed equal deformations. As previous works report [12], when exchanges with divalent ions are performed the preferential occupancy site is in the water molecules position. In the structure of AV-7 the plane (020), figure 60, crosses the 8 ring channel and is coincident with the structural water molecules. Therefore, any variation in this plane intensity is related to this position occupancy and therefore to the success of ion exchange.

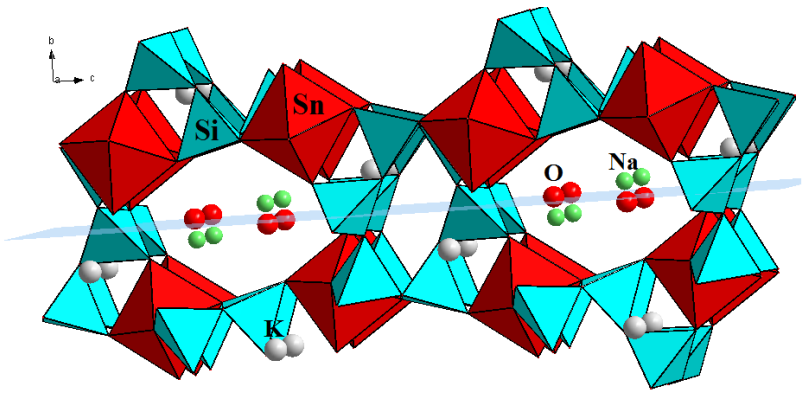

Figure 60. AV-7 simulated structure with plane (020).

The 15.3° 2theta diffraction plane (020) intensity was compared with a reference plane (002) in all ion exchange forms of AV-7. In the as-synthesized AV-7 the difference from the two planes intensities is around 30%. For the Zn-AV-7 ion exchange sample the difference from the two planes intensities is around 70%. This means that a change in AV-7 chemical composition by ion exchange with divalent 8 coordination ions can cause variations in this intensities ratio.

The ion exchange with Al^{3+} resulted in intensity difference of 30% which is the same as in the as-synthesized AV-7. This indicated that no alterations happened in the channel and therefore the exchange was not realized. This clearly indicated that the failed exchanges had not affected the diffraction planes and that the successful ones increased this perceptual difference. Lead ion exchange experiments did just that, both times of ion exchange showed values around 55%. The strontium ion exchange sample, even with very low crystallinity levels, showed also an increase to 50% on planes intensity difference. This analysis alone does not prove the ion exchange success, however, if confirmed by EDS this method could be used for primary ion exchange success evaluation.

Furthermore, as figure 61 shows the intensity difference does not depend on the time of ion exchange but only of the ion involved. In this case, this type of analysis can be used to determinate the chemical composition of an unknown AV-7 exchanged form. If considered that every element has its unique diffraction coefficient then it is possible to distinguish the different ions accommodated in the pore system.

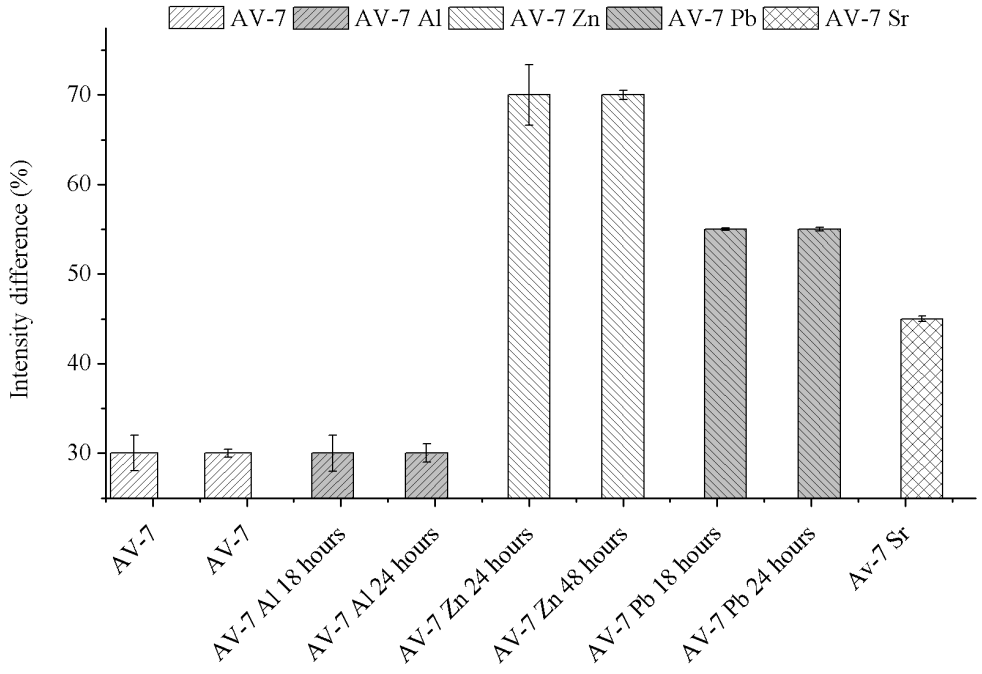

Figure 61. Peak intensity difference between planes (002) and (020) in several AV-7 forms.

Since there are no ion exchanges reported on AV-7 there is no way to compare and validate this approach for analysis. However, if other attempted exchanges behave the same way and if the EDS results confirm the successful of ion exchange this method could be considered optimal for AV-7 ion exchange evaluation. After that it is necessary to understand why these different elements present this difference in this specific plane. If a physical property of the ions is link to this behavior this analysis could gain even higher importance. It is also necessary to prove by EDS that the different shifts come from ion type only and not by exchange percentage. Nevertheless, even if this effect is only related to the amount of ion exchange it can be used to calculate the amount of foreigner ions captured in this microporous framework. In this case it is necessary to understand the relation between the intensity drop and the amount of ion exchanged.

7.5 Isomorphous substitutions

7.5.1 Substitutions by zirconium

When preparing the precursor for the isomorphous substitutions by zirconium it was possible to see that even with large amounts of zirconium ions this precursor remained transparent. This was an interesting factor since this work is pioneer in that kind of hydrothermal synthesis of tin silicates or mixed metal tin silicates. Some trials showed sandy white powders, others milky solutions that after drying resulted in fine white powders. The remaining trials presented very hard agglomerates with high porosity. Table 38 shows the synthesis results for all the isomorphic substitutions by zirconium in tin silicate compositions.

Table 38. Synthesis results from the isomorphous substitutions with 20% (I_{S1} to I_{S4}) and 40% (I_{S5} to I_{S6}) of zirconium.

Trial	Synthesis result
I_{S1}	Fine white powder
I_{S2}	Small amount of white powder
I_{S3}	Large amount of white powder
I_{S4}	Cohesive material
I_{S5}	Sandy white powder
I_{S6}	Sandy white powder
I_{S7}	Solid porous cylinder, white material
I_{S8}	Agglomerated material soft material

All the synthesized materials were analyzable by XRD and the results are shown on figure 62. These analyses showed that the different compositions resulted in phases already seen in the stannosilicates standard synthesis (synthesis chapter 7.2). I_{S1} showed a mixture between AV-6 and AV-7 and no indication that zirconium could had entered the framework. Le Bail analysis and structural comparison showed that this phase had the original dimensions of AV-7 and AV-6. This confirmed the absence of zirconium and the failure of substitution. The structures of AV-7 and AV-6 were present in equal percentage 51% to 49% respectably. I_{S2} was identified as pure AV-6 with a difference in unit cell volume of 0.85%. This very small variation indicated that no zirconium was present in the framework and that the substitution was a failure again. I_{S3} and I_{S4}, that were sodium based silicates, presented the characteristic low crystalline materials. I_{S3} presented a powder pattern similar to the unknown phase from the sodium based stannosilicates. The low angle diffraction peak was well defined but the remaining powder pattern was near amorphous so no indexation was possible. I_{S4} showed a powder pattern not consistent with any silicate structure and therefore had no interest in analysis. IS_5 and IS_6 had increased amount of zirconium in the solution (40% in weight), nevertheless, these powder patterns showed

pure forms of AV-7. The materials produced with AV-7 structure had a deviation in volume inferior to 3%. This indicates that the material was completely formed out of tin and no zirconium had entered the framework. Apart from the attempt of substitution, the decrease in available tin enabled the formation of AV-6 and allowed the formation of pure AV-7. The I_{S6} sample had no sodium in the composition proving again that it is possible to form sodium free AV-7 sieves. I_{S7} and I_{S8} showed similar results to the 20% substitution sodium compositions (IS_3 and IS_4).

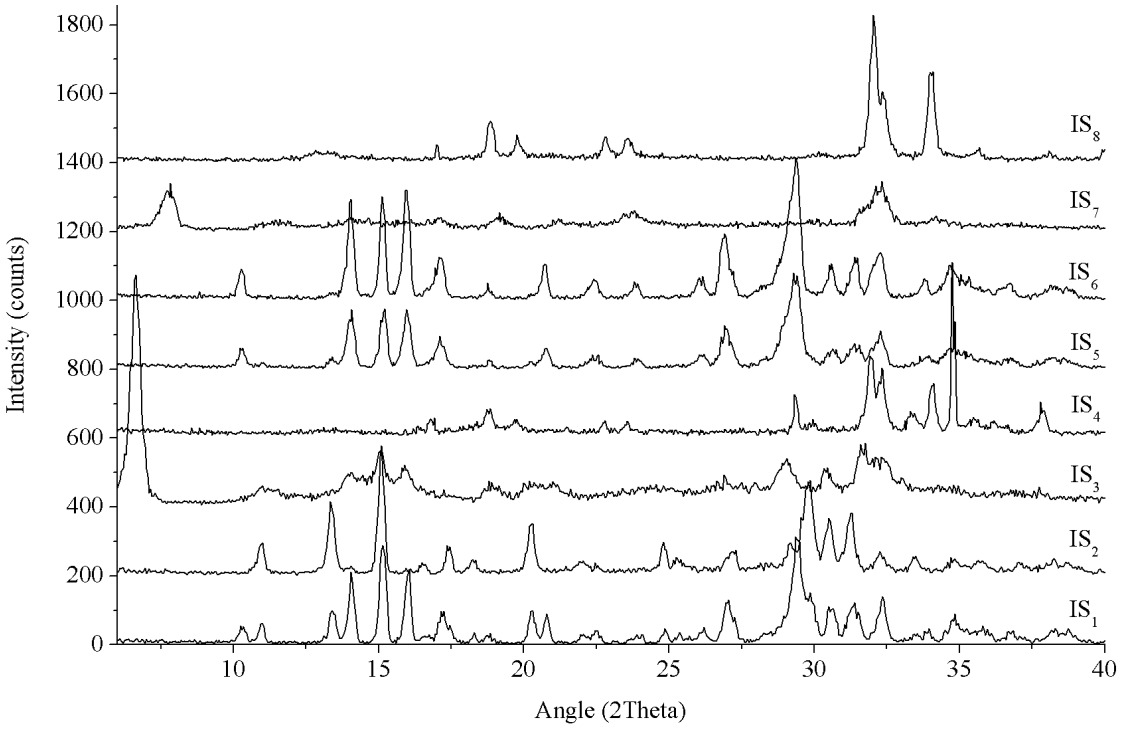

Figure 62. Experimental powder XRD patterns of the zirconium isomorphous substitutions on stannosilicates, performed at 200°C for 2 days.

7.5.2 Substitution by titanium

The close resemblance between titanium and tin silicates was a good indication for the formation of mixed octahedral frameworks. The compositions used followed low concentration values of titanium to high concentration values of titanium. This allowed to test if higher concentrations of titanium result in the synthesis of titanium silicate frameworks. Trials I_{S9} to I_{S20} were realized by the same hydrothermal synthesis procedure of the zirconium exchanges. However, due to the source of Ti ($TiCl_3$) the solution transparency was lost. Some trials resulted in black solutions others grey gels and the remaining ones resulted in different color solutions. All these precursors were prepared in the same conditions and the resulting material can be seen on table 39, where it is also possible to see the type of solution before entering the autoclave.

Table 39. Type of precursor and synthesis result of all isomorphous substitutions with titanium. Performed at 200°C for 2 days.

Trial	Solution Color / state / pH	Synthesis result
I_{S9}	Black/ Solution / 13	Two colored powder
I_{S10}	Black/ Solution / 13	Soluble transparent material and white powder
I_{S11}	Grey / Gel / 14	Solid block of white material
I_{S12}	Black/ Solution / 10-11	Very fine white powder
I_{S13}	Black/ Solution / 13	White powder
I_{S14}	Black/ Solution / 13	Cohesive material white
I_{S15}	Grey / Gel / 7	Yellow soft agglomerated material
I_{S16}	Black/ Solution / 6-7	White powder
I_{S17}	Green / Solution / 14	White powder
I_{S18}	Brown / Solution / 14	Black powder
I_{S19}	Violet / Solution / 7	Yellow soft material
I_{S20}	Black / solution / 12	Large amount of soft white powder

Not all the synthesis products came out as powder. For trial IS_{11} it was necessary to scratch the solid block in order to obtain XRD analyzable material. At the macro scale IS_{11} was a solid porous material that could capture high quantities of liquids. This solid was shaped into a cubic form for density calculation and internal channels visualization. By geometrical evaluation method the calculated density was 0.31(4) g/cm^3, showing that this was a very light material. The 60% substitution trials (IS_{17} to IS_{20}), that were in fact titanium based silicates (since the composition had more Ti that Sn), formed different colored solutions, figure 63. These different precursors had different pH values and different compositions but nevertheless the change in color was not expected.

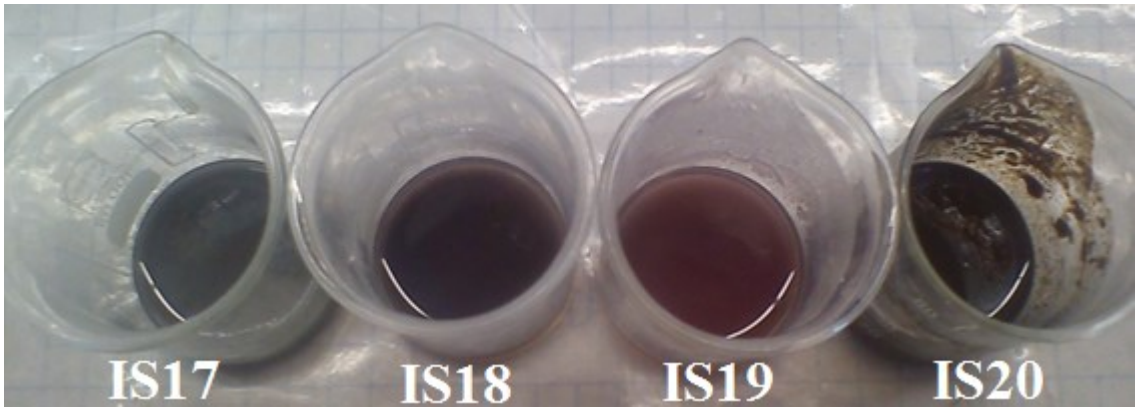

Figure 63. Titanium-tin precursors, 60% titanium 40% tin compositions.

Despite the large difference in the results, all trials were analyzable by XRD. The obtained powder patterns showed a general lack of crystallinity. It also showed a much higher amorphous percentage of trials that in the Zr substations (more than 50% of the samples resulted in amorphous materials), figure 64. AV-7 was the only structure formed with good quality and only

appeared in its more favored composition, $6.6K_2O$ -$3.33Na_2O$-$0.5(xSnO_2$ –$yTiO_2)$ -$5SiO_2$ ·H_2O. The remaining trials presented very low crystallinity possibly indicating that the synthesis time was too short. I_{S11} proved to be an amorphous solid block. I_{S10} showed all the features of an AV-6 powder pattern. Despite its low crystallinity the trial seemed to be a pure form of Sn-umbite. There was no difference in volume or unit cell dimensions so no titanium was present in the octahedral positions. This also happen to all the produced materials that came out with an AV-7 structure. All samples had a change in volume inferior to 1.5% indicating that its structure was only composed of tin as octahedral element. The effects of sodium and potassium were seen again in these compositions. Has said in the synthesis chapter, all compositions that have sodium and potassium are the more reactive and produce more crystalline materials. However, there was another factor that may have influenced these results, the use of $TiCl_3$. This source of titanium was not very reactive in the precursor, if other source is used the same compositions may result in different materials.

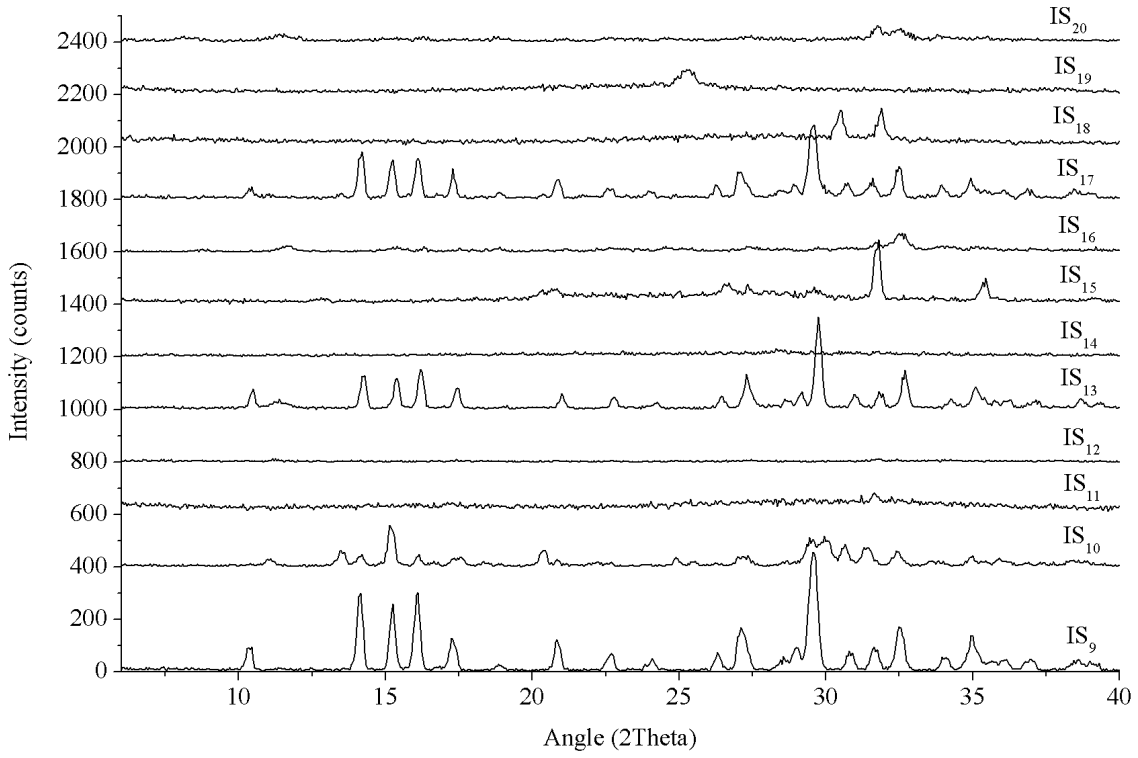

Figure 64. Experimental powder XRD patterns of the titanium isomorphous substitutions performed at 200°C for 2 days.

7.5.3 Influence of the precursor agitation and synthesis time on the substitutions of tin by zirconium and titanium.

In order to understand if the formed structures were the stable forms of the tested compositions, new trials were performed at different parameters. The increase of parameters like time of agitation of the precursor or time of synthesizes (temperature exposure) may allow the

formation of different structures. The I_{SS} trial, performed with a precursor agitation of 30 minutes and a time for heating of 4 days, showed improved crystallinity. The three compositions tested, one zirconium and two titanium compositions, were chosen by different aspects. I_{SS1}, the composition of trial I_{S7}, was chosen because it presented a unique powder pattern with very low crystallinity. I_{SS2}, composition of trial I_{S17}, was chosen due to its formation of AV-7. With the increase in the synthesis time titanium could substitute some of the tin and form a mixed AV-7 phase. I_{SS3}, composition of trial I_{S20}, was chosen to try the formation of a crystalline material from a sodium based composition. It was expected that with the increase of both precursor agitation and time in oven the materials would gain much higher crystallinity. Figure 65 shows the experimental powder patterns obtained from the I_{SS} trial. I_{SS1} changed from a near amorphous material to highly crystalline phase not similar to any tin silicate. In the presence of zirconium, the material did not suffered crystallinity loss with the increase of time. As seen before, in sodium compositions the increase of synthesis time leads to the structural destruction. With only 20% of zirconium the material formed a well-defined structure that could have mixed octahedral occupancy. I_{SS2} showed the same AV-7 structure that in the 2 days synthesis. The difference came from the presence of an unknown peak, possibly an impurity of titanium. I_{SS3} presented a powder pattern very different from the normal tin silicate powders with very high crystalline levels.

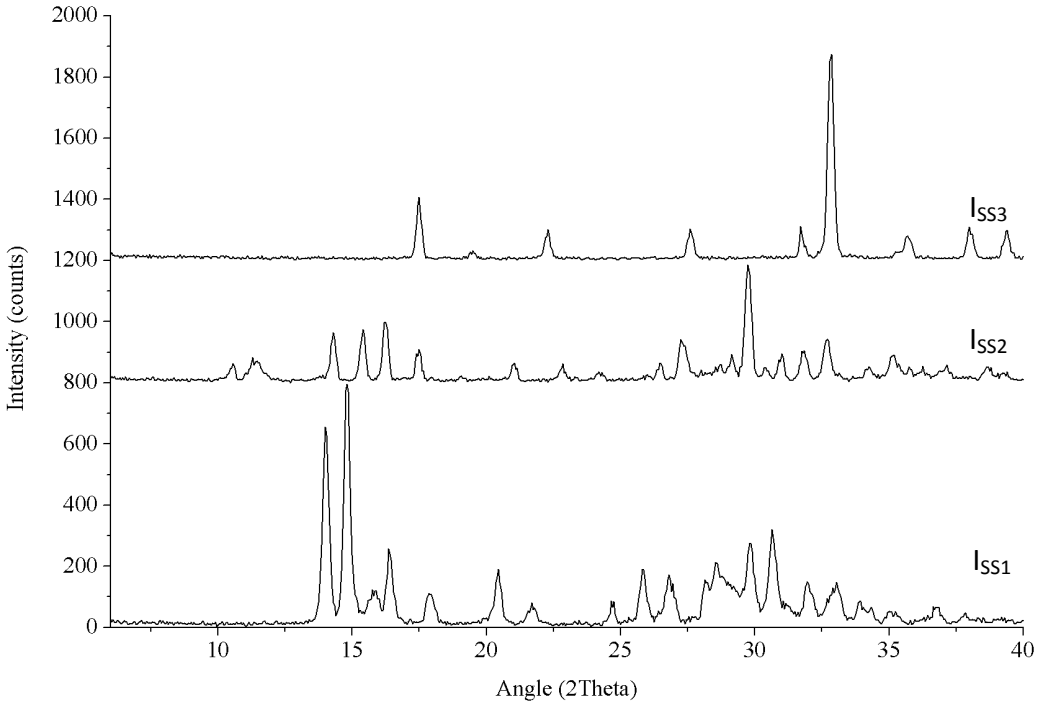

Figure 65. Experimental powder XRD patterns from trial I_{SS}. Synthesis at 200°C for 5 days.

The analysis of trial I_{SS1} showed that none of the known tin silicates matched the obtained powder pattern. Nevertheless some similarities were found when compared with a

zirconium silicate structure. The mixed occupancy of tin and zirconium and the substitution of potassium for sodium in AV-15 may justify the bad quality of the calculated pattern. However, there were no certainties that this was the correct space-group since the fit was not perfect. There was also no confirmation of the mixed octahedral occupancy without a chemical composition analysis. Other space-groups were tested but all showed less resemblance to synthesized phase. The monoclinic space-groups did not match with the experimental data. These Le Bails presented to many non-described diffraction peaks. AV-15 space-group and dimensions however, was the best and the most plausible result, figure 66. Nevertheless, the crystallographic data of table 40 is only a first try in the identification of this unknown powder pattern. I_{SS2} was refined to AV-7 structural dimensions (space-group and unit cell size) by Le Bail method presenting no variations from the standard values. The long exposure to titanium made no changes on the early formed AV-7. This indicated that the stannosilicate phase has good chemical stability and that the prepared composition clearly favors the tin silicate formation. The detected impurity was represented by a single diffraction peak and its most probable source is the free titanium surrounding AV-7. The I_{SS3} trial showed a typical titanium silicate phase called natisite (PDF 01-085-0512). This small unit cell structure is composed by sodium, titanium and silicon and since there were no alterations in the powder pattern the in the precursor did not enter the octahedral sites. An impurity was also found in this trial but this time it was easily identified. The XRD pattern of the impurity matched with NaCl (PDF 01-071-3741) and it appeared in the material due to insufficient filtration. Table 40 and figure 66 show the Le Bail refinement parameters and the calculated and experimental curves of the synthesized materials.

Table 40. Crystallographic data from the isomorphous substitutions performed for 5 days synthesis at 30 minutes of precursor agitation time. Substitutions by zirconium and titanium.

	I_{SS1}	**I_{SS2} (AV-7)**	**I_{SS3} (Natisite)**
Rwp	33.2(1)	17.1(5)	30.8(3)
GOF	3.3(4)	1.2(6)	1.4(2)
Space group	$C222_1$	$P2_1/c$	P4/nmmS
Volume (Å^3)	1015.6(4)	995.76(4)	215.01(8)
Crystal size (nm)	43.4±0.1	34.4±0.1	65.4±0.1
a (Å)	7.80(5)	6.33(5)	6.49(1)
b (Å)	10.86(1)	12.48(5)	5.10(3)
c (Å)	11.99(9)	12.99(2)	
β(º)	90	104.4(8)	

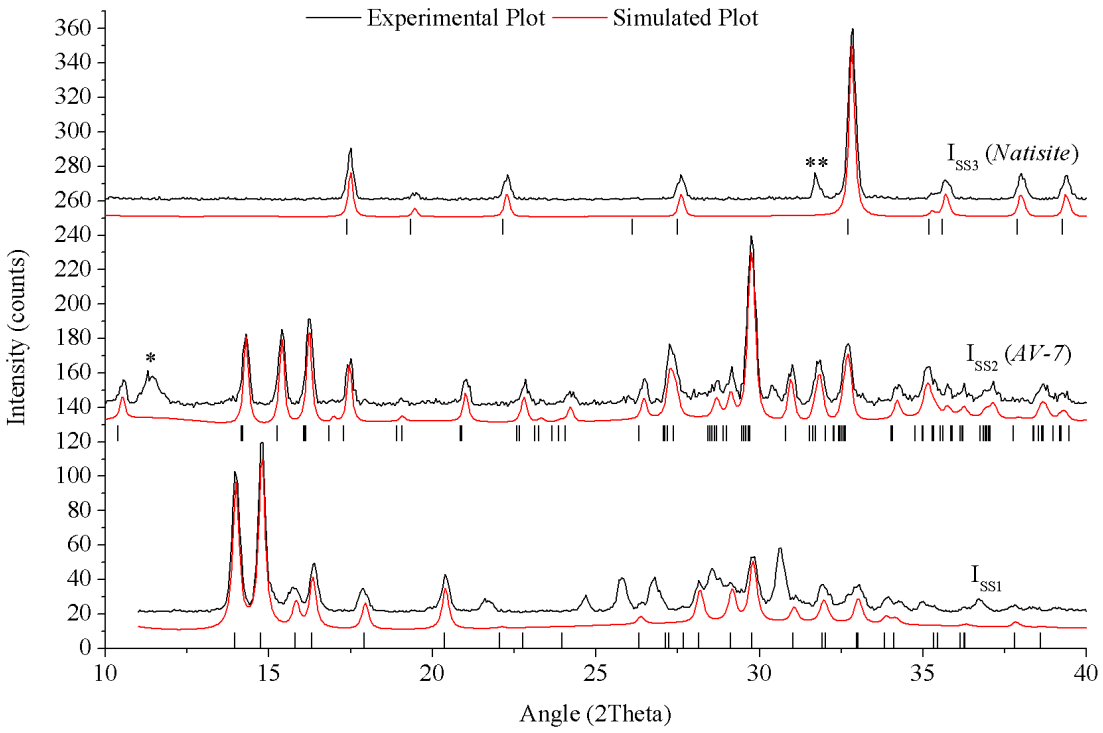

Figure 66. Experimental and simulated powder XRD patterns of the isomorphous substitutions for 5 days and 30 minutes precursor agitation.

After 23 tries of isomorphous substitutions only one sample presented a powder pattern that could indicate a mixed octahedral occupancy. I_{SS1} showed a powder pattern different from the known tin and zirconium silicates, but so far it was impossible to be indexed.

7.5.4 Substitutions by germanium and bismuth

The preparation of solutions for synthesis was different form the ones used so far but in the germanium compositions the transparency of the precursor was still preserved. The difference in germanium solutions was the dissolution of GeO_2, instead of water it was added to the alkaline water solution. For the bismuth substitutions samples transparency was lost, the clear solution turned black after $BiCl_3$ dissolution. In addition to the change of color the solution viscosity also increased indicating that some of the bismuth immediately precipitated. Table 41 shows the precursor type and the synthesis results of these isomorphous substitutions. After drying the germanium substitutions showed sandy aspect and a very large amount of white powder, Ge_2D_2 provided 1.37 grams. Bismuth substitutions samples showed for the sodium composition a grey powder and for the potassium composition a mixture of black and white powders. The last mixed color trial indicated that bismuth had separated itself from the rest of the elements and precipitated alone. This showed that the substitution was unsuccessful even without XRD analysis.

Table 41. Precursor type and synthesis result from the isomorphous substitutions by germanium and bismuth.

Trial	Precursor type	Synthesis result
Ge_2D_2	Clear solution	Large amount of white powder
Ge_1D_4	Clear solution	White powder
Bi_2D_2	Black gel	Grey powder
Bi_1D_4	Black gel	Mixed material white powder/black precipitates

After powder analysis only the first three samples were worthy for XRD analysis. The results, seen on figure 67, showed that the sodium based silicate compositions (Ge_1D_4 and Bi_1D_4) produced similar crystalline phases. These phases were similar to the unknown phase seen in the sodium based tin silicates trial, Trial C_{20}. Both phases had the characteristic 7° 2theta high intensity peak but with a small shift. This shift may indicate difference in the octahedral occupation but since the original structure was not identified there is no firm confirmation. The germanium composition showed higher crystallinity than the original phase (trial C_{20}) and more diffraction peaks were now visible. The bismuth substitution had one extra peak that could be some kind of impurity caused by bismuth remains. The final trial, the germanium substitution on a potassium based composition, resulted in almost pure AV-7 with high crystallinity. The amount of material produced was higher than any other synthesis (1.39 g). The germanium oxide present in the precursor had some influence in the formation of precipitates.

The impurity detected on the bismuth isomorphic substitution was pure bismuth (PDF 01-085-1329). The sodium phases both withstand 5 days of synthesis without framework dissolution. This was an improvement compared to the normal sodium stannosilicate that presented structural instability after 2 days synthesis and low crystallinity when synthesized successfully. This improvement, however, still did not allow structure identification. Sample Ge_2D_2, performed in a 2 days synthesis, showed after Le Bail analysis a powder pattern formed out of a mixture between AV-6 and AV-7. The formed AV-7 was 1.6% larger than the normal one indicating that some germanium may have taken some octahedral or tetrahedral positions inside the AV-7 framework. Within the mixed phase material AV-7 was 70% of all crystalline material and once again, this AV-7 structural configuration was achieved in a sodium free composition. The remaining 30 % of crystalline material belonged to the AV-6 phase. The agitation of the precursor for 15 min might be responsible for this mixed phased material. If the time for agitation is increased to more than 15 min (30 or more) AV-7 appeared in a pure form.

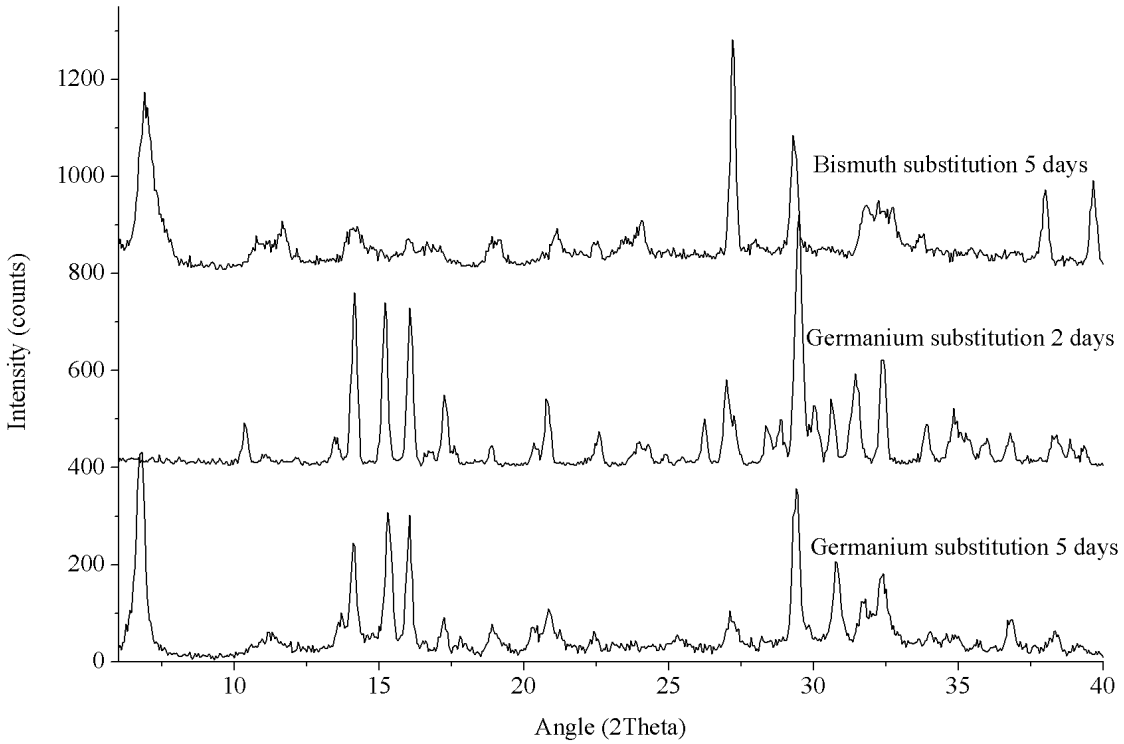

Figure 67. Experimental powder XRD patterns from isomorphous substitutions by germanium and bismuth. Sodium compositions synthesized for 2 days and potassium compositions for 2 days, all at 200°C.

The EDS results confirmed the presence of germanium and a change in the elements ratio, table 42. Both AV-6 and AV-7 have a 1 to 3 ratio of Sn to Si, the chemical results showed a percentage of Si inferior to 2.5. This could indicate that these structures have both silicon and germanium as tetrahedral units. There was no confirmation in which of the phases the silicon was exchanged but there was no doubt that this was a chemically different stannosilicate.

Table 42. Chemical composition of the germanium exchanged AV-7 (trial Ge_2D_2).

Elem	Weight percentage (%)	Atomic percentage (%)	Error (%)	Element ratio
Ge	1.69	0.61	0.0089	0.122
Si	12.79	11.86	0.101	2.372
K	24.85	16.55	0.2334	3.31
Sn	21.86	4.8	0.1801	0.96
Other elements	38.81	66.19	0.0877	-

The SEM images, figure 68, supported the XRD results showing two differently shaped particles. The larger well-shaped particles (marked in blue) belong to AV-7 and the smaller shapeless particles (marked in red) to AV-6. It can also be seen some AV-7 nanorods (marked in green) that have already been seen in other synthesis (figure 51).

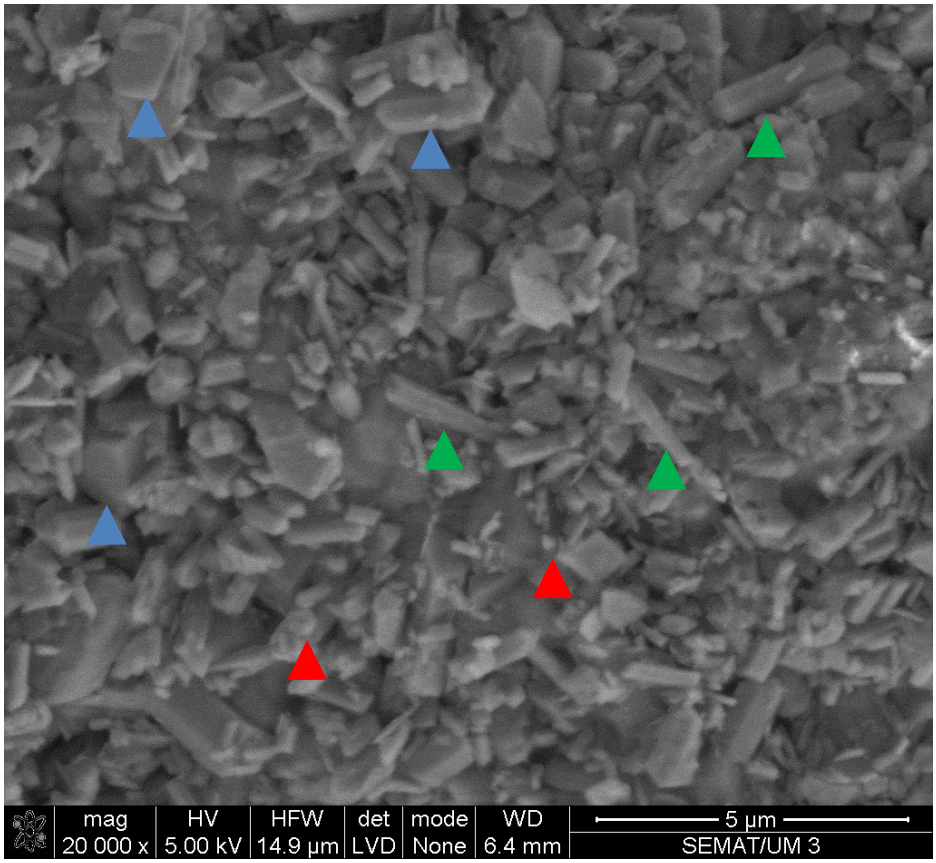

Figure 68. SEM image of potassium AV-7, isomorphous substation with germanium, AV-7 particles (blue) AV-6 particles (red) AV-7 nanorods (green).

Among all isomorphous substitutions only the one realized with participation of germanium has given the indication of being a mixed occupancy tetrahedral-octahedral framework. However, the changes in powder pattern are so small that the germanium detected by EDS may be outside of the crystalline microporous sieve.

7.6 Stannosilicates-thermal properties

7.6.1 Heating at 750ºC for 4 hours

The powders were taken from the oven and by visual observation it was possible to see that sample E_6 (an amorphous material produced with sodium silicon and tin) had changed from yellow to a white powder. Cu-AV-6 also changed the color, from bluish to a dark burn brown. The brown color came from the oxidation of the superficial copper chloride (not totally removed in the filtration process). By XRD analysis, figure 69, it was possible to see that all the exchanged forms of AV-7 turned into amorphous materials. Cr-AV-7 and Zn-AV-7 were expected to have lower thermal resistance since the entrance of different ions creates instability in the framework. The AV-7 sample that was used to try an ion exchange with Na however, was not chemically different since the ion exchange did not occur. Nevertheless this sample followed the behavior of the chemically changed AV-7's and lost all crystallinity. The attempt of ion exchange has provoked a

instability in the framework in the same proportion was the actual exchanges do. This may happen due to the formation of OH^- connections inside the every framework during the exposure to the ion exchange solution. However this is still to be proven. For ion exchange materials it is known that the ion exchange results in structural distortion and formation of local instabilities due to the charge and ionic radius differences between the included ions. This causes the structure to collapse earlier than the unchanged AV-7 upon the same thermal exposure. The as-synthesized AV-7 showed after exposure some amorphization but not in the levels seen in the other chemical types of this stannosilicate.

AV-6 had preserved its framework after the thermal exposure. Its framework showed an unchanged powder pattern similar to the as-synthesized phase. The structure suffered from dehydration but recovered in full. The Zn-AV-6 also preserved some of the crystalline features. The monoclinic phase part of ion exchanged sample (this part is where the zinc ions are stored) turned amorphous leaving the unchanged orthorhombic Sn-umbite as the single crystalline phase on the material. The totally exchanged Cu-AV-6 re-crystallized into a totally different nanosized phase, cassiterite. This was also the crystalline form obtained by the amorphous powder (trial E_6) exposed to the same thermal conditions. The sodium phases C_{20} and AV-10 turned to amorphous materials after this 750°C exposure. The large amount of defects present in both structures contributed to its rapid collapse at these high temperatures.

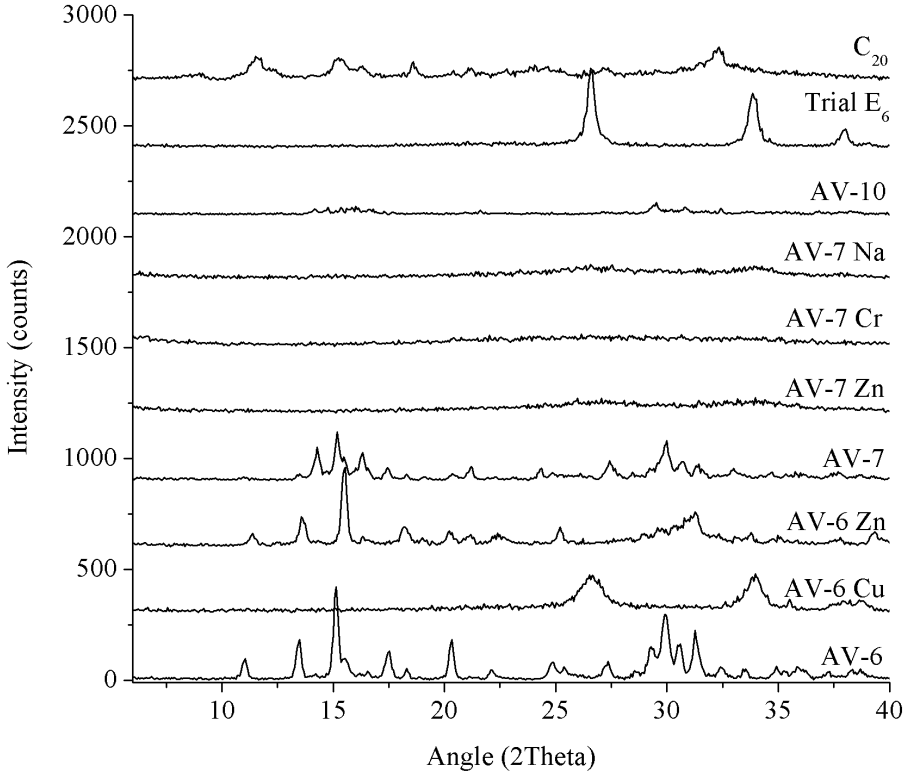

Figure 69. Experimental powder XRD patterns of the samples exposed to 750°C for 4 hours.

Cu-AV-6 and the amorphous material of trial E_6 showed the structure of the tin oxide cassiterite (PDF 01-072-1147). High resolution powder patterns showed that the cassiterite produced from high temperature transformation of AV-6-Cu was contaminated with crystalline copper oxide, tenorite (PDF 048-1548). Despite this impurity, the thermal exposure of this ion exchanged form showed an unreported high temperature transformation to a nanosized oxide structure. The Le Bail refinement process showed that both materials produced had nanosized structures, of 12 nanometers to the structure obtain from the ion exchanged form and of 24 nanometers to the cassiterite obtained from trial E_6, table 43. As figure 70 shows the separation between cassiterite and tenorite is clear. The cassiterite resulting from the amorphous trial had more time to crystallize.

Table 43. Crystallographic data of thermally exposed samples E6 and Cu-AV-6. Exposure for 4 hours at 750°C.

	AV-6 Cu after 750°C	**E6 after 750°C**
Rwp	19.3(6)	17.3(2)
GOF	1.1(4)	1.0(3)
Space group	P42/mnm	P42/mnm
Volume (Å^3)	71.30(3)	71.64(9)
Crystal size (nm)	12±1	24±1
a (Å)	4.73(3)	4.73(9)
c (Å)	3.18(2)	3.19(1)

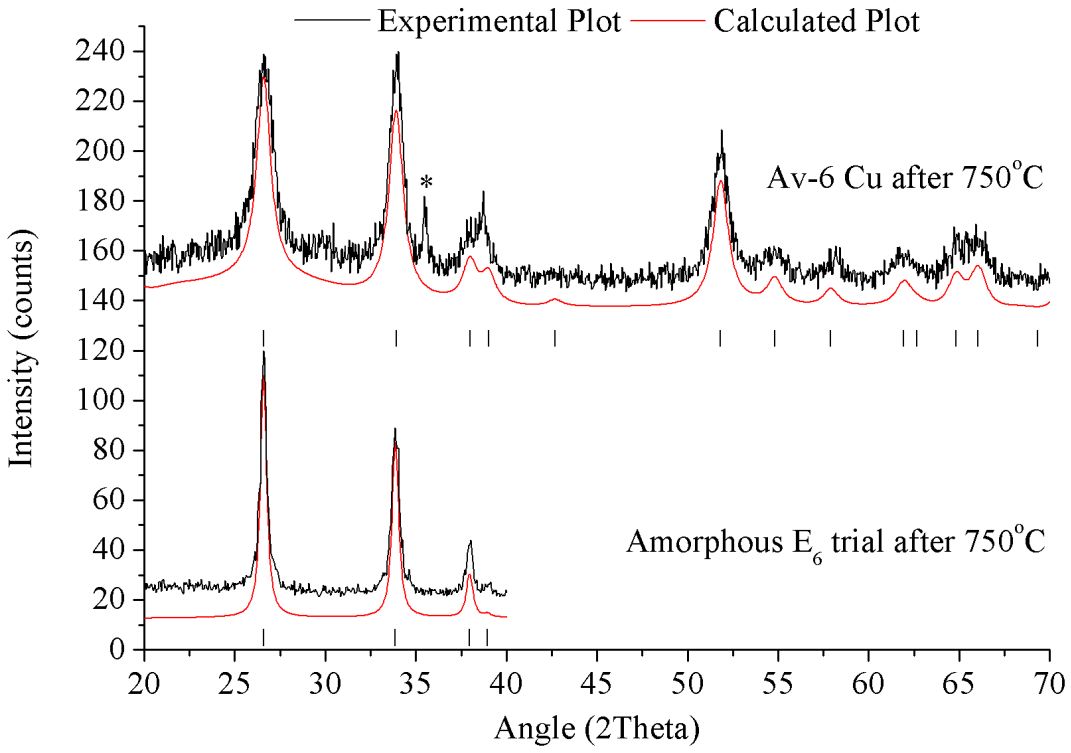

Figure 70. Experimental and simulated curves after Le Bail refinement of the cassiterite formed by thermal exposure of samples E6 and Cu-AV-6.

The transformation of amorphous material into nanosized cassiterite was unexpected but of small interest in terms of stannosilicates thermal properties. However, the Cu-AV-6 high-temperature transformation into cassiterite was a unique behavior in this type of frameworks. The normal thermal transformation of AV-6 is Sn-AV-14 or Sn-wadeite depending on the temperatures of thermal exposure. Copper had a vital role in the formation of this phase so it is possible that during the heating process some other phenomena may have happened differently from the typical behavior of AV-6.

7.6.2 Detailed analysis of AV-6 and AV-6-Cu thermal stability

The thermal behavior of AV-6 was already studied and reported [54]. In that study it was possible to see that this framework has a negative thermal expansion after 200°C and that the expansion is reversible as the samples temperature drops again. This negative thermal expansion was detected by the shift of the diffraction peaks. In this work the same thermal study was performed in order to compare the behavior of AV-6 and Cu-AV-6.

The two chemically different phases showed different behavior at high temperatures, figure 71. The change in the powder pattern of AV-6 was correspondent to a negative thermal expansion. This phenomenon was already reported [54] but in this sample the expansion happen at higher temperatures. The main reason for this higher temperature reaction was the presence of normal pressure in the surrounding environment. In the previous report [54] the thermal study was performed in a vacuum environment causing the water release and consequent negative expansion to happen at lower temperatures. This change was seen in the powder pattern by an intensity increased peak and a slight movement on some diffraction planes. In terms of unit cell the c-axis suffered higher contraction making the volume drop after the 300°C. For Cu-AV-6 this negative expansion appeared at lower temperature (200°C). To this chemical form of AV-6 the expansion caused even more changes in the powder pattern. The volume drop was near 2 times the one seen on AV-6 due to the contractions of b- and c- axes (figure 71). The exchange of potassium for copper accelerated and intensified the negative thermal expansion but also introduced thermal instability. The AV-6 sample reached 700°C without any crystallinity drop, Cu-AV-6 started amorphization after 500°C. This amorphization lead to the recrystallization of cassiterite at 750°C as it was seen in the previous point.

By Le Bail analysis it was possible to understand that AV-6 changes its space-group at 300°C, from orthorhombic $P2_12_12_1$ to monoclinic $P2_1/c$. This change happens without any crystallinity loss and with complete reversibility as shown in figure 72. Figure 72 shows powder

patterns of the test samples (AV-6 and Cu-AV-6) after thermal exposure. It can be seen that the AV-6 structure recovers to the orthorhombic space-group from any temperature. This recovery was complete and did not change the materials unit cell. This indicated that AV-6 can dehydrate and rehydrate without suffering any irreversible change at the structural level. This easy transition between the orthorhombic and the monoclinic space-groups helps to understand why the same change happens when this structure is successfully ion exchanged.

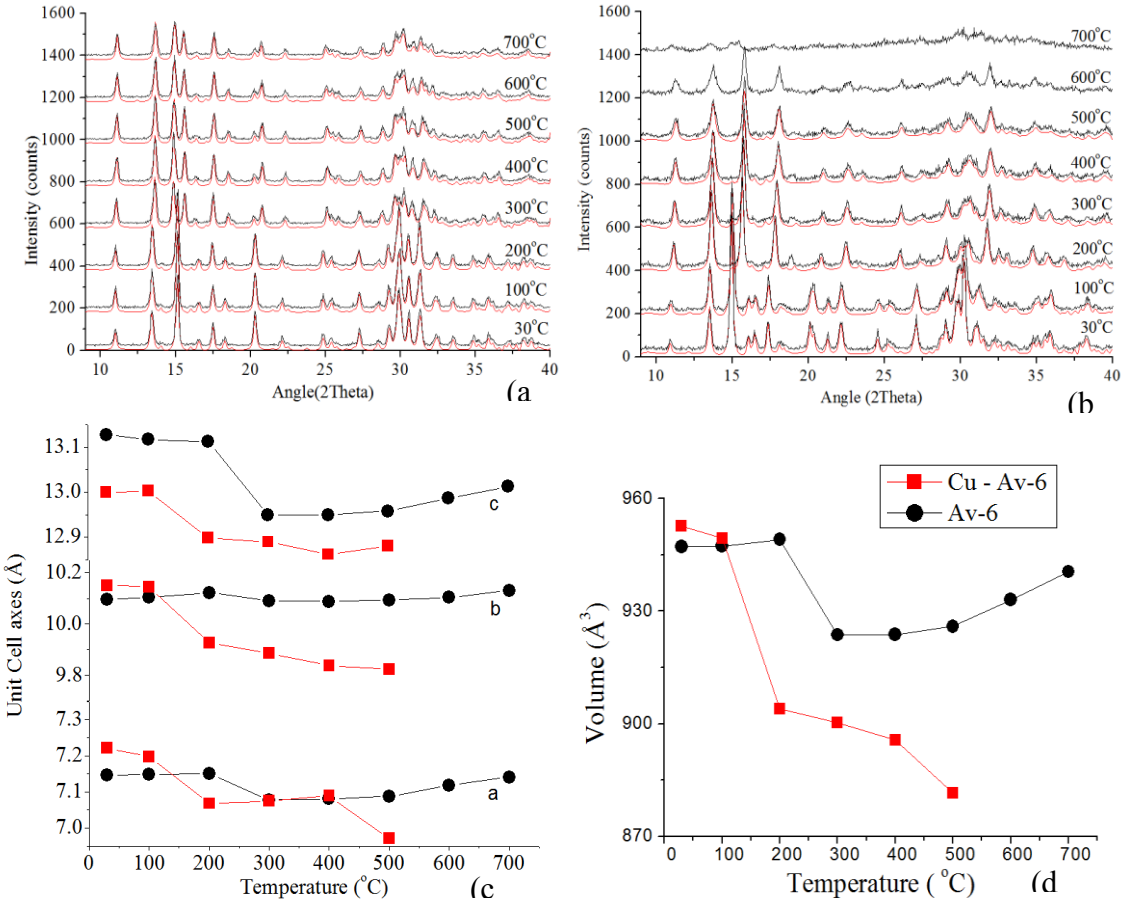

Figure 71. Experimental (Black) and calculated (red) PXRD patterns of AV-6 (a) and AV-6-Cu (b) performed at different temperatures. Unit cell axes (c) and lattice volume (d) of AV-6 and AV-6-Cu at different temperatures.

In Cu-AV-6 the transformation at high temperatures was of different nature. The contraction happened at lower temperatures, 200°C, and by analyzing the after exposure powder patterns it was possible to see that the negative thermal expansion was not fully recuperated. The copper inside the porous framework does not allow full rehydration. In fact since the water molecules on Cu-AV-6 are placed in mixed occupancy with copper, once they are removed by high temperature its full return is not possible. After 100°C the unit cell of this material has no recovery on the a and b axes (figure 72c) This explains the early amorphization of Cu-AV-6, after water release the 8-ring pore occupancy changes and the materials gets structurally instable.

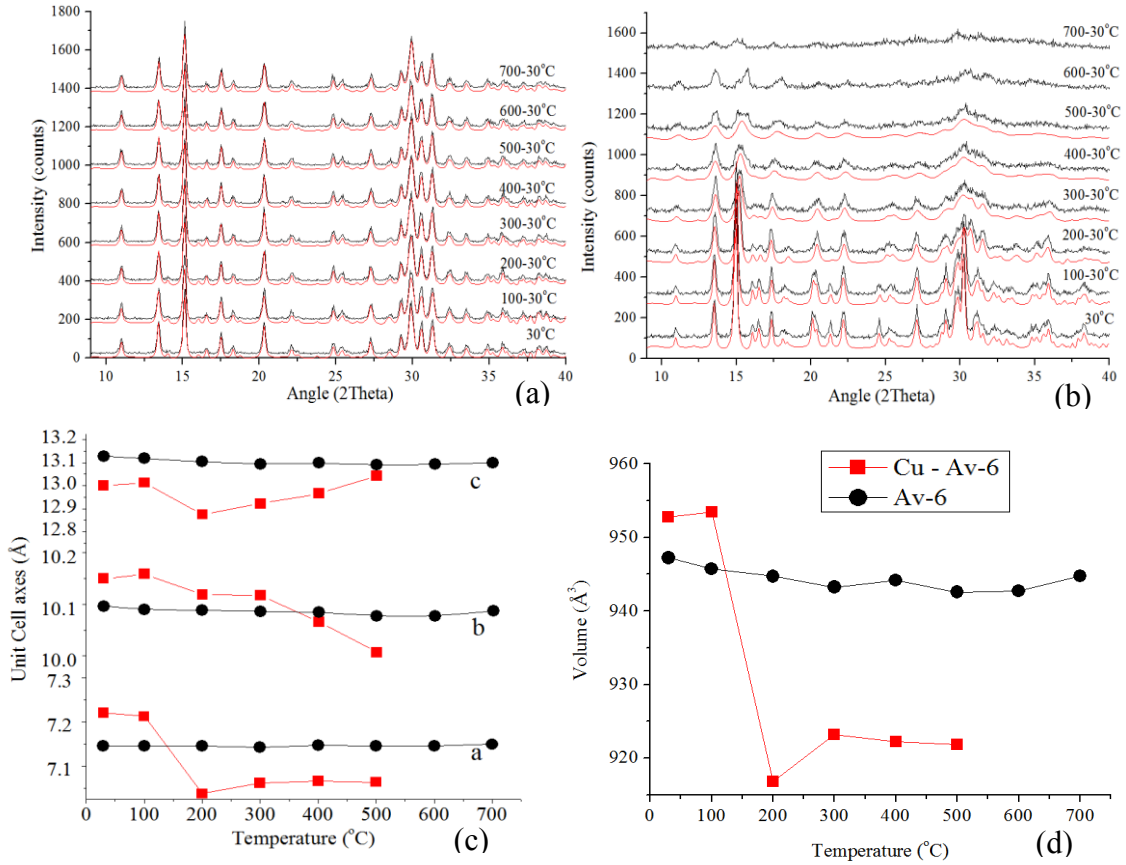

Figure 72. Experimental (black) and calculated (red) PXRD patterns of AV-6 (a) and AV-6-Cu (b) performed at ambient temperature after heating at different temperatures. Unit cell axes (c) and lattice volume (d) of AV-6 and AV-6-Cu at ambient condition.

The preservation of the original unit cell dimension proves the stability of AV-6 up to 750°C. As for Cu-AV-6, the ion exchange made the structure more vulnerable. The instabilities introduced by the capture of Cu^{2+} decreased the material thermal stability and removed its ability to fully rehydrate. Nevertheless it was also this incorporation of copper that allowed this ion exchange material to recrystallize into cassiterite after total amorphization. This transformation started at 700°C and was completed at 750°C.

7.6.3 Heating at 800ºC for 4 hours

In this study were used samples from isomorphous substitutions, ion exchange of AV-7 and potassium bases stannosilicates. After thermal exposure for 4 hours the powders were visually analyzed and none of the samples had melted. The F_1 powder had changed from grey to white powder, the typical color of bismuth oxide. Cu-AV-7 also changed from a blue to green, this color change happen due to the dehydration of copper chloride present at the sample surface Contrarily to Cu-AV-6 this phase did not turn brown but remained with a more light coloring. This could indicate that there is more to the color aspect than the state of the remains of copper chloride. The structural modifications that happened to the stannosilicate may have also influenced the change of color. All other powders presented the original shape and colors

indicating that no major transformation happened during thermal exposure. Nevertheless the XRD results after that exposure, figure 73, showed that the materials crystalline structure had changed in all samples.

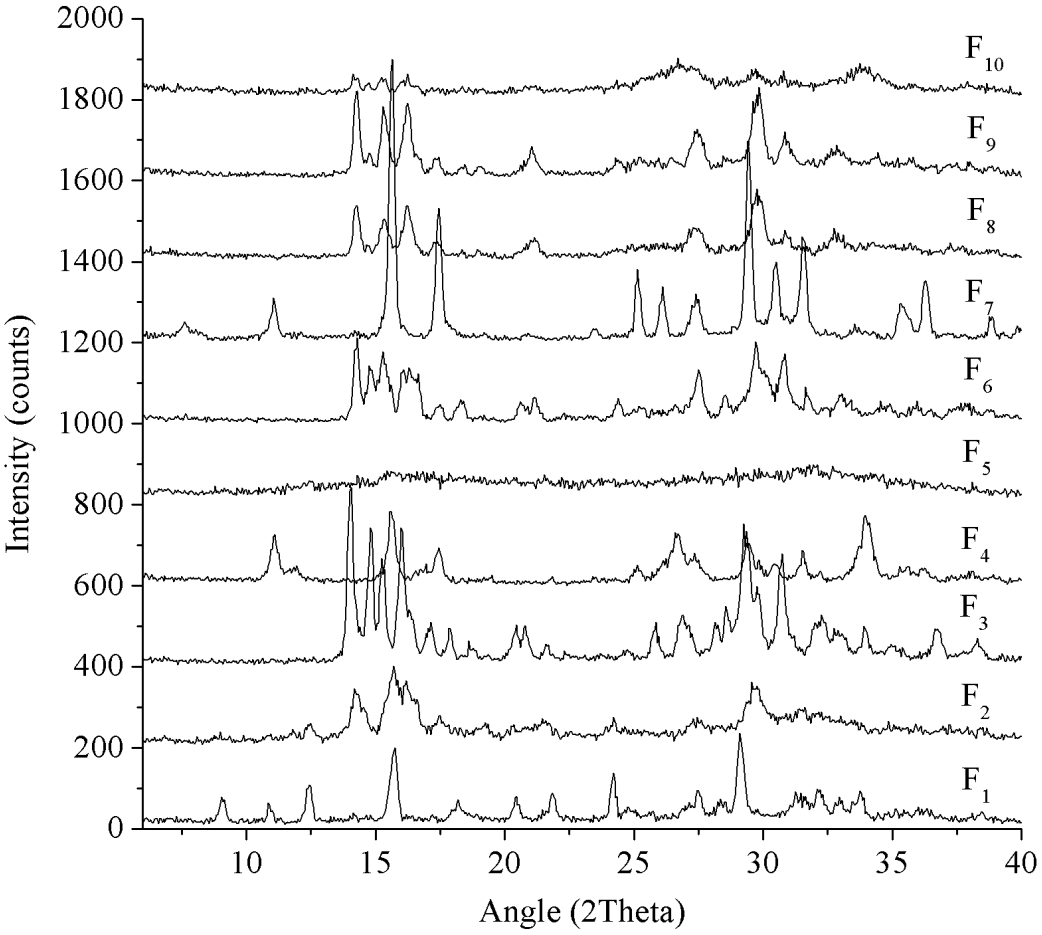

Figure 73. Experimental powder XRD patterns of the thermally exposed samples. Exposure at 800°C for 4 hours.

The result of the thermally exposed bismuth isomorphous substitutions (F_1) was identified as a mixture of unknown impurities and bismuth oxide. Even during the precursor preparation this material showed separation between bismuth and the other elements and after thermal exposure it was clear that this material was no longer a microporous silicate.

The majority of the stannosilicates heated at 800°C remained crystalline after exposure and there was no formation of cassiterite. The transformation seen at 750°C on Cu-AV-6 was not repeated for AV-7-Cu at 800°C (F_{10}). This two exchanged structures behaved differently upon high temperature exposure. The pure form of AV-7 (F_6) clearly degraded with exposure, like in the test at 750°C. The crystallinity loss was high but at 800°C this sample showed some emerging diffraction peaks that indicated a start of structural change. The other form of AV-7, Ge-AV-7 (F_7), behaved differently from the regular framework. Instead of a simple loss of crystallinity, after the

exposure, this sample revealed a completely different high crystalline structure. The structure was identified as Sn-AV-11, the high temperature transformation of AV-6 and AV-7. Never reported at such a low temperature, this transformation was clearly accelerated by the presence of germanium. The Le Bail refinement, figure 74, showed that all AV-7 had transformed into Sn-AV-11 leaving only traces of AV-6. That AV-6 was still present at its initial orthorhombic space-group but with much inferior volume, table 44. There were no proves that germanium had entered the AV-7 framework but even if only present in the material as an amorphous oxide, this material had some effect in the AV-7. Its thermal stability was clearly reduced because none of the other samples of AV-7 exposed to 750°C or 800°C showed this level of transformation. The sample also presents a small impurity in the low-angle 2theta values. This contamination was not identified but it probably comes from germanium oxide residing outside the framework.

Table 44. Crystallographic data from sample F_7. Le bail refinement using AV-6 and Sn-AV-11 data.

	Sn-AV-11	**AV-6**
Rwp	21.1(7)	
GOF	1.4(1)	
Space group	R3 (146)	$P2_12_12_1$
Volume (Å^3)	1326.02(2)	915.85(7)
Crystal size (nm)	50.5±0.1	34.7±0.1
a (Å)	10.16(3)	7.078(3)
b (Å)	-	10.07(9)
c (Å)	14.82(3)	12.83(7)

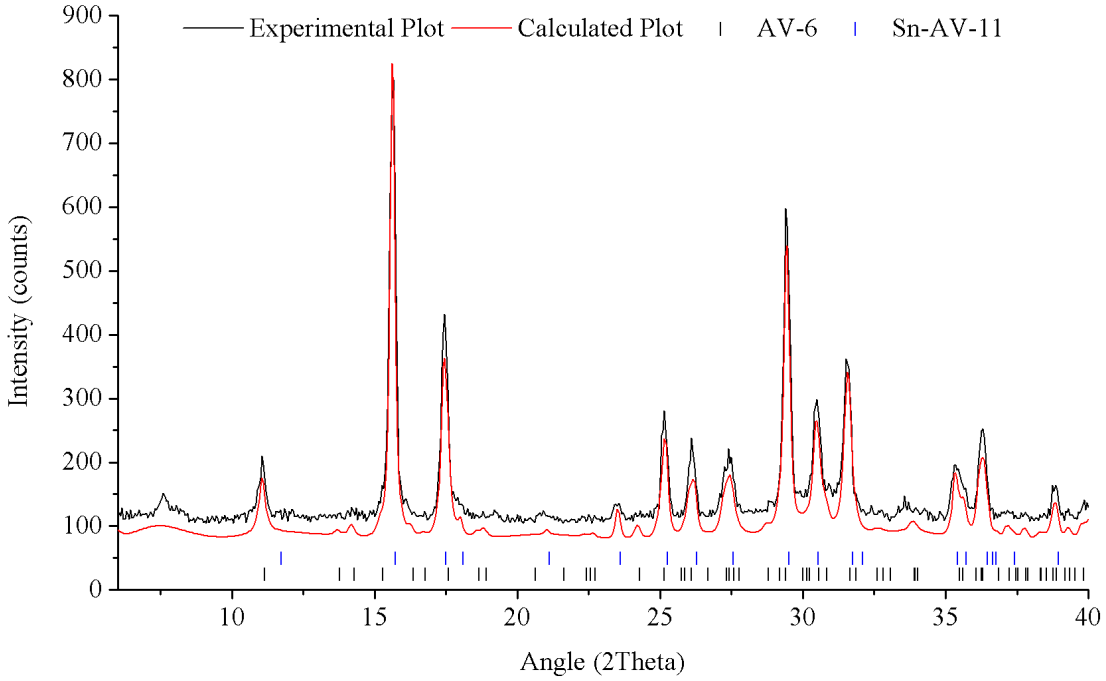

Figure 74. Experimental and simulated powder XRD patterns obtained by Le Bail refinement. Collected on sample F_7, mixture of Sn-AV-11 and AV-6.

The potassium stannosilicate layered phase (F_4) also had a unique behavior when heated. By the amount of extra diffraction peaks seen in its powder pattern it appeared that this structure had changed into a different phase. After Le Bail analysis this material should very close resemblance to Sn-AV-11, figure 75. The high temperature exposure did not fully transform the crystal structure, since there were still diffraction peaks of the initial layered phase, turning it into a mixed phase material. The layered phase does not share the same pore or framework disposition of AV-6 and AV-7 nevertheless this structure has the same high temperature transformation as AV-6 and AV-7. In some aspects the layered phase is very similar to Sn-AV-11. They share the same element ratio 1 to 1 to 1 in Sn, Si and K needing no element release for the transformation. The same does not happen with AV-6 and AV-7 that have a 3 to 1 ratio of Si and Sn. In these phases the remaining silicon oxide stays out of the structure as amorphous material. It seems that this layered phase started its transformation to Sn-AV-11 earlier than AV-6 or AV-7 but 800°C during 4 hours were not enough for total transformation.

Table 45. Crystallographic data of Le Bail refinement of sample F_4.

	Layered phase	**Sn-AV-11**
Rwp	23.9(9)	
GOF	4.9(8)	
Space group	P-31m	R3
Volume (Å^3)	209.36(1)	1308.75(5)
Crystal size (nm)	16.9±0.1	15.2±0.1
a (Å)	5.58(3)	10.17(1)
c (Å)	7.75(5)	14.61(1)

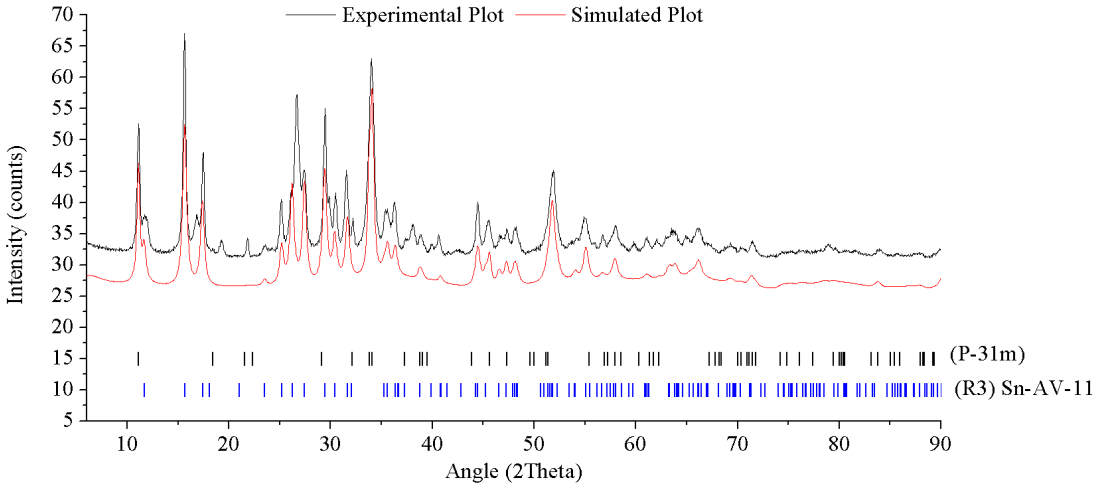

Figure 75. Le Bail refinement of the high resolution powder XRD pattern of trial F_4. Experimental (black) calculated (red).

The F_3 sample, which had unknown structure, suffered some minor changes but didn't appear to have suffered a recrystallization. The thermally exposed material showed a similar

pattern to the one it had before. It is possible that the differences between patterns are due to the material dehydration but without understanding exactly what this material is there was no possible characterization to be made.

The Zn-AV-7 forms (F_8 and F_9) showed greater resistance to structural change when compared with normal AV-7 (F_6) or AV-7-Cu (F_{10}). The powder patterns of these exchanged forms kept more similar peaks to the AV-7 than the thermally exposed AV-7. As proven before, the zinc enters in the 8-ring pores exchanging all of the sodium and potassium from that position. This introduces some hydroxide bonds but also increases the strength of connection on the 8-ring pore since zinc as a higher charge than sodium and potassium. With reinforced pores the Zn-AV-7 material can withstand higher temperatures without the loss of the characteristic diffraction peaks.

The 72 hours exchanged material presented even better results than the 24 hours sample indicating that the more zinc is in the porous framework the more thermal resistance it possesses. The Le Bail refinement to the 72 hours AV-7-Zn after 800°C exposure showed that this material was still represented by the crystallographic data of AV-7. Small changes were seen in the cell volume, table 46, and on some of the diffraction peaks, figure 76. These changes came from the irreversible dehydration phenomenon that occurs on the ion exchange frameworks. Like on Cu-AV-6, after water release the Zn-AV-7 structure cannot rehydrate and therefore loses structural stability.

Table 46. Crystallographic data for Zn-AV-7 after 800°C for 4 hours.

	AV-7-Zn 800ºC
Rwp	11.1(1)
GOF	2.4(9)
Space group	$P2_1/c$
Volume (Å^3)	924.56(4)
Crystal size (nm)	32.6±0.1
a (Å)	6.42(2)
b (Å)	11.58(5)
c (Å)	12.88(1)
β(◦)	105.29(2)

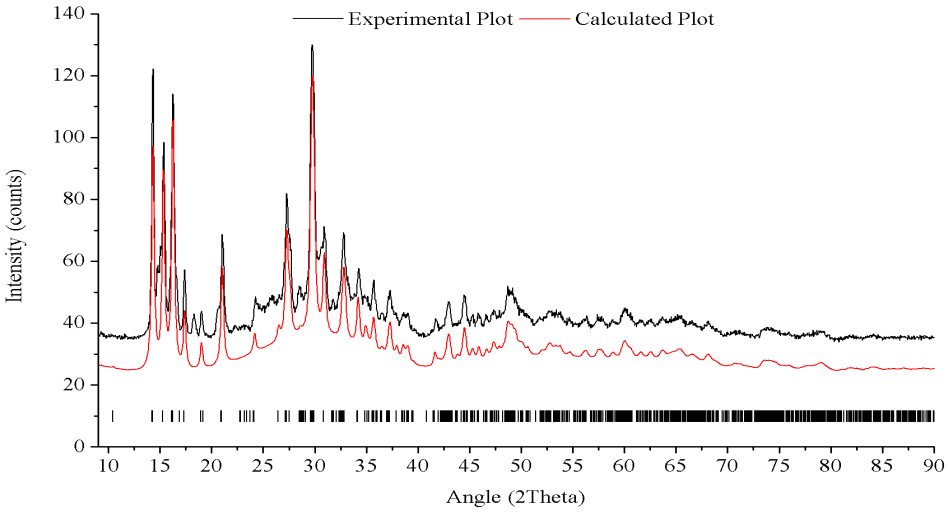

Figure 76. Experimental and calculated patterns of AV-7-Zn after 800°C for 4 hours.

This result was contradicted by the result of the 750°C exposure where the AV-7-Zn sample turned to an amorphous material. The result obtained at 800°C had higher confirmation since two samples were tested and both times of exchange presented the same thermal stability. It is possible that the 750°C the exposed AV-7-Zn sample had large amounts of defects prior to oven entry. This defects lead to a loss on thermal stability and an early amorphization.

7.6.4 Heating at 1000ºC for 5 hours

At this high temperature the main purpose was to understand which samples could withstand the thermal exposure without melting. Samples H_5 and H_6 melted during thermal exposure and due to the porous nature of the ceramic tile used for support they were irretrievable. The unknown sodium phase endured well at 800°C but it appears that now with zirconium (H_5) its solid state phase ends before 1000°C. The amorphous material (H_6) and its chemically equal solid block (H_7) also melted. By its aspect H_7 only melted at the block surface (Figure 77). The material suffered enormous retraction but with all sides equally reduced and with the same cubic shape it had before entering the oven. The average size retraction was 44% leading to a volume retraction of 83%. The solid block had a weigh variation of 8% transforming its density from 0.27g/cm^3 before high temperature exposure to 1.44g/cm^3 after 1000°C for 5 hours. The material was now covered by a glassy surface and had lost the ability to perform water absorption. Upon visual inspection all other

Figure 77. Solid block (Sample H7).

samples were still in this powder form and the H_1 trial, amorphous before the thermal exposure, had change from yellow to a white powder (just like sample E_6 on the 750°C thermal exposure).

All the powders and the solid block were analyzed by XRD and the results, figure 78, showed that the high temperature transformations were much more developed. The two retrievable amorphous samples, H_1 and H_7, showed after thermal exposure the same crystalline phase, cassiterite.

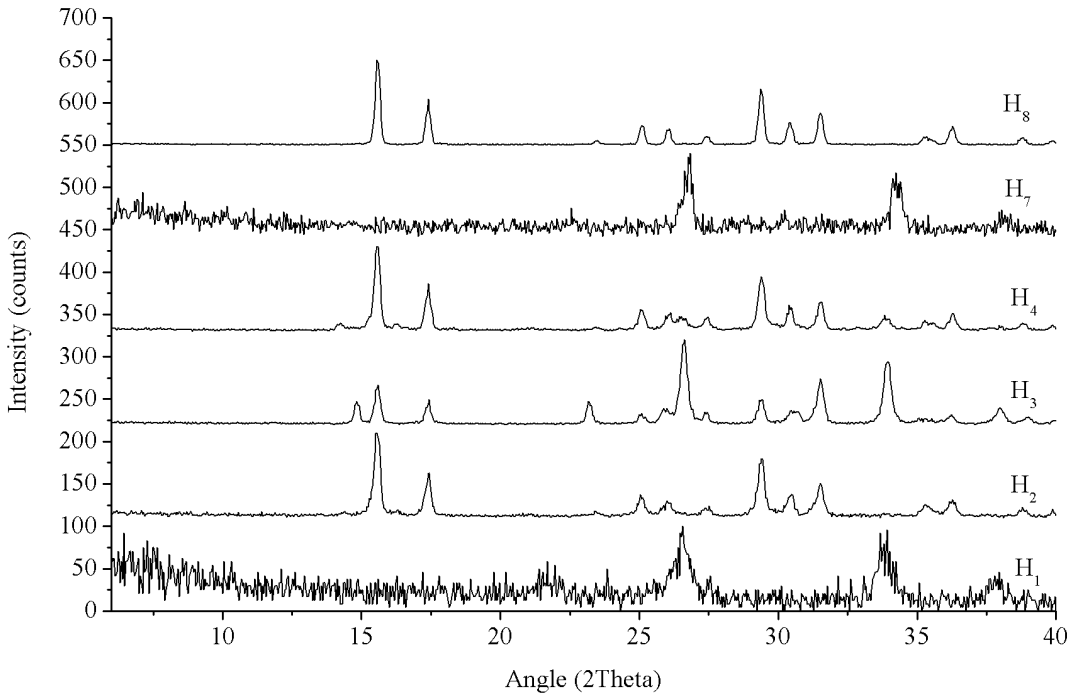

Figure 78. Experimental powder XRD patterns of the thermally exposed samples. Exposure at 1000°C for 5 hours.

H_2 and H_4, representing AV-6 and AV-7 showed similar patterns. Both materials had near pure Sn-AV-11 indicating that the transformation to its high temperature form has not completed. On H_8 (the germanium substation that produced 70% AV-7 and 30% AV-6 material) however, that transformation was complete. The Sn-AV-11 structure seemed pure proving that germanium had some effect on the thermal properties of the mixed phase stannosilicate. H_3, that represented the potassium layered stannosilicate, showed signs of the two high temperature transformations mentioned above. The powder pattern of this material had the characteristic diffraction peaks of cassiterite, Sn-AV-11 and some other phases.

With high resolution XRD analysis H_4 showed even more diffraction planes and after EVA matching it was possible to see that this material suffered more than one transformation. The potassium layered stannosilicate (H_4) when exposed to 1000°C lost all its initial characteristics and decomposed into 4 different phases. These phases were cassiterite (PDF 01-072-4275), Sn-

AV-11 identified thanks to its titanium analog (PDF 01-072-4275), Sn-wadeite (PDF 00-027-0446) and a silicon oxide form (PDF 00-052-1425). The three tin phases appeared naturally. Sn-AV-11 was already forming at 800°C and it must have ended its transformation before 1000°C. As the thermal exposure at 1000°C continued some of the Sn-AV-11 started to transform into Sn-wadeite. Since Sn-wadeite as different Sn-Si ratio the extra tin was amorphous and crystallized as cassiterite. All this transformations left some remnants of Si that crystallized separately in its oxide form. All these phases can be identified in the high resolution powder pattern, figure 79, where the Le Bail refinement allowed to performed plane identification and full pattern simulation. The dimensions and crystal sizes of all the high temperature transformation phases can be seen at table 47.

Table 47. Crystallographic data from the Le Bail refinement of trial H_3. Obtained using a high resolution powder XRD pattern.

Rwp	10.72			
GOF	1.59			
	Sn-AV-11	**Sn-Wadeite**	**SiO_2**	**Cassiterite**
Space-group	R3	P63/m	I2/a	P42/mnm
Crystal size (nm)	49.9	55.8	41.3	41.5
Volume (Å^3)	1327.9(3)	409.7(1)	456.2(1)	71.22(9)
a (Å)	10.16(2)	6.87(7)	8.93(3)	4.73(2)
b (Å)	-	-	4.73(4)	-
c (Å)	14.84(6)	10.00(1)	10.78(6)	3.18(1)
B (º)	-	-	89.88(8)	-

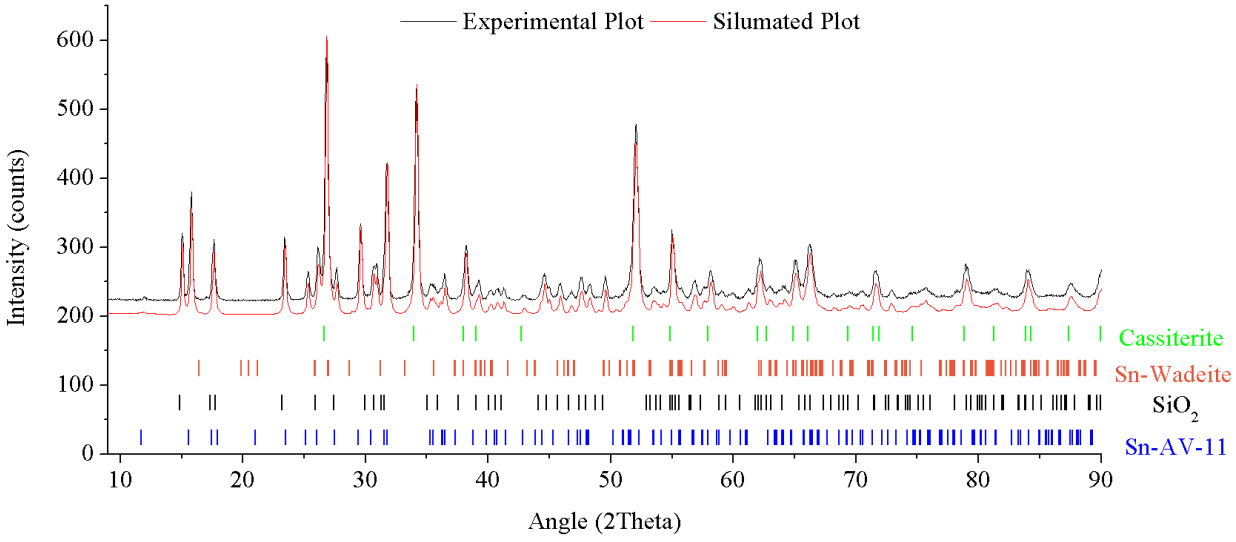

Figure 79. Experimental, calculated and plane occupation patterns of the Le Bail refinement for trial H_3.

H_2, H_4 and H_8 were confirmed as Sn-AV-11 by Le Bail refinement. However, only the H_8 sample presented a pure form of this phase. Both H_2 and H_4 had remnants of its original phases,

AV-6 and AV-7 respectively. The thermal stability of the as-synthesized AV-6 and AV-7 was higher than the isomorphous substituted material (H_8). Even if no germanium was detected in the initial structure its effects were yet again proved by this higher temperature exposure. Germanium increases the material reactivity speeding up the transformation process. This can be seen by the total elimination of any extra diffraction peak in the H_8 sample. At 800°C this material had already started the transformation to Sn-AV-11 but the powder pattern still presented two major impurities. At this temperature the transformation was completed and no traces of germanium were found. This indicated that this element remained in its amorphous state even at 1000°C. The Le Bail results show the differences between the three materials. In figure 80 it is possible to see the remains of AV-6 and AV-7 on the thermal exposed materials and on table 48 the lattice dimensions of all the Sn-AV-11's formed.

Table 48. Crystallographic data from the materials transformed into Sn-AV-11.

	H_2	**H_4**	**H_8**
R-Bragg	3.6(3)	3.8(7)	6.0(9)
Space-group	R3	R3	R3
Volume (Å^3)	1321.1(4)	1321.9(5)	1323.7(8)
Crystal size (nm)	40.5	52.4	78.8
a (Å)	10.14(5)	10.15(1)	10.15(9)
c (Å)	14.82(2)	14.81(6)	14.81(1)

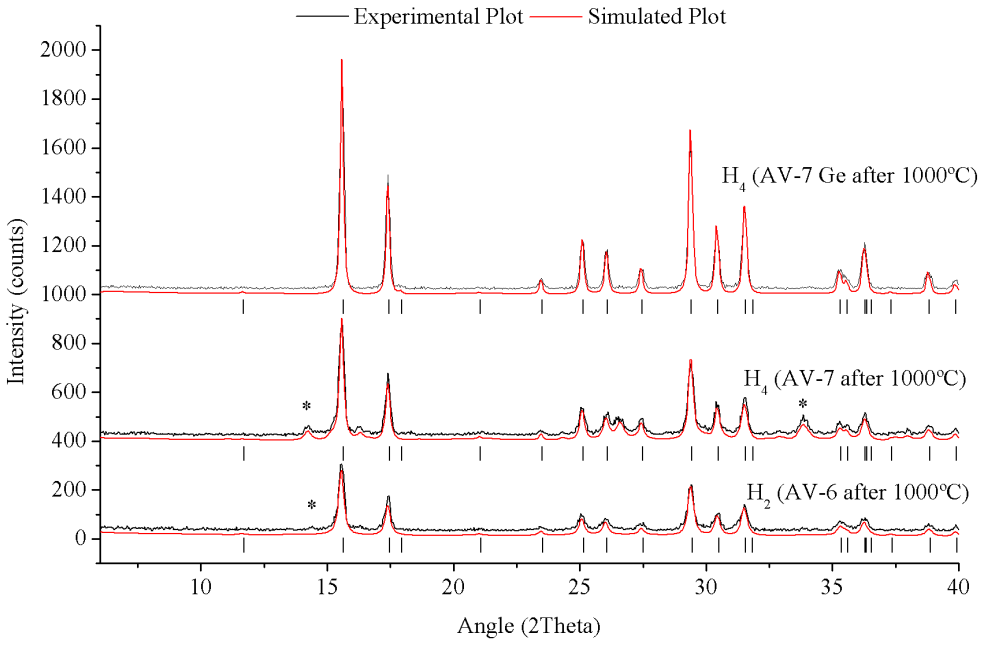

Figure 80. Experimental and simulated plots of the Sn-AV-11 heated at 1000°C for 5 hours.

For the initial amorphous samples, H_1 and H_7, the thermal exposure resulted in transformation to cassiterite. This, yet again, nanosized crystals were dispersed in amorphous silica without any other crystalline impurity. The Le Bail refinement showed the phases unit cells and the actual size of these particles, table 49. The simulated curves, figure 81, confirmed the absence of other crystalline forms.

This was the fourth time cassiterite was produced from high temperature transformation. Three out them were produced from heating amorphous materials with different chemical compositions. The fourth was produced via thermal degradation of Cu-AV-6 and was contaminated with crystalline copper oxide.

Table 49. Crystallographic data for cassiterite. Le Bail refinement of samples H_1 and H_7.

Space-group	P42/mnm	P42/mnm
Cell Volume (Å^3)	72.13(1)	70.76(7)
Crystal Size (nm)	14.5±1	32±1
a (Å)	4.75(3)	4.73(4)
c (Å)	3.19(1)	3.15(6)

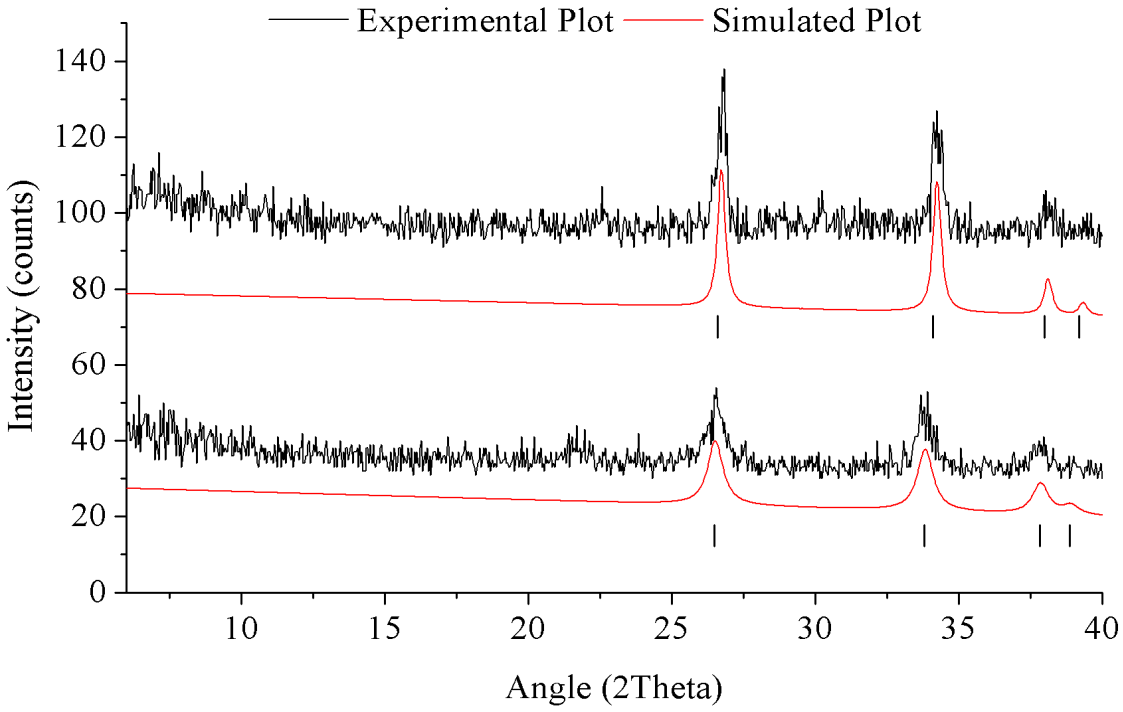

Figure 81. Experimental and calculated curves of samples H_1 and H_7. Le Bail refinement of cassiterite.

VIII Conclusions

After more than 400 experiments including synthesis, ion exchange, isomorphous substitutions and thermal treatment this work produced more than 300 samples. As a result more than 300 XRD powder patterns were collected. All in order to understand the unique phenomena that is involved in the production of stannosilicates using a transparent precursor. All this work served not only to identify the typical stannosilicate structures formed at each composition but also to produce new frameworks and to identify unique behaviors of the synthesis process. This work resulted in one publication in international journal and created the first synthetic materials called after the University of Minho (UM-1 and UM-2)

8.1 Synthesis using a transparent precursor

This newly developed method started as a great incognita for what would be the optimal compositions for the synthesis of the already known stannosilicate structures. The first syntheses allowed understanding what compositions would favor each structure. As the experience has advanced it was also possible to prove that not only initial batch composition is responsible for the successful phase formation. This work managed, for the first time to produce different stannosilicate structures by changing the precursor agitation time. This work also used different compositions with a single alkaline element to search in crystallization fields that have never been explored. By studying the effect of each alkaline element (sodium and potassium) it was possible to understand its individual role in all stannosilicate compositions. The reduced time of synthesis (2 days) also showed that stannosilicates have fast synthesis. This production speed makes a large difference in terms of mass production for industrial purposes.

8.1.1 Sodium stannosilicates

These compositions were the least successful trials of all synthesis. The crystalline phases only appeared in medium sodium and tin compositions but even those were far from high crystalline materials. The pH given by the sodium hydroxide presence produced very aggressive solutions that destroyed most of the crystalline material. From the synthesis parameters study it was possible to conclude that more time of synthesis only progressed the destructive effect. Despite that, the synthesis of sodium based silicates resulted in new material. It was found that this material has a lattice with relatively big volume (more than 1400Å^3) and possibly a porous framework. It was produced by several compositions indicating that it was the most chemically favored phase of all sodium-based tin silicates. From the studies performed it was possible to conclude that this phase its only stable until 2 days synthesis at 200°C. To its forming composition any longer time than 2 days in oven produces a non-silicate material. However, due

to the low crystallinity of all samples this phase was not indexed. The other synthesized material, AV-10, also appeared with low quality. The time of synthesis may have done the same damage as to the other phase. Several adjustments were made to improve these phases crystallinity but none of them had success. This sodium based tin silicates were the first compositions to reveal the effect of precursor agitation time. The change from 15 to 30 minutes of precursor agitation time made a composition of the unknown sodium phase produce a material with all the characteristics of AV-10.

8.1.2 Potassium stannosilicates

This field was created to enhance the production of AV-6. The compositions tested were very similar to the chemical composition of this stannosilicate. AV-6 appeared as the dominant phase, however, there were other frameworks synthesized. AV-7 appeared in a free sodium phase proving that this element is not decisive for its crystallization. The synthesis of a potassium AV-7 showed that the framework is flexible to different charge stabilizers. These two phases AV-7 and AV-6, appeared in many compositions together as mixed phase material. This showed that these two frameworks have similar initial building units and that probability to form one or the other is close to 50%. In fact the study of the precursor agitation time came to prove just that. That study also proved that it is possible to control the resulting structure by allying chemical composition and precursor agitation time. AV-7 framework showed the need for high agitation times in order to grow as a single phase and eliminate the AV-6 nucleus.

In terms of synthesis success, the potassium based silicates also proved to have some deficiencies. The synthesized powders were most of the times of small size, enabling filtration. Like in the sodium based tin silicates there were some compositions that did not form any solid material. However, comparing to the sodium base tin silicates these powders had much higher crystallinity and no tendency to dissolute in long time synthesis.

In these potassium based tin silicates it was also possible to produce a new type of framework called UM-2. This layered potassium tin silicate had very small volume but interconnected chains of SnO_6 octahedra. These chains were separated by SiO_4 tetrahedra and the formed layers separated by potassium ions and water molecules. This phase has unknown properties but from the structural information gathered here it is possible to say that it could have possible applications in linear electronics or composite materials.

8.1.3 Sodium and potassium based tin silicates

The sodium and potassium based stannosilicate compositions are the most widely used. The presence of small amounts of sodium increases the precursor activity leading to a faster synthesis. The presence of potassium chemically stabilizes the precursor allowing it to form high crystalline materials. These two elements together provide properties to the precursor that none of the single alkaline compositions possess. In terms of success of synthesis, the use of sodium and potassium in the precursor ensures the formation of crystalline material even in short time precursor agitation and synthesis. Using these two alkaline elements there were no problems with chemical stability at long/short time synthesis or low crystallinity. The potassium in the precursor leads to materials with well-defined powder patterns of highly crystalline phases.. The sodium leads to fast grain size growth and results in good quantities of crystalline material. These compositions were optimal to produce Na-K-AV-7 but since the sodium often stays out of the crystallization process the formation of AV-6 is also possible. To guaranty the formation of AV-7 the precursor agitation time must be high and to produce AV-6 the agitation must be kept at minimum. These typical compositions were important to prove that the transition between AV-6 and AV-7 is also possible in sodium and potassium precursors. It also showed that it is possible to produce high quality materials at short synthesis time making this process more industrially profitable.

8.2 Ion exchange forms

These tests were used to characterize AV-6 and AV-7 in terms of ion exchange abilities. The tests were used to understand which element had higher reactivity to each structure and to obtain some chemically different forms of AV-6 and AV-7.

The exchanges performed on AV-6 did not reveal any unknown behavior. Nevertheless the tests helped to develop the already discovered Cu-AV-6, looking for its ion exchange limits and thermal stability. The ion exchange experiments done on AV-6 also revealed that zinc has affinity to the microporous framework but its capturing process is much slower. After 48 hours of exchange the materials crystalline structure was not completely changed. The ion exchange result was a mixture of Zn-AV-6 and AV-6 meaning that the orthorhombic to monoclinic transformation was not complete. Aluminum and lead ion exchange experiments showed that this framework is destroyed not by the pH of the ion exchange solution but by the external ion activity. In terms of reactivity, it was also seen that, in these ion exchange conditions, sodium and chromium had no affinity to this microporous sieve. The exchange with aluminum showed some

signs of changing the structure of AV-6 to the monoclinic space-group but the EDS results showed that no Al^{3+} was in the stannosilicate framework.

The ion exchanges experiments done on AV-7 showed some new unexpected results. This structure showed a unique behavior when ion exchanged, presenting different powder patterns depending on the coordination of the captured ion. The sixth coordinated ions that were successfully exchanged (copper and chromium) made a great change on the material crystalline structure. Both Cu-AV-7 and Cr-AV-7 had a shift in the (020) plane. The 8-ring pore occupants completely changed its position in order to accumulate this different coordination ion. Chromium showed a much faster exchange than copper mainly due to the ion valence difference. The trivalent ions had much higher affinity to the microporous framework. The eighth coordinated ions that were successfully exchanged (zinc, lead and strontium) had all divalent charge and did not affect the position of plane (020). In fact, the only change in the powder patterns that indicated its presence was the drop of intensity of the same plane. The amount of intensity loss at each ion exchange experiment was directly influenced by the nature of the captured ion. Each ion (zinc, lead and strontium) had its characteristic intensity loss. When the difference between planes was 30% the material was at the as-synthesized AV-7 form, 70% indicated exchange with zinc, 55% indicated exchange with lead and 50% exchange with strontium. This difference in intensity depending on the captured ion can be used for sensor applications. Detecting lead in consumable waters is a very likely application. By introducing AV-7 in that water it is possible to know by XRD if the liquid is contaminated. The quick times of exchange also help in the use in this application. The exchange with lead was performed in 18 hours. These preliminary tests suggest that this material can be used for filtration or sensory applications. However, it is still necessary to study the influence of multi ion exchange solutions to understand if this stannosilicate captures ions in a selective way.

8.3 Isomorphous substitutions

This attempt to modify the stannosilicates existing phases was not successful. None of the tried compositions revealed a clear modification of the framework characteristics. The purpose was to create modified porous materials with differently sized pores. However, all attempts to modify AV-7, AV-6 or any other phase failed and the majority of the products produced were not even crystalline.

Previous reports [20] produced a Sn-Zr umbite material so some kind of interaction was expected when performing the isomorphous substitution experiments. The Zr-Sn-umbite was the

most probable phase to be produced in these compositions. However that was not possible within the conditions that were attempted. Both 20% and 40% of substitution failed and the only crystalline silicates produced were AV-6 and K-AV-7. During these experiments with zirconium it was a material with an unindexed powder pattern. This material presented some characteristics of a zirconium silicate (AV-15) but no confirmation was possible. This phase had significant changes in powder XRD pattern when compared with the original AV-15. Those changes could be induced by the presence of a mixed octahedral occupation or simple by the presence of unknown impurities. This material appeared in a long time synthesis (5 days) indicating that some recrystallization phenomenon may had occurred. Increasing the time of synthesis in other isomorphic substitution experiments could had increased the odds of structural modification In order to form zirconium silicate building units the temperature or the synthesis time should have been much higher.

The isomorphic substation by titanium experiments also should no modifications of structures. The titanium source used in these trials was not the best. The lack of crystalline titanium forms indicated that $TiCl_3$ had very reduced reactivity in the precursor. From the tried compositions, the only crystalline forms obtained had the single contribution of tin and as percentage of titanium increased (from 20% then 40% and finally 60%) the tin silicates gradually lost their crystallinity. The sodium and potassium compositions produced pure AV-7 showing no interference from the large amounts of titanium in the precursor. A titanium silicate was produced in a sodium composition with 60% of titanium and 5 days of synthesis. In 5 days and with only sodium as alkaline element there were no conditions to form any tin silicate (as proven in the synthesis chapter), only natisite (titanium silicate) was possible to produce. To make this isomorphous substitutions work the single increase of time or synthesis temperature appeared to be not enough, probably a change in the source of titanium would improve the chances of obtaining a mixed octahedral silicate phase.

Despite the few attempts for substitution by germanium showed some detectable changes. No mixed octahedral or tetrahedral phase was discovered but effects of adding small amounts of germanium into the precursor were clearly noticed. The first was the increased amount of product retrieved from the autoclave when using this element. The trials that normally produced quantities of powder inferior to 1 gram produced, with small quantities of germanium, near 1.5 grams. The second effect was the increase in crystallinity in all the produced materials. Both AV-7 and the sodium tin silicate unknown phase had increased crystallinity induced by the external presence of germanium atoms. The third and final effect was the acceleration of the AV-

7 high temperature transformations. The Ge-AV-7 turned to Sn-AV-11 200°C below the normal temperature.

The isomorphous substitutions by bismuth failed due to the rapid precipitation of bismuth during precursor preparation. The synthesis resulting material had always two mixed phases, chemically and structurally different. One formed from the precursor elements (sodium, potassium, silicon and tin) the other formed out of the precipitated bismuth. This bismuth at normal synthesis remained in its metal form and at high temperatures it turned into its oxide form.

8.4 Thermal Properties

The heating of AV-6 and Cu-AV-6 showed difference in the thermal behavior of the two phases. Upon heating the structural changes in Cu-AV-6 are irreversible while the ones in AV-6 are completely reversible (up to 800 °C). Cu-AV-6 dehydrated at 200°C become distorted and slowly degrade when the temperature is further increased. At 700°C Cu-AV-6 gets completely amorphous and at 750°C transforms to a nanosized tin oxide with cassiterite structure.

These thermal tests it was also possible to find all the high temperature transformations of the potassium layered tin silicate. Starting the transformation to Sn-AV-11 before 800°C and completed before 1000°C. At this temperature this phase decomposed into Sn-wadeite, cassiterite and silicon oxide.

The transformations of AV-6 and AV-7 corresponded to the previous reports. These phases started to turn into Sn-AV-11 around 1000°C not finishing this transformation after 5 hours of exposure. The ions exchanged forms of these materials decomposed and turn amorphous at 750°C. This happen to all but the Zn-AV-7 that after 4 hours at 800°C still showed the main structural characteristics of its beginning phase. In fact this ion exchanged form showed more thermal stability than the normal AV-7 that at 800°C has nearly amorphous.

To report was also the transformation of all the amorphous samples into cassiterite when exposed to high temperatures (>750°C). This materials had unknown composition but turn from a room temperature amorphous state onto a good quality cassiterite.

8.5 Final considerations

The main achievements of the present work can be summarized as follows:

-Creation of crystallization fields for the synthesis of various stannosilicates;

- Synthesis of stannosilicates using potassium based tin silicates;

-Discovery of a new layered phase of potassium stannosilicates;

- Revealed the effect of the precursor agitation time on the run product;

-Synthesized the first sodium free AV-7;

-Performed the first successful ion exchange experiments on AV-7;

-Modeled the structural changes performed by each ion on the AV-7 framework;

-Studied the effects of non-structural effect of Ge on the thermal properties of AV-7.

- Synthesized cassiterite by decomposition of ~~an~~ ion exchanged AV-6.

IX References

[1]- Cheetham, A.K. Peter Day. Solid State Chemistry. Clarendon Press, 1992;

[2]- F. Ramôa Ribeiro, Alírio E. Rodrigues, L. Deane Rollmann, Claude Naccache. Zeolites: Science and Technology. 1984;

[3]- Cundy, C.S., & Cox, P. a. Chemical reviews, 103(3), (2003), 663-702;

[4]- G.D. Ilyushin, Inorganic Materials, 29, (1993), 1128-1133;

[5]- www.hypotheticalzeolites.net/NEWDATABASE/BRONZE_UNIQ/;

[6]- J. Rocha, M. W. Anderson, Eur. J. Inorganic Chemistry. (2000), 801-818;

[7]- Z. Lin, J. Rocha, P. Brandao, A. Ferreira, A. P. Esculcas, J. D. P. de Jesus, A. Philippou, M. W. Anderson, The journal of Physical Chemistry. B 101, (1997), 7114-7120;

[8]- B. Mihailova, V. Valtchev, S. Mintova, L. Konstantinov, J. Mater. Sci. Lett. 16(1997) 1303-1304;

[9]- M. S. Dadachov, A. LeBail, Eur. J. Solid State Inorg. Chem. 34 (1997) 381–390;

[10]- Z. Lin, J. Rocha, P. Ferreira, A. Thursfield, A.J. Agger, M.W. Anderson, J. Phys. Chem. B 103 (1999) 957-963;

[11]- D. M. Poojary, A. I. Bortun, L. N. Bortun, A. Clearfield, Inorg. Chem. 36 (1997) 3072–3079;

[12]- S. R. Jale, A. Ojo, F. R. Fitch, Chem. Commun. (1999) 411–412;

[13]- Döbelin, N., & Armbruster, T. Microporous and Mesoporous Materials, 99(3), (2007), 279–287;

[14]- Döbelin, N., & Armbruster, T. Materials Research Bulletin, 42(1), (2007) 113–125;

[15]- Thomas, B., Das, B. B., & Sugunan, S. Microporous and Mesoporous Materials, 95(1-3), (2006) 329–338;

[16]- Coleman, N. J., Lewis, S. P., Mendham, A. P., & Trivedi, V. Journal of Porous Materials, 17(6) (2009);

[17]- Ferdov, S., Shikova, E., Ivanova, Z., Dimowa, L. T., Nikolova, R. P., Lin, Z., & Shivachev, B. L. RSC Advances, 3(23), (2013) 8843;

[18]- Sebastián, V., Bosque, J., Kumakiri, I., Bredesen, R., Ansón, A., Maciá-Agulló, J. a., Linares-Solano, Á., et al. Microporous and Mesoporous Materials, 142(2-3), (2011), 649–654;

[19]- S. Ferdov, Z. Lin, R. Sá Ferreira. Microporous and Microporous Materials. 96, (2006), 363-368;

[20]- Pertierra, P., Salvadó, M. A., Garci'a-Granda, S., Bortun, A. I., Khainakov, S. A., & Garci'a, J. R. Inorganic Chemistry Communications, 5(10), (2002), 824–828;

[21]- Zanardi, S., Dalconi, M. C., Gambaro, C., Bellussi, G., Millini, R., Rizzo, C., & Carati, A. Microporous and Mesoporous Materials, (2009), 117(1-2);

[22]- Lin, Z., Ferreira, A., & Rocha, J. Journal of Solid State Chemistry, 175(2), (2003), 258–263;

[23]- Lin, Z., Rocha, J., Pedrosa de Jesus, J. D., & Ferreira, a. Journal of Materials Chemistry, 10(6), (2000), 1353–1356;

[24]- Millini, R., Carati, A., Bellussi, G., Cruciani, G., Parker, W. O., Rizzo, C., & Zanardi, S. Microporous and Mesoporous Materials, 101(1-2), (2007), 43–49;

[25]- Lin, Z., & Rocha, J. Microporous and Mesoporous Materials, 94(1-3), (2006), 173–178;

[26]- Ferreira, a, Lin, Z., Rocha, J., Morais, C. M., Lopes, M., & Fernandez, C. Inorganic chemistry, 40(14), (2001), 3330–5;

[27]- Lo, F.-R., & Lii, K.-H. Journal of Solid State Chemistry, 178(4), (2005), 1017–1022;

[28]- Miguel A.R. Peixoto. Síntese e trocas iónicas em silicatos de estanho, Projeto Individual, MIEMAT, Universidade do Minho. 2012;

[29]- Publishing, W. A., & York, N. HANDBOOK OF HYDROTHERMAL TECHNOLOGY. (2001). New York.

[30]- http://abulafia.mt.ic.ac.uk/shannon/radius.php?Element=Ti, used for reading and values checking.

[31]- http://abulafia.mt.ic.ac.uk/shannon/radius.php?Element=Sn, used for reading and values checking.

[32]- Zagorodni, Andrei. A. Ion exchange Materials - Properties and Applications. (2007) Elsevier;

[33]- Fewox, C. S. Ion exchange behavior among metal trisilicates: Probing selectivity, structure and mechanism. (August, 2008);

[34]- Aiello, R., Nagy, J. B., Giordano, G., Katovic, A., & Testa, F. Comptes Rendus Chimie, 8(3-4), (2005) 321–329;

[35]- http://www.ctcms.nist.gov/wulffman/docs_1.2/;

[36]- Burton, A. W., Ong, K., Rea, T., & Chan, I. Y. Microporous and Mesoporous Materials, 117(1-2), (2009), 75–90.

[37]- Norbert Stribeck, X-Ray Scattering of Soft Matter, 2007;

[38]- http://www.semat.lab.uminho.pt;

[39]- http://www.icdd.com;

[40]- TOPAS V3.0, General profile and structure analysis software for powder diffraction data, Bruker AXS, Karlsruhe, Germany;

[41]- R.W. Cheary, A.A. Coelho, Journal of Applied Crystallography. 25, 109 (1992);

[42]- http://www.iucr.org/resources/cif;

[43]- A. Kern, A.A. Coelho, R.W. Cheary, Convolution based profile fitting, in Diffraction analysis of the microstructure of materials, ed. by E.J. Mittemeijer, P;

[44]- Shah, P., Ramaswamy, a. V., Lazar, K., & Ramaswamy, V. Microporous and Mesoporous Materials, 100(1-3), (2007), 210–226;

[45]- Ng, E.-P., Chateigner, D., Bein, T., Valtchev, V., & Mintova, S. Science (New York, N.Y.), 335(6064), (2012), 70–3;

[46]- - http://abulafia.mt.ic.ac.uk/shannon/radius.php?Element=Cr;

[47]- http://abulafia.mt.ic.ac.uk/shannon/radius.php?Element=K;

[48]- Peixoto, M. A. R., & Ferdov, S. Journal of Porous Materials, (2013);

[49]- http://abulafia.mt.ic.ac.uk/shannon/radius.php?Element=Cu;

[50]- http://abulafia.mt.ic.ac.uk/shannon/radius.php?Element=Zn;

[51]- http://abulafia.mt.ic.ac.uk/shannon/radius.php?Element=Pb;

[52]- http://abulafia.mt.ic.ac.uk/shannon/radius.php?Element=Al;

[53]- Ferreira, A., Lin, Z., Soares, M. R., & Rocha, J.. Journal of Solid State Chemistry, 183(12). (2010). 3067–3072;

[54]- Pertierra, P., Salvadó, M. a., García-Granda, S., Khainakov, S. a., & García, J. R. Thermochimica Acta, 423(1-2), (2004), 113–119;

Appendix

Appendix 1

Chemical compositions of all the products synthesized in this thesis.

Casos	Composição química	NaOH (g)	$SnCl_2$ (g)	SiO_2 (g)	H_2O (g)
C1	$5Na_2O$-$5SiO_2$-$0,5SnO_2$-$500H_2O$	1.778	0.402	1.335	40.000
C2	$10Na_2O$-$5SiO_2$-$0,5SnO_2$-$500H_2O$	3.555	0.402	1.335	40.000
C3	$15Na_2O$-$5SiO_2$-$0,5SnO_2$-$500H_2O$	5.333	0.402	1.335	40.000
C4	$20Na_2O$-$5SiO_2$-$0,5SnO_2$-$500H_2O$	7.111	0.402	1.335	40.000
C5	$5Na_2O$-$5SiO_2$-SnO_2-$500H_2O$	1.778	0.803	1.335	40.000
C6	$10Na_2O$-$5SiO_2$-SnO_2-$500H_2O$	3.555	0.803	1.335	40.000
C7	$15Na_2O$-$5SiO_2$-SnO_2-$500H_2O$	5.333	0.803	1.335	40.000
C8	$20Na_2O$-$5SiO_2$-SnO_2-$500H_2O$	7.111	0.803	1.335	40.000
C9	$5Na_2O$-$5SiO_2$-$1,5SnO_2$-$500H_2O$	1.778	1.204	1.335	40.000
C10	$10Na_2O$-$5SiO_2$-$1,5SnO_2$-$500H_2O$	3.555	1.204	1.335	40.000
C11	$15Na_2O$-$5SiO_2$-$1,5SnO_2$-$500H_2O$	5.333	1.204	1.335	40.000
C12	$20Na_2O$-$5SiO_2$-$1,5SnO_2$-$500H_2O$	7.111	1.204	1.335	40.000
C13	$5Na_2O$-$5SiO_2$-$2SnO_2$-$500H_2O$	1.778	1.606	1.335	40.000
C14	$10Na_2O$-$5SiO_2$-$2SnO_2$-$500H_2O$	3.555	1.606	1.335	40.000
C15	$15Na_2O$-$5SiO_2$-$2SnO_2$-$500H_2O$	5.333	1.606	1.335	40.000
C16	$20Na_2O$-$5SiO_2$-$2SnO_2$-$500H_2O$	7.111	1.606	1.335	40.000
C17	$5Na_2O$-$5SiO_2$-$2,5SnO_2$-$500H_2O$	1.778	2.007	1.335	40.000
C18	$10Na_2O$-$5SiO_2$-$2,5SnO_2$-$500H_2O$	3.555	2.007	1.335	40.000
C19	$15Na_2O$-$5SiO_2$-$2,5SnO_2$-$500H_2O$	5.333	2.007	1.335	40.000
C20	$20Na_2O$-$5SiO_2$-$2,5SnO_2$-$500H_2O$	7.111	2.007	1.335	40.000

Casos	K_2O	Na_2O	SiO_2	SnO_2	H_2O	KOH (g)	NaOH (g)	$SnCl_2$ (g)	SiO_2 (g)	H_2O (g)
D1	6.67	3.33	5	0.5	500	3.378	1.185	0.402	1.335	40
D2	8.00	2.00	5	0.5	500	4.053	0.711	0.402	1.335	40
D3	8.57	1.43	5	0.5	500	4.343	0.508	0.402	1.335	40
D4	8.89	1.11	5	0.5	500	4.504	0.395	0.402	1.335	40
D5	6.67	3.33	5	1	500	3.378	1.185	0.803	1.335	40
D6	8.00	2.00	5	1	500	4.053	0.711	0.803	1.335	40
D7	8.57	1.43	5	1	500	4.343	0.508	0.803	1.335	40
D8	8.89	1.11	5	1	500	4.504	0.395	0.803	1.335	40
D9	6.67	3.33	5	1.5	500	3.378	1.185	1.204	1.335	40
D10	8.00	2.00	5	1.5	500	4.053	0.711	1.204	1.335	40
D11	8.57	1.43	5	1.5	500	4.343	0.508	1.204	1.335	40
D12	8.89	1.11	5	1.5	500	4.504	0.395	1.204	1.335	40
D13	6.67	3.33	5	2.0	500	3.378	1.185	1.606	1.335	40
D14	8.00	2.00	5	2.0	500	4.053	0.711	1.606	1.335	40
D15	8.57	1.43	5	2.0	500	4.343	0.508	1.606	1.335	40
D16	8.89	1.11	5	2.0	500	4.504	0.395	1.606	1.335	40
D17	6.67	3.33	5	2.5	500	3.378	1.185	2.007	1.335	40
D18	8.00	2.00	5	2.5	500	4.053	0.711	2.007	1.335	40
D19	8.57	1.43	5	2.5	500	4.343	0.508	2.007	1.335	40
D20	8.89	1.11	5	2.5	500	4.504	0.395	2.007	1.335	40

Trial	K_2O (moles)	SiO_2 (moles)	SnO_2 (moles)	H_2O (moles)	KOH (g)	SiO_2 (g)	$SnCl_2$ (g)	H_2O (g)
P1	5	2.5	0.5	500	2.53(3)	0.66(7)	0.40(1)	40±0.5
P2	10	2.5	0.5	500	5.06(6)	0.66(7)	0.40(1)	40±0.5
P3	15	2.5	0.5	500	7.60(1)	0.66(7)	0.40(1)	40±0.5
P4	5	5	0.5	500	2.53(3)	1.33(5)	0.40(1)	40±0.5
P5	10	5	0.5	500	5.06(6)	1.33(5)	0.40(1)	40±0.5
P6	15	5	0.5	500	7.60(1)	1.33(5)	0.40(1)	40±0.5
P7	5	2.5	1	500	2.53(3)	0.66(7)	0.80(2)	40±0.5
P8	10	2.5	1	500	5.06(6)	0.66(7)	0.80(2)	40±0.5
P9	15	2.5	1	500	7.60(1)	0.66(7)	0.80(2)	40±0.5
P10	5	5	1	500	2.53(3)	1.33(5)	0.80(2)	40±0.5
P11	10	5	1	500	5.06(6)	1.33(5)	0.80(2)	40±0.5
P12	15	5	1	500	7.60(1)	1.33(5)	0.80(2)	40±0.5
P13	5	2.5	1.5	500	2.53(3)	0.66(7)	1.20(2)	40±0.5
P14	10	2.5	1.5	500	5.06(6)	0.66(7)	1.20(2)	40±0.5
P15	15	2.5	1.5	500	7.60(1)	0.66(7)	1.20(2)	40±0.5
P16	5	5	1.5	500	2.53(3)	1.33(5)	1.20(2)	40±0.5
P17	10	5	1.5	500	5.06(6)	1.33(5)	1.20(2)	40±0.5
P18	15	5	1.5	500	7.60(1)	1.33(5)	1.20(2)	40±0.5

Appendix 1

Trial	ZrO_2	SnO_2	SiO_2	K_2O	Na_2O	H_2O	$ZrCl_2$ (g)	$SnCl_2$ (g)	SiO_2 (g)	KOH (g)	NaOH (g)	H_2O (g)
IS1	0.1	0.4	5	6.66	3.33	500	0.104	0.321	1.335	3.374	1.184	40.000
IS2	0.1	0.4	2.5	5	0	500	0.104	0.321	0.668	2.533	0.000	40.000
IS3	0.3	1.2	5	0	5	500	0.311	0.963	1.335	0.000	1.778	40.000
IS4	0.5	2	5	0	20	500	0.518	1.606	1.335	0.000	7.111	40.000
IS5	0.2	0.3	5	6.66	3.33	500	0.207	0.241	1.335	3.374	1.184	40.000
IS6	0.2	0.3	2.5	5	0	500	0.207	0.241	0.668	2.533	0.000	40.000
IS7	0.6	0.9	5	0	5	500	0.621	0.722	1.335	0.000	1.778	40.000
IS8	1	1.5	5	0	20	500	1.036	1.204	1.335	0.000	7.111	40.000

Trial	BiO_2	SnO_2	SiO_2	K_2O	Na_2O	H_2O	$BiCl_2$ (g)	$SnCl_2$ (g)	SiO_2 (g)	KOH (g)	NaOH (g)	H_2O (g)
Bi_1D_4	0.6	0.9	5	0	5	500	0.840	0.722	1.335	0.000	1.777	40
Bi_2D_2	0.3	1.2	5	10	0	500	0.420	0.963	1.335	5.067	0	40

Trial	GeO_2	SnO_2	SiO_2	K_2O	Na_2O	H_2O	GeO_2 (g)	$SnCl_2$ (g)	SiO_2 (g)	KOH (g)	NaOH (g)	H_2O (g)
Ge_2D_2	0.3	1.2	5	10	0	500	0.139	0.963	1.335	5.067	1.777	40
Ge_1D_4	0.3	1.2	5	0	5	500	0.139	0.963	1.335	0	0	40

Appendix 1

Trial	ZrO_2	SnO_2	SiO_2	K_2O	Na_2O	H_2O	$ZrCl_2$ (g)	$SnCl_2$ (g)	SiO_2 (g)	KOH (g)	NaOH (g)	H_2O (g)
IS9	0.1	0.4	5	6.66	3.33	500	0.069	0.321	1.335	3.374	1.184	40
IS10	0.1	0.4	2.5	5	0	500	0.069	0.321	0.668	2.533	0.000	40
IS11	0.3	1.2	5	0	5	500	0.206	0.963	1.335	0.000	1.778	40
IS12	0.5	2	5	0	20	500	0.343	1.606	1.335	0.000	7.111	40
IS13	0.2	0.3	5	6.66	3.33	500	0.137	0.241	1.335	3.374	1.184	40
IS14	0.2	0.3	2.5	5	0	500	0.137	0.241	0.668	2.533	0.000	40
IS15	0.6	0.9	5	0	5	500	0.411	0.722	1.335	0.000	1.778	40
IS16	1	1.5	5	0	20	500	0.685	1.204	1.335	0.000	7.111	40
IS17	0.3	0.2	5	6.66	3.33	500	0.206	0.161	1.335	3.374	1.184	40
IS18	0.3	0.2	2.5	5	0	500	0.206	0.161	0.668	2.533	0.000	40
IS19	0.9	0.6	5	0	5	500	0.617	0.482	1.335	0.000	1.778	40
IS20	1.5	1	5	0	20	500	1.028	0.803	1.335	0.000	7.111	40

Appendix 1

Trial	Na_2O (moles)	SiO_2 (moles)	SnO_2 (moles)	H_2O (moles)	NaOH (g)	SiO_2 (g)	$SnCl_2$ (g)	H_2O (g)
E1	1	2.5	1	40	0.356	0.668	0.803	40
E2	2.5	2.5	1	40	0.889	0.668	0.803	40
E3	2.5	5	2	40	0.889	1.335	1.606	40
E4	1	5	2	40	0.356	1.335	1.606	40
E5	5	5	2	40	1.778	1.335	1.606	40
E6	1	2.5	2	40	0.356	0.668	1.606	40

Appendix 2

Crystallographic data of the layered phase model created. All distance and angles respect the theoretical physical values. The structure is still not at its final state but the obtained parameters are very close to the final solution.

Position	Atom	x	y	z	Occupancy
Sn1	Sn+4	0.3333	0.6667	0.1385	1
K1	K+1	0.6667	1.3333	0.3661	1
Si1	Si+4	0	1	0.2159	1
O3	O-2	0	1	0	1
O4	O-2	0.1607	0.8393	0.2922	1
O5	O-2	0.5	1	0	1
Ow	O-2	0	1	0.5	1

Atoms connected	Number of connections	Distance (Å)
Sn-O5	2x	1.9184
Sn-O5	1x	1.9188
Sn-O4	1x	2.0308
Sn-O4	2x	2.0312
K-O4	2x	2.833
K-O4	2x	2.8333
K-O4	2x	2.8335
K-O4	1x	3.0856
K-O4	2x	3.0859
Si-O3	1x	1.6435
Si-O4	3x	1.651
Si-Ow	1x	2.1626

Atoms connected	Angle (°)
O5-Sn-O5	92.704
O5-Sn-O5	92.691
O5-Sn-O4	88.584
O4-Sn-O4	90.123
O4-K-O4	116.168
O4-K-O4	128.213
O4-K-O4	100.272
O4-K-O4	156.976
O3-Si-O4	110.597
O4-Si-O4	108.323